044430

SOME EFFECTS OF ROUGHNESS ELEMENTS ON BOUNDARY LAYER GROWTH

A MASTER'S THESIS

in

Mechanical Engineering

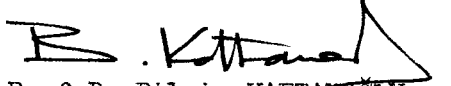Middle East Technical University

044430

By

Melda (ÖZDİNÇ) ÇARPINLIOĞLU

September 1986

Approval of the Graduate School of Natural and Applied Sciences.

Prof.Dr.Bilgin KAFTANOĞLU

Director

I certify that this thesis satisfies all the requirements as a thesis for the degree of Master of Science in Mechanical Engineering Department.

Assoc.Prof.Dr. Ömer T.GÖKSEL

Chairman of the Department

We certify that we have read this thesis and that in our opinion it is fully adequate, in scope and quality, as a thesis for the degree of Master of Science in Mechanical Engineering Department.

Assoc.Prof.Dr. Ömer T.GÖKSEL

Supervisor

Examining Committee in Charge :

Assoc.Prof.Dr.Ömer T.GÖKSEL

Assoc.Prof.Dr.Mazhar ÜNSAL

Assoc.Prof.Dr.Süleyman SARITAŞ

ABSTRACT

SOME EFFECTS OF ROUGHNESS ELEMENTS ON BOUNDARY LAYER GROWTH

ÇARPINLIOĞLU (ÖZDİNÇ) Melda

M.S. in Mechanical Engineering

Supervisor : Assoc.Prof.Dr.Ömer T. GÖKSEL

September 1986, 132 Pages

The effects of an isolated and a row of roughness elements on boundary layer transition, recovery length of turbulent boundary layer, and wake development were investigated by using the available experimental results in the literature.

The present correlations are analysed, by making several comments about them.

The effect of upstream flow history on the transition characteristics of roughness elements are studied; and correlations which consider this effect are obtained.

Correlations are proposed also for recovery lengths, and simple expressions which describe the critical dimensions of a spherical roughness element are obtained.

Correlations are proposed for the turbulent wake growth behind an isolated spherical roughness element .

Key Words : boundary layer, transition, roughness element.

ÖZET

SINIR TABAKASI GELİŞİMİNDE PÜRÜZLÜLÜK ELEMANLARININ BAZI ETKİLERİ

ÇARPINLIOĞLU (ÖZDİNÇ) Melda

Yüksek Lisans Tezi, Makina Mühendisliği Bölümü

Tez Yöneticisi : Doç.Dr. Ömer T. GÖKSEL

Eylül 1986, 132 Sayfa

Tek ve bir sıra pürüzlülük elemanlarının sınır tabakası geçişi, türbülanslı sınır tabakasının toparlanma mesafesi ve türbülanslı bölge gelişimine etkileri literatürdeki mevcut deneysel neticelerin kullanılmasıyla incelendi.

Mevcut eşilişkilerin analizi, çeşitli yorumlarla yapıldı.

Akım geçmişinin pürüzlülük elemanlarının geçiş karekterleri üzerindeki etkisi incelendi ve bu etkiyi dikkate alan eşilişkiler elde edildi. Ayrıca toparlanma mesafeleri için de eşilişkiler önerildi ve küresel bir pürüzlülük elemanının kritik boyutlarını tanımlayan basit ifadeler elde edildi.

Tek küresel pürüzlülük elemanı arkasındaki türbülanslı bölge gelişimi için eşilişkiler önerildi.

Anahtar Kelimeler : Sınır tabakası, geçiş, pürüzlülük elemanı.

ACKNOWLEDGEMENTS

TABLE OF CONTENTS

vii

LIST OF TABLES

LIST OF FIGURES

x

xi

xiii

xiv

NOMENCLATURE

H	Shape Factor, $\dfrac{\delta^*}{\Theta}$
k	Roughness height
R	Reynolds number
R_k	Roughness Reynolds, number $\dfrac{Uk}{\nu}$ based on the free stream velocity
R_{kcs}	Critical value of R_k for the start of transition
R_{kce}	Critical value of R_k for the end of transition
R_{kk}	Roughness Reynolds number based on the velocity at the roughness height, u_k , in the undisturbed laminar boundary layer at the roughness position $\dfrac{u_k\,k}{\nu}$
R_{kkcs}	Critical value of R_{kk} for the start of transition.
R_{kkce}	Critical value of R_{kk} for the end of transition
R_x	Reynolds number based on chordwise length x, $\dfrac{Ux}{\nu}$
R_{x_k}	Roughness position Reynolds number
R_{x_T}	Start or end of transition Reynolds number
$R_{x_{Tcs}}$	Critical value of R_{x_T} for the start of transition
$R_{x_{Tce}}$	Critical value of R_{x_T} for the end of transition
R_{x_L}	Reynolds number based on distance X_L
$R_{x_{W_T}}$	Reynolds number based on turbulent wake starting distance, X_{W_T} ,
R_{W_T}	Turbulent wake width Reynolds number
R_{δ^*}	Displacement thickness Reynolds number
R_Θ	Momentum thickness Reynolds number
U	Free stream velocity
u	Velocity of flow in the boundary layer

u_k	Velocity at the roughness height in the undisturbed laminar boundary layer at the roughness position.
U_τ	Skin friction velocity,
U_k	Free stream velocity at $x = x_k$
X_k	Chordwise position of the roughness element
X_T	Chordwise position of the start or the end of transition
X_R	Chordwise position of the end of recovery region
X_L	Distance to the end of recovery region behind the roughness element, $X_R - X_k$
X_{W_T}	Chordwise position of the turbulent wake apex
MRL	Minimum recovery distance
n	Number of the elements in the row
S	Spacing of the elements in the row
T	Turbulence intensity of free stream
z	Spanwise coordinate measured from the centerline of the flat plate.
δ	Boundary layer thickness
δ^*	Displacement thickness
θ	Momentum thickness
δ^*_k	Displacement thickness of the undisturbed laminar boundary layer at $x = x_k$
θ_k	Momentum thickness of the undisturbed laminar boundary layer at $x = x_k$
λ_θ	Pohlhausen's pressure gradient parameter, $\dfrac{\theta^2}{\nu} \cdot \dfrac{dU}{dx}$
λ_{θ_k}	Value of λ_θ at $x = x_k$
μ	Dynamic viscosity
ν	Kinematic viscosity
ρ	Density
τ_o	Skin friction

CHAPTER 1

INTRODUCTION

Transition from laminar to turbulent flow is the result
of the build up of the disturbances in the boundary layer. In
natural transition, this build up occurs over long distances.
In order to induce transition ahead of its naturally oc -
curring position " tripping " must be done by a roughness element
fixed onto or near the surface. The presence of such a rough -
ness element shortens the surface distance required for distur -
bances to cause transition by changing the flow configuration
completely. Transition of this type is known as forced transi -
tion. Two and three dimensional roughness elements can be used
as tripping devices.

In the available literature, measurements of transition
behind the roughness elements have been done under zero, ad-
verse, and favourable pressure gradients. The effects of rough-
ness elements upon the boundary layer development have been inves-
tigated also. Before the data in the available literature were
re - analysed, the experimental set - ups and the instrumentation
of the investigators were also carefully checked so that any error
in their experimental set - up or the instrumentation did not affect
their results. Those data collected by investigators who did not
clearly give explanations about their experimental set - up or their
measurement techniques were disregarded. Several different measure-
ment techniques have been used by different investigators to detect
transition. Roughness elements of various shapes and sizes have been
used by various investigators in different nature. The correlations
obtained by these investigators are not generally in good agreement

1

with each other and furthermore some of them are incomplete. All of the investigators considered in this study did not give emphasis on the effect of upstream flow history upon the transition and wake characteristics of roughness elements.

Under the light of the above argument there seems to be a necessity in the unification of the correlations made by different authors. This can be done by using the available data in the literature and introducing the effect of upstream flow history on transition characteristics of the roughness elements. In this work new correlations between the important variables were made which are simple and applicable to relevant flow conditions.

Chapter 2 gives a complete review of the previous work on boundary layer transition with special emphasis on forced transition.

Several comments are made on the available correlations in chapter 3. New correlations on the transition characteristics of laminar boundary layer are proposed by using the available data in the literature.

Boundary layer development behind a roughness element and wake growth of a spherical roughness element is investigated in chapter 4, and some new correlations are presented.

Chapter 5 is about the effects of row of spherical roughness elements upon boundary layer transition.

CHAPTER 2

LITERATURE SURVEY

2.1. INTRODUCTION

Although a great many experimental as well as theoretical investigations on transition from laminar to turbulent flow have been made; the transition problem is not completely solved due to the reason that phenomena associated with it is rather complex. In this chapter, both theoretical and experimental studies on transition conducted upto now will be briefly discussed.

2.2. GENERAL ASPECTS OF TRANSITON

The phenomenon of transition from laminar to turbulent flow which is fundamental for the science of fluid dynamics was first investigated in relation to flows through straight pipes and channels. At the end of the nineteenth century, O. Reynolds was the first one who investigated systematically the laminar and turbulent flow patterns. He discovered the law of similarity which now bears his name and which states that transition from laminar to turbulent flow always occurs at nearly the same Reynolds number.

The transition in a boundary layer flow was first investigated much later than the transition in a pipe flow. In 1914, L. Prandtl succeeded in showing that the flow in the boundary layer undergoes transition and the problem of calculation of drag is affected by transition. Theoretical investigations in the process of transition from laminar to turbulent flow are based on the acceptance of Reynolds's hypothesis that the latter occurs as a consequence of an

instability developed in the laminar boundary layer.

In the past, a number of investigators attempted to solve the theoretical problem of the stability of the laminar flow by determining under what conditions small disturbances in the form of velocity variations present in flow would increase or decrease with time.

Much work has been done on the mathematical foundations of Reynolds's hypothesis first by O. Reynolds himself and later by L. Rayleigh. These efforts have led to complicated calculations. About 1930, Tollmien (1) made important advances in the application of the mathematical theory and published a theory of stability which was confirmed later by Schlichting. Tollmien - Schlichting theory was based on the assumption that small disturbances of any wavelength lying within a certain region would be amplified; whereas disturbances of shorter or longer wavelength would be damped. The amplified disturbances were assumed to grow until they caused a breakdown of laminar flow. The theory which was based on the linearized perturbation equation of boundary layer was universally discredited by scientists and engineers mainly because no evidence of disturbances had ever been found in boundary layers. The first experimental verification of this theory has been achieved by Schubauer - Scramstad (2) in 1940. They discovered sinosoidal velocity fluctuations which were termed as "laminar boundary layer oscillations", to distinguish these fluctuations from the irregular fluctuations oberved by other investigators in the laminar boundary layer of a flat plate. Schubauer - Scramstad used a wind tunnel having a turbulence level of much less than 0.1 percent in observing the laminar boundary layer oscillations. The oscillations were found to consist of a wave motion in the boundary layer. Amplified, damped and neutral waves were found and these characteristics together with wave velocities and type of wave motion were in accordance with the theory of selective amplification and damping proposed by Tollmien - Schlichting. The mechanism of transition was later con -

4

firmed by the works of Klebanoff - Tidstrom (3), Klebanoff - Tidstrom-Sargent (4), Tani (5), Tani - Komada (6), Squire (7). Squire analytically verified that   for small disturbances the two dimensional waves are more unstable than oblique waves traveling at an angle to the main flow. Then it was found that the two - dimensional Tollmien - Schlichting wave first appears as an indication of an eventual breakdown of laminar flow into turbulence. As a result of experiments and theoretical studies on the instability of laminar boundary layer the following transition mechanism can be assumed:

A Tollmien - Schlichting wave may be set up by the selective amplification of pre - existing small disturbances. As the wave travels downstream it damps or amplifies in the way predicted by the linearized stability theory, and at the same time wave is deformed into a three dimensional configuration. If the wave remains small in intensity, it does not result in the onset of turbulence. If the wave intensity exceeds a certain amount, non linear development takes place. The appearance of non linear development, which is characterized by the rapid amplification of wave intensity; rapid increase in wave three dimensionality, and distortion in mean velocity profile leads to the breakdown of laminar flow. Breakdown of laminar flow occurs as a result of three dimensional development of the wave as a whole.

Dryden (8) in 1931 and Taylor (9) in 1936 suggested that transition was caused by incipient or permanent separation of the boundary layer. But later Liepmann - Fila (10), Tani - Sato (11), Hama - Long - Hegarty (12) showed that separation of the laminar boundary layer was not a prerequisite for transition.

Hama - Long - Hegarty investigated the flow on a flat plate behind a cylindrical trip wire attached transversely to the surface. Their observations led to the following conclusions :

1- Weak two dimensional vortices remain almost two dimensional.

5

2- Strong two dimensional vortex lines have a definite tendency to form three dimensional vortex loops, in shear flows with a marked transverse wavelength. As swept downstream, the waviness is intensified as a result of the interaction between the mean velocity gradient and the induction effect of the deformed vortex line. Thus a strong vortex line picks up three dimensional disturbances and intensifies their effect.

3- The transverse wavelength is dependent on the mean velocity distribution and it's different in wakes and in boundary layers.

4- The formation of the three dimensional vortex loop must occur before a turbulent spot can originate near the top of the vortex loop.

5- The mechanism of final breakdown is not clear.

6- Local seperation does not necessarily lead to immediate transition.

In summary of the results they suggested that the cause of transition on a smooth plate may be due to the formation of vortex loops. Later Hama - Nutant (13) showed that warped vorticity field acts to set up a high shear layer within the boundary layer which then breaks down to form a loop of concentrated vortex filaments.

Meanwhile a different approach to the problem of transition has been provided by Emmons (14) through his water table experiments. He showed that at random times and at random places tiny spots of turbulence appeared. He observed that spots grow as they move downstream in a wedge shaped region and the locus of the successive spot positions appear straight and at the same angle as the continuous turbulence from a wake. The turbulence in transition was seen to be essentially intermittent and final breakdown of laminar flow was observed when these spots took over the entire boundary layer flow field. In short, Emmons concluded that a transition region was

6

a region of formation and growth of turbulent spots. Schubauer – Klebanoff (15) later investigated the propagation of a turbulent spot by means of a spark technique developed by Mitchner and they verified the Emmons'spot theory. Schubauer – Klebanoff concluded that a transition region may be roughly divided into two parts, namely :

1- An initial stage where initial breakdowns occur and spots form and begin to grow .

2- A final stage consisting of spot growth with new breakdowns prohibited.

Dhawan – Narasimha (16) proposed a universal intermittency distribution for boundary layers on a flat plate and predicted the skin friction and the velocity profiles in the transition region by utilizing Emmons'spot theory. Nagel (17) extended this theory to hypersonic flows. Chen – Thyson (18) used spot theory for boundary layers on flat plates or cones to include those of blunt bodies and they found that spot formation rate depends on local Mach number as well as transition Reynolds number.

Morkovin (19) described the transition process in a different way and analyzed it as an electrical system. He considered the boundary layer as a filter amplifier of a highly non – linear character and external disturbances such as noise, vibration and free stream turbulence were taken as inputs·Parameters like pressure gradient, surface roughness, heat transfer were considered to be operation modifiers; but due to non – linearity of the system it was not possible to see the effects of modifiers separately. Morkovin has drawn attention to the fact that the sequence of events leading to transition is not universal and process of instability remains unknown.

The effects of turbulence level of free stream, pressure gradient, flow history, heat transfer on transition of a laminar

7

boundary layer were investigated also at different times.

Schubauer - Scramstad (2) investigated the influence of turbulence intensity, T, of the free stream on transition of boundary layer on a flat plate under zero streamwise pressure gradient. They observed that a decrease in turbulence intensity up to a value of 0.0008; causes an increase in the transition Reynolds number, $R_{x_T} = \dfrac{Ux_T}{\nu}$; where U is the free stream velocity, X_T is the length from the leading edge of the plate to the observed transition position. For values of T lower than 0.0008, decrease in T does not cause any change in the transition Reynolds number which is known as the critical transition Reynolds number. This effect is shown in Figure 2.1.

Turbulence intensity also influences the distance between the points of instability and transition. P.S. Granville (20) correlated the results of Hall - Hislop (21), Schubauer - Scramstad (2), and Dryden (22). This is shown in Figure 2.2 by plotting $\Delta R_\theta = R_{\theta_T} - R_{\theta_i}$ versus T; where $R\theta_T$ is $\dfrac{U\theta_T}{\nu}$ and R_{θ_i} is $\dfrac{U\theta_i}{\nu}$; Reynolds numbers based on momentum thickness of the boundary layer at the transition and instability positions respectively. It was seen that the points of instability and transition become closer to each other as turbulence intensity increases.

The rate of amplification of unstable disturbances also influences the above mentioned distance. This rate of amplification is strongly dependent on the streamwise pressure gradient. R. Michel (23) discovered a simple empirical relation on this manner and A.M.O Smith (24) succeeded in confirming this relation on the basis of the stability theory. His results can be seen in Figure 2.3.

P.S. Granville (20) studied on the influence of the streamwise pressure gradients. His results were plotted together with the results of several different investigators. As is seen in Figure 2.4 all of these results arrange themselves on a single curve in a plot of $\Delta R_{\theta} = R_{\theta_T} - R_{\theta_i}$ versus $\bar{K} = $

$$\frac{1}{x_T - x_i} \int_{x_i}^{x_T} K \, dx \quad \text{where} \quad K \text{ is the Pohlhausen parameter,}$$

$$K = \frac{\theta^2}{\nu} \cdot \frac{dU}{dx} \quad \text{and} \quad x_T \text{ and } x_i \text{ are the chordwise positions of}$$

transition and instability. From Figure 2.4 it is seen that the distance between the instability and transition points is greater for favourable pressure gradients ($\bar{K} > 0$) than for adverse pressure gradients ($\bar{K} < 0$).

It was also found that at a certain turbulence level the effect of adverse pressure gradient in promoting transition was greater than the effect of favourable pressure gradient in retarding it. It was seen that the effect of pressure gradient as a whole becomes less significant as the level of turbulence increases.

2.3 THE INFLUENCE OF ROUGHNESS ON TRANSITION

It has been known since the thirties that a dirt particle or similar isolated roughness on the surface in the region of laminar flow may induce transition at a point ahead of its naturally occurring position.

The existence of roughness elements gives rise to additional disturbances in the laminar stream which have to be added to those generated by turbulence that are already present in the boundary layer. If the disturbances created by the roughness element are bigger than those due to turbulence , it must be expected that a lower degree of amplification will be sufficient to affect transition. On the other hand if the disturbances of the roughness element are small as compared with the existing ones, the presence of the roughness element would be

9

expected to have no effect on transition.

The very extensive experimental data collected upto date includes information on the effect of two dimensional, three dimensional, three dimensional and distributed roughness elements on transition from laminar to turbulent flow. Many of the investigations include data on the influence of pressure gradients, turbulence intensity and compressibility together with the roughness effects.

2.3.1 Transition Characteristics of Spherical Roughness Elements

Transition characteristics of spherical roughness elements have been investigated by Schubauer - Klebanoff - Tidstrom (25), Gregory - Walker (26), Weske (27), Peterson - Horton (28), Tani (29), Mochizuki (30), Hall (31), Göksel (32), Fraser - Milne (33), Yeğen (34), Albayrak (35).

Klebanoff et al (25) investigated transition behind a row of roughness elements on a flat plate under zero pressure gradient. They measured the start of transition. They found that as the wind speed is increased transition point moved almost instantaneously towards the row of elements. They also concluded that the critical condition for transition is affected by the stability limit of the boundary layer.

They accepted the critical condition as the transition oc - curring at the roughness location and defined the critical roughness Reynolds number as $R_{kk} = \dfrac{u_k k}{V}$ where; u_k is the velocity at the height of the roughness element, k is the height of the element, above the surface, V is the kinematic viscosity of the fluid. The critical roughness Reynolds numbers R_{kk} were found to be in the range of 490 - 578. Peterson - Horton (28) investigated the movement of start of transition behind a spherical roughness element

under favourable pressure gradient. Due to the strong favourable pressure gradient they applied, they found greater critical roughness Reynolds number values than Klebanoff et al's ones. They showed that the end of transition moved much more slowly towards the element than did the start, but they didn't measure particular values for the end of transition.

Mochizuki (30) performed experiments on a flat plate by using bearing balls of various diameters as spherical roughness elements. The resulting flow patterns were examined by smoke emitted from various heights and positions relative to the sphere. The end of transition point was defined as the apex of the turbulent wedge behind the roughness element. She concluded that in the transition process, flow pattern passes through the vortical state until finally developing into turbulence. She found critical roughness Reynolds number $R_{kk} = \dfrac{u_k \cdot k}{v}$ values for the end of transition varying between 600 - 1000.

Hall (31) made experiments under zero, favourable and adverse pressure gradients. For the zero pressure gradient case, he found the critical roughness Reynolds numbers $R_{kk} = 533$ for the start of transition, and the value between 750 - 800 for the the end of transition. He concluded that both favourable and adverse pressure gradients cause an increase in the critical roughness Reynolds numbers R_{kk} for the start and the end of transition. He also pointed that the end of transition never reaches the roughness position.

Göksel (32) has investigated transition behind isolated and a row of spherical roughness elements upon a flat plate under zero pressure gradient. He has correlated the critical roughness Reynolds numbers $R_k = \dfrac{Uk}{v}$ with roughness location Reynolds numbers $R_{x_k} = \dfrac{Ux_k}{v}$ for the start and the end of transition. For a row of spherical roughness elements he showed that the effect of spacing between the roughness elements is more pronounced at smaller rough-

ness location Reynolds numbers R_{x_k} . He also observed that both the start and the end of transition moved rapidly towards the element with increasing unit Reynolds numbers, $(\frac{U}{\nu})$. The point of the end of transition was found to move slowly towards the element when it was compared with the movement of the start of transition. In his study; he also correlated the minimum roughness Reynolds numbers which can't move the positions of the start and the end of transition towards the roughness element from the naturally occurring position with roughness location Reynolds numbers, (Rx_k).

Yeğen (34) investigated the movement of transition under zero, adverse and favourable pressure gradients but he gave special emphasis on the case with an adverse pressure gradient. He correlated the critical roughness Reynolds numbers, (R_k), for the start and the end of transition with the Reynolds number based on the displacement thickness of the boundary layer at the roughness location, $R_{\delta^*_k}$. He obtained the same relationship between above mentioned dimensionless parameters for zero, adverse and favourable pressure gradients. His findings indicated that R_k and $R_{\delta^*_k}$ is independent of the pressure gradient for a certain range of λ_Θ. He has concluded that there is no systematic effect of λ_Θ on the critical roughness Reynolds numbers for the start and the end of transition for $- 0.052 \leq \lambda_\Theta \leq + 0.053$. He also found that under adverse pressure gradients the critical roughness Reynolds numbers for the start and the end of transition behind a row of roughness elements of $S/k > 2$ are the same as the corresponding roughness Reynolds numbers for a single roughness element.

Albayrak (35) performed experiments on a flat plate to investigate the effects of favourable pressure gradient on the transition characteristics of spherical roughness elements. He concluded that in zero and favourable pressure gradients the start of transition appeared to move instantaneously from its naturally occurring position to a position very close to the element as was investigated

12

by many of the previous observers. While the end of transition app-
roaches to the element more gradually as it comes near to the element
and stops at a finite distance from it. Albayrak also proposed
correlations for the start and the end of transition, between the
critical roughness Reynolds numbers and corresponding critical
roughness position Reynolds numbers. He concluded that the proposed
correlations are applicable for zero, adverse and favourable pres-
sure gradients for the range of $- 0.052 \leqslant \lambda\Theta_k \leqslant + 0.055$. Where
$\lambda\Theta_k$ is the shape factor defined as $\lambda\Theta_k = \frac{\Theta_k^2}{\nu} \cdot \frac{dU}{dx}$. In his
work he succeeded in showing the relationships between the critical
roughness Reynolds numbers based on the velocity at the height of
the roughness element for the start and the end of transition and
the roughness Reynolds number which is based on the displacement
thickness of the boundary layer at the roughness position. But due
to the scatter of his experimental results he couldn't obtain exact
relationships between $R_{kkcs} - R_{\delta^*_k}$ and $R_{kkce} - R_{\delta^*_k}$. Where
R_{kkcs} and R_{kkce} are the critical roughness Reynolds numbers based
on the velocity at the roughness height for the start and the end of
transition respectively. He noticed that the critical roughness
Reynolds number values decrease when $R_{\delta^*_k}$ value increases. It was
also found that R_{kkcs} and R_{kkce} values obtained for favourable
pressure gradients are higher than the values obtained for zero pres-
sure gradient; and the effect of the shape factor $\lambda\Theta_k$ is more pro-
nounced on the values of R_{kkce} than on the values of R_{kkcs}.

2.3.2 Transition Characteristics of Other Forms of Roughness
       Elements

Von Doenhoff-Horton (36) performed experiments on an airfoil
with distributed carborandum particles which were attached on the
nose of the airfoil in the favourable pressure gradient region.
They observed the effect of stagnation point on the distance
between the start and the end of transition. They showed that

13

when the roughness elements were located away from the stagnation point, distance between the start and the end of transition was long, but as the elements were moved towards the stagnation point the transition length was decreased and even approached to zero. Göksel's experiments behind spherical roughness elements upon a flat plate under zero pressure gradient confirmed the same effect of transition length.

Holstein (37) made experiments on a flat wooden plate upon which an emery paper was attached. He indicated that the effect of distributed roughness in reducing the transition Reynolds number is much greater than the effect of a single roughness element. But unfortunately his results were considered not to be exact since the thickness of the emery paper was not included in the roughness height calculation.

Braslow (38) indicated that in supersonic flows the length of transition behind the roughness elements was long while in incompressible flows this length was short even with the turbulent wedge close to the element.

Gregory – Walker (26) observed the movement of the turbulent wedge behind cylindrical, and conical roughness elements. The movement of the turbulent wedge to the element was found to be instantaneous in accelarating flows. Their observations are thus in agreement with those of Von Doenhoff – Horton, and Mochizuki. Since they couldn't measure the movement of the start of transition they didn't determine the relative movement of the start and the end of transition.

B.H. Carmichael (39 - 40) measured transition behind upright cylindrical roughness elements on a flat plate. He investigated transition characteristics of multiple elements as well as single cylindrical elements. He developed an improved method for the prediction of the critical roughness size sufficient to trip the laminar boundary layer to turbulent state. He proposed a correlation between roughness Reynolds number, $R_k = \dfrac{Uk}{\nu}$, and quantity $\dfrac{k^2}{\Theta_k d}$. ($\dfrac{k^2}{\Theta_k d} = \dfrac{k}{\Theta_k} \cdot \dfrac{k}{d}$; $\dfrac{k}{d}$:

roughness fineness ratio, $\frac{k}{\theta_k}$: roughness relative height).

He used audio stethoscope technique for transition detection, and he considered the generation of bursts in the flow at a certain frequency as an indication of the start of transition . For cylinders of equal height and diameter the average critical roughness Reynolds number $R_{kk} = \frac{u_k k}{\nu}$ was found to be about 700 for the start of transition. He concluded that for a pair of similar elements placed one diameter away from each other, the critical Reynolds number which is based on dimater of the roughness $R = \frac{Ud}{\nu}$ will decrease about 50% from that of a single element, while in a field of elements which is composed of a large element with a number of smaller ones with three dimater spacing, no effect of small elements upon transition is seen. He also investigated the spanwise and streamwise spacing effects on transition.

Tani et al (41) investigated the transition characteristics of cylindrical elements in a zero pressure gradient. They defined the transition point by 50% intermittency factor, thus their criterion actually determines the flow midway between the start and the end of transition points. They said that transition point moved gradually towards the roughness element with increasing unit Reynolds number and stopped at a finite distance from the element. They have also proposed a correlation between ,R_{kk} ,roughness Reynolds number based on the velocity at the height of the roughness element and, R_{x_k}, roughness position Reynolds number, by using the results of their measurements along with those of Klebanoff et al's and Mochizuki's results.

Fage (42) made measurements on roughness elements of various shapes under favourable pressure gradient. Fage's data were the first to show that a roughness element could move transition forward without necessarily bringing it to the element.

Stüper (43) investigated cylindrical roughness elements on a plate with and without pressure gradient; he drew the following con-

15

clusion : The sensitivity of the laminar boundary layer to irregularities on an otherwise smooth surface was not greatly altered by a favourable pressure gradient in the range of Reynolds numbers covered by the experiments and with the amount of turbulence present in the tunnel.

Hall - Gibbings (44) developed a criterion for the tolerable roughness in a laminar boundary layer. They investigated both the effects of two and three dimensional roughness elements. They provided a correlation between the Reynolds numbers $R_k = \frac{Uk}{V}$ and $R_{x_k} = \frac{Ux_k}{V}$ for the tolerable roughness size of two and three dimensional roughness elements. They considered the simplest case of a boundary layer on a flat plate under zero pressure gradient.

2.3.3 Flow Structure Behind Three Dimensional Roughness Elements

The visual observations of Mochizuki (30) and Gregory - Walker (26) showed that there are two sets of streamwise vortices in the wake of a three dimensional roughness element at the roughness Reynolds numbers below its critical value:

1 - Horse shoe shaped vortex encircling the front of the roughness element.

2 - Pair of closely spaced vortex filaments originating from the spiral filaments which rise vertically from the points on the plate behind the roughness element. These filaments are at about the level of the top of the element. While horseshoe vortex is located close to the plate.

The sense of rotation is such that momentum is to be transported downward towards the plate by means of a horseshoe vortex and upwards by means of a closely spaced vortex filaments. The effect of these vortices is seen to redistribute momentum so that

16

distortion in the mean velocity field appear in the boundary layer downstream of the roughness element.

Tani et al (41) concluded that three dimensional deformation of the mean velocity field was considered to account for critical behaviour of transition movement. The wake of a three dimensional roughness element is wedge shaped. It is composed of fully turbulent and intermittent regions. The spread angles which show lateral growth of these wedge shaped regions by different observers are inconsistent with each other. Schubauer - Klebanoff (15) found a half included vertex angle of 6.4^o and 10.6^o for fully turbulent and intermittent regions respectively. The edges of the wedges were found to be straight.

Mochizuki (30) observed that upto and including critical Reynolds numbers the sides of the wedge were composed of straight lines which were linked at a certain position downstream of the element. The wedge angle changed from 5° to 10° near the roughness element and 10° to 11° away from the element. At supercritical Reynolds number the boundary of the wedge could be represented by a single straight line and a wedge angle of 2.5^o to 5°.

Fraser - Milne (33) gave half included vertex angles of fully turbulent and transition wedges as 4.6^o and 9.1^o.

Göksel (32) with his experiments under zero pressure gradient behind single spherical roughness elements has investigated the mean flow quantities. He said that wedge angle behind spherical roughness element increases in downstream direction. He also concluded that the width of the intermittent wake could be expressed as a function of flow conditions at the roughness position and distance from the roughness element. For a row of spherical roughness elements he also proposed correlations between width of turbulent and intermittent wedges with conditions at the roughness position and distance from the roughness elements.

17

Göksel also investigated the turbulent boundary layer development behind a roughness element and he defined the region behind the roughness element through which the perturbations due to the roughness decay as the recovery region. He proposed a correlation between the dimensionless recovery length and dimensionless parameter of $R_k \frac{k}{\delta^*_k}$. Where δ^*_k is the displacement thickness of the boundary layer at the roughness location.

Yeğen (34) later investigated the boundary layer development behind a roughness element on a flat plate under adverse pressure gradients. He generalized the criterion for the recovery length concept proposed by Göksel and concluded that the dimensionless recovery length $\frac{R_x - R_{x_k}}{k}$ is a function of $R_k \left(\frac{k}{\delta^*_k} \right)^{n = -1}$.

Albayrak (35) also studied this problem; and he used a favourable pressure gradient. He obtained a good correlation of data of his experiments with the results of Göksel and Yeğen by defining a correlation parameter, $\Delta = \frac{R_{x_k} - R_{x_{kcs}}}{R_{x_{kce}} - R_{x_{kcs}}}$. He found that there exists a roughness Reynolds number for which recovery length may be minimum. Minimum recovery length was found to occur at about $\Delta = 21$. He also concluded that there exists a relationship between parameters Δ and $R_k \frac{k}{\delta^*_k}$. Albayrak, as a result said that it is not possible to trip a laminar boundary layer for the values of $R_k \frac{k}{\delta^*_k} \leqslant 10^3$.

2.3.4 Flow Structure Behind Two Dimensional Roughness Elements

Tani et al (51) investigated the transition behind a cylindrical two dimensional roughness element on a flat plate under zero pressure gradient. They concluded that transition does not take place right behind the element, rather the change is gradual, and the roughness element effect transition far downstream. They also obtained a good correlation of data by plotting the transition Reynolds number $\left(R_{x_T} = \frac{Ux_T}{v} \right)$ against the ratio of the roughness height to the

18

displacement thickness of the boundary layer at the roughness location.

$$\left(\frac{k}{\delta^{*}_{k}} \right).$$

Tani - Sato (11) later performed experiments again with cylindrical roughness elements. They concluded that for a zero pressure gradient case, transition behind a two dimensional element depends only on the ratio of the roughness height to the boundary layer thickness at the roughness position ($\frac{k}{\delta_k}$). They observed that if this ratio is small the boundary layer flow separates at the element but reattachnes to the plate at some distance producing scarcely any disturbance. Transition occurs in the reattached boundary layer, and a sinosoidal velocity fluctuation is observed at a distance downstream from the roughness element. They also said that when the ratio of $\frac{k}{\delta_k}$ is large transition occurs in the separated layer before it reattaches to the plate. They also suggested that for a given roughness element at a given position on the plate, transition moves forward and the transition Reynolds number, $R_{\delta_T} = \frac{U \delta_T}{V}$, where δ_T is the boundary layer thickness at the transition position, continues to decrease as the free stream velocity is increased. At a certain value of $\frac{k}{\delta_k}$ transition reaches the element and transition Reynolds number begins to increase as the free stream velocity is further increased. However the available data in their published work does not strictly support their above argument. In their study they defined the transition point as the location at which the intermittency factor of velocity fluctuation attains the value 0.5. Tani - Sato with their work achieved to decompose the complex phenomenon of transition due to roughness into simpler types;transition of laminar boundary layer type,and transition of laminar - separated layer type.

Liepmann - Fila (10) investigated the flow characteristics in the wake of large two dimensional roughness elements. They observed the effects of these elements both in laminar and turbulent boundary layers. The results of their studies in the wake of roughness

19

elements show that the existence of a separation profile does not necessarily lead to transition, meanwhile they also noticed that a laminar boundary layer can separate and reattach itself without transition taking place. If transition occurs in the detached layer, the velocity profile in the reattached boundary layer will approach the normal turbulent boundary layer profile very rapidly. They also showed that separation bubbles behind the element varied in length depending upon the condition of the boundary layer at the reattachment. The bubble became shorter as the element's size relative to that of boundary layer increased and the reattachment changed from laminar to turbulent.

2.3.5 Roughness Effects on Airfoils

For boundary layer flow upon an airfoil the Tollmien-Schlichting theory shows that the stability of the flow is greatly dependent on the pressure gradient and hence on the chordwise position. The Reynolds number at which amplification of small disturbances occurs may vary with chordwise position by several powers of 10. The movement of transition with the height of a single roughness element is dependent on airfoil pressure distribution and hence on airfoil shape. In the absence of sufficient data it can be concluded that over certain ranges of airfoil chord Reynolds number, the transition Reynolds number of the boundary layer flow is a function of free stream turbulence, pressure gradient, and surface roughness.

The papers of Fage (42), Tani et al (45) contain some data on roughness effects on transition in the boundary layers of airfoils.

There are other experiments conducted on the effects of roughness elements on flow over airfoils; one of them are those of Loftin (46) in which only the critical Reynolds number of the airfoil for drag rise was determined from wake survey measurements. He concluded that :

1 - The Reynolds number at which one row of spanwise projections causes premature transition is primarily a function of the projection geometry and the Reynolds number based on the height of the projection and the velocity at the tip of the projection, provided the height of the projection is small compared with the boundary layer thickness.

2 - The laminar boundary layer is more sensitive to surface projections than to surface grooves or sanding scratches.

Liepmann (10) has shown that, on a clean aerofoil , transition occurs on a convex surface at the same Reynolds number as on a flat one. Hence it could be postulated that convex curvature does not influence transition due to surface irregularities.

Gregory - Walker (26) discussed the permissible height of an excresence which affect the boundary layer transition on an aerofoil. They proposed a relationship between the Reynolds numbers $\frac{U_\tau k}{\nu}$ and $\frac{U\delta^*}{\nu}$, regardless of whether the excrescences were conical or cylindrical. Here U_τ is the friction velocity defined as $\sqrt{\frac{\tau_0}{\rho}}$. They found an expression for the critical height of the excrescence on an aerofoil surface which was confirmed later by Loftin. Gregory - Walker studied on the vortex structure occurred behind the roughness and showed that the dominant vortex pattern appears to be a horseshoe vortex encircling the front of the excrescence, with twin elements trailing downstream.

Cowled (47) made a survey for the existing state of the know ledge on transition in laminar boundary layers on aerofoil surfaces and extended the single element criteria to multiple arrangements of irregularities.

2.4 CONCLUSIONS

In this chapter, a general literature survey on boundary layer transition from laminar to turbulent flow was made. Since the major interest in this study is transition caused by roughness elements, attention was given to the effect of roughness elements among several other factors affecting transition. However many of the investigations conducted up to date include the effects of other factors and especially of pressure gradient on transition.

Because the phenomena associated with transition is very complicated to be explained theoretically, the present state of knowledge on transition is basically achieved as a result of experimental studies which had started a long time ago.

It was observed that different criteria were used for the definition of the transition point, this caused a difficulty in comparing the results of various experiments. Several different flow observation techniques and various shapes of roughness elements have also been used.

Available data of the previous experiments were investigated and attempts were made to obtain new and complete correlations. These are given in the succeeding chapters.

CHAPTER 3

TRANSITION CHARACTERISTICS OF ROUGHNESS ELEMENTS

3.1 INTRODUCTION

The results of the previous work on forced transition were
analysed under the light of the present status of the knowledge.
Several comments about them were made, and the available data of
the previous experiments were presented by forming new correlations.

3.2 FORCED TRANSITION

Forced transition is defined as artificially caused tran-
sition by using two dimensional or three dimensional roughness
elements. The commonest two dimensional element is a wire attached
on the surface in spanwise direction. Various shapes of three
dimensional elements were used in the past, but generally the elements
of equal width and height were preferred. Due to their ease in
manufacture and availability, spheres are the most familiar three
dimensional roughness elements of all.

When roughness elements occur whether they are naturally pre-
sent or are used as artificial tripping means; two things must be
known about them.

1 - Critical dimensions of the roughness which are effective
on transition

   i) Minimum height of roughness below which no influence on
transition exists.

   ii) Critical height of the roughness element which causes
transition to occur at the element itself.

23

2 - Nature of the flow about the roughness.

The first physical concept about the roughness size was due to Schiller (48) . He suggested that a trip wire induces transition when its Reynolds number reaches a definite value at which vortices were shed from the apex of the element.

Schiller determined the value of this minimum roughness Reynolds number as $R_k = \dfrac{U_\tau k}{V} = 13.$ Goldstein (49) made a similar attempt and defined the minimum height by again a constant roughness Reynolds number of $R_k = \dfrac{U_\tau k}{V} = 7.$

Tani - Hama - Mituisi (45) assumed that the critical height of a trip wire is given by expression $R_k = CONSTANT = \dfrac{U_\tau k}{V}$; this constant was found to be 15. While Fage - Preston (52) proposed that this constant was about 20. Later, it was shown that the expressions of this type, provide rough estimates on roughness effects. Instead of these very simple relationships functional relations between the related variables for every different case should be determined.

The effect of a tripping element of given shape placed on a flat plate in an incompressible fluid stream of constant turbulence and with a zero streamwise pressure gradient was first investigated by many authors, due to its relative simplicity.

Tani - Hama - Mituisi (51), Dryden (53) showed that the transition Reynolds number, $R_{x_T} = \dfrac{U x_T}{V}$, is only a function of $\dfrac{k}{\delta^*_k}$ for a trip wire. The experimental results arrange themselves on the curve shown in Figure 3.1

$$R_{x_{T_c}} = 2.96 \left(\frac{x_k}{k} \right)^2 \left(\frac{k}{\delta^*_k} \right)^2 \tag{3.1}$$

Equation 3.1 is for the critical condition of $x_T = x_k$ ie. transition

occurring at the roughness position.

However in this represantation, there is no evidence of the position of the start and the end of transition. This plot can be taken as showing a mean position in the transition region although the use of a single transition point seems to be meaningless.

Meanwhile Tani - Sato (11) proposed somewhat different correlation for the critical condition as is shown in Figure 3.2

$$(\frac{U \delta_T}{\nu}) \ (\frac{k}{\delta_k}) \ = \ 840 \qquad\qquad (3.2)$$

This relation is applicable except at very low values of $\frac{k}{\delta_k}$. Because $\frac{k}{\delta_k^*}$ is dependent on the roughness location, x_k, and the local free stream velocity at roughness location ,U_k, it is a good measure of local flow conditions. Therefore equation 3.2 is expressed in the following form :

$$(\frac{U \delta_T}{\nu}) \ = \ 2520(\frac{\delta_k^*}{k}) \qquad\qquad (3.3)$$

In their represantation Tani - Sato specified the transition point as the point where the intermittency factor attains the value of 0.5 . It is seen that the local flow conditions at the roughness position are very important on the transition characteristics of laminar boundary layer, providing that the effect of turbulence intensity of the free stream is taken to be negligible.

Tani - Komoda - Komatsu - Iuchi (41) used upright cylindrical three - dimensional elements as tripping devices on a flat plate; they used again the 50% intermittency factor criteria as the point of tran- sition. They proposed the following correlation for the critical con- dition of $x_T = x_k$.

25

$$R_{x_{T_c}} = 2.08 \left(\frac{x_k}{k} \right)^{4/3} \left(\frac{ku_k}{V} \right)^{2/3} \qquad (3.4)$$

which can also be written as

$$R_{x_{T_c}} = 0.997 \left(\frac{x_k}{k} \right) \left(\frac{Uk}{V} \right)_c \qquad (3.5)$$

Göksel (32) studied the effects of spherical roughness elements on transition, by using surface pitot tubes , and determined the start and the end of transition points separately. He proposed the following correlations for the critical condition.

$$\log_{10} R_{kcs} = 0.1882 \log_{10} R_{x_{T_{cs}}} + 1.9609 \qquad (3.6)$$

$$\log_{10} R_{kce} = 0.2314 \log_{10} R_{x_{T_{ce}}} + 1.7579 \qquad (3.7)$$

Where R_{kcs} , R_{kce} are defined as the roughness Reynolds numbers at which start and end of transition would have occurred at the element respectively.

Similarly Yeğen (34), Albayrak (35) and Hall (31) used surface pitot tubes and determined the start and the end of transition seperately; and they reject the correlations based on 50% intermittency factor concept.

However, when the correlation proposed by Tani et al (41) for upright cylindrical elements which is given in equation 3.5 ; was used for the experimental results of Göksel (32), Hall (31), Yeğen (34) and Albayrak (35) for spherical roughness elements, it was found that the results deviate in an acceptable range from the actual ones. This fact is seen in table 3.1. Furthermore Figure 3.3 and Figure 3.4 show the relationship between correlations proposed by Tani et al and Göksel for the start and the end of transition respectively.

Inspection of table 3.1 and of Figures 3.3 and 3.4 results that the using of 50% intermittency factor criteria for transition point determination is not so far from the reality, contrary to the previously accepted fact. Since the criteria defines somewhat a midpoint in the transition region, correlation given by Equation 3.5. which describes a single point in the transition zone is seen to be applicable for the entire zone. Therefore as shown in Figures 3.3 and 3.4, Tani et al's correlation must be valid for the start and the end points of transition.

It can be concluded that the previous rejection of taking of a single point in transition region is not realistic, although determination of the start and the end points of this region is more useful.

It can also be said that the shape of a three dimensional element does not seem to be an effective factor on its transition characteristics; providing that $k < \delta_k$. Instead the height of the element above the surface must be taken into consideration in determining its effect.

As a last study on the transition characteristics of spherical roughness elements, Albayrak (35) proposed correlations for the start and the end of transition which determine the critical condition and which can be applicable for zero, adverse and favourable pressure gradients for a range of $-0.052 \leqslant \lambda_{\theta_k} \leqslant +0.053$.

His correlations are as follows :

$$\log_{10} R_{kcs} = 0.1803 \log_{10} R_{x_{T_{cs}}} + 2.002 \qquad (3.8)$$

$$\log_{10} R_{kce} = 0.1979 \log_{10} R_{x_{T_{ce}}} + 1.9481 \qquad (3.9)$$

which were in a similar form of the correlations proposed by Göksel with modified constants arising from the effect of streamwise pressure gradients.

Since in the given range of $\lambda \Theta_k$ same correlations for the start and the end of transition can be used; it can be concluded that presence of a streamwise pressure gradient does not alter the effect of roughness on boundary layer transition. In other words pressure gradient effect seems to be of secondary importance.

3.3 COMMENTS ON PREVIOUS ANALYSIS

The effect of two and three dimensional roughness elements on transition and on flow structure behind them are different from each other as was stated previously by several investigators.

A separation bubble occurs behind a trip wire and the boundary layer both over the bubble and over the reattachment region is very unstable. Disturbances can therefore build up very quickly and cause transition. Two - dimensional tripping devices can therefore produce turbulent flow over their whole width. Three - dimensional devices only produce a trailing wedge of turbulence behind them; thus they generate trailing vorticity which distorts the boundary layer profile reducing its stability. Thus a two - dimensional element seems to be more dangerous than a three - dimensional one.

Hall - Gibbings (44) concluded that a laminar boundary layer can't be tripped by a three - dimensional element near the limit of stability of the laminar boundary layer while a two - dimensional element can.

Göksel (32) suggested that the transition length behind a spherical roughness element vanishes when roughness position Reynolds number, R_x, is less than 5.85×10^4. Since the known stability limit of the laminar boundary layer was $R_\Theta = 420$ which approximately corresponds to $R_x = 5.85 \times 10^4$; he concluded that a laminar boundary layer can't be tripped at or below its stability limit by a three - dimensional element.

We know that the stability limit of a laminar boundary layer under zero streamwise pressure gradient was modified as $R_{\delta^*} = 520$ (54) which is considerably greater than the previously accepted value.

It will be interesting thus, to evaluate the results of the previous experiments on this new basis.

The experimental results of Hall (31), Göksel (32), Yeğen (34), Albayrak (35) were used in order to show the variation of the critical transition Reynolds number, $R_{x_{T_c}}$, with the critical roughness Reynolds number, R_{k_c} , for the start and the end of transition . As can be seen from Figure 3.5, contary to the previous statement, it seems, it is possible to trip the laminar boundary layer by a spherical roughness element below the modified stability limit; i.e, $R_{\delta^*} = 520$ corresponding to $R_x = 9.14 \times 10^4$.

The difference between the given limits of stability of laminar boundary layer and the physical reason behind the above men - tioned phenomenon can be explained as follows :

It is known that transition of laminar boundary layer to tur- bulent one occurs through a region called as the transition region. For this reason instead of a single transition point use , the start and the end points of the transition region must be determined. Similarly it seems that it is better to define an " instability region " than the use of a single limit for instability. Probably there is an instability region whose upper limit is the known theo- retical limit of instability which corresponds to $R_{x_{i_u}} = 9.14 \times 10^4$. The lower limit of this region can be taken as $R_{x_{i_L}} = 6 \times 10^4$. This agrees well with the experimental results. It seems that when the roughness location Reynolds number, R_{x_k} , is between these two limits; ie, $6 \times 10^4 \leq R_{x_k} \leq 9.14 \times 10^4$; it is possible to trip the boundary layer from laminar to turbulent flow by even a three - dimen-

sional roughness element. The lower limit of the instability region corresponds to the Reynolds number below which all individual os - cillations decay. Throughout the instability region at least some of these oscillations are amplified and at the upper limit the oscillations are strengthened enough to cause transition from laminar to turbulent flow. It can be concluded that; although the tripping of laminar boundary layer by a three - dimensional element seems to be possible below the upper limit of instability region, it seems that below the lower limit of this region it is impossible to trip the boundary layer by a three - dimensional roughness element.

3.4 NEW CORRELATION ATTEMPTS ON TRANSITION CHARACTERISTICS OF ROUGHNESS ELEMENTS.

It is interesting to note that there is no attempt in the available literature to consider the effect of the flow history upstream of the tripping element on the transition of boundary layer from laminar to turbulent flow. As transition is the result of the build up of disturbances in the boundary layer, transition following a roughness element will be the result of the effect of the roughness and the degree of disturbance pre - existing in the boundary layer ahead of the roughness. Since the examination of the experimental results is facilitated by the use of dimensional analysis; it will be convenient to start with it.

It has been shown that (50) in the absence of a streamwise pressure gradient the variation of any property " P " of the flow resulting from the effect of a tripping device of height , k , above the surface can be described in terms of two non - dimensional groups as

$$P = f \left(k, U, \nu, \delta \right)$$ (3.10)

If P is a velocity or length

and

$$P = f \left(\ k, \ \ U, \ \mu \ , \rho \ , \ \delta \ \right) \qquad\qquad (3.11)$$

If P is a force ,

The values of all independent variables of above functional relations are the local values at the position of the trip.

In both cases two non – dimensional groups will describe the variations in " P " . There are two convenient arrangements of the two governing non – dimensional groups :

1 – Two Reynolds numbers, one for the trip and one for the boundary layer.

2 – One Reynolds number of either for trip or for boundary layer, and the ratio of trip height to boundary layer thickness, usually $\dfrac{k}{\delta^*_k}$.

In a zero streamwise pressure gradient case, the boundary layer's Reynolds number at the trip location completely describes the boundary layer's upstream history and therefore its degree of disturbance.

Boundary layer's Reynolds number may be taken as one of the following :

$$R_{\delta^*_k} = \frac{U \, \delta^*_k}{\nu} \quad , \quad R_{\Theta_k} = \frac{U\Theta_k}{\nu} \quad , \quad R_{x_k} = \frac{Ux_k}{\nu}$$

In this study, among the above mentioned parameters, $R_{\delta^*_k} = \dfrac{U\delta^*_k}{\nu}$ is preferred due to :

1 – In a zero pressure gradient case, δ^*_k is directly related to the other boundary layer parameters and to x_k through the Blasius boundary layer relations.

2 – Ease in calculation of $R_{\delta^*_k}$ for the available data of the previous experiments when compared with the calculation required for other non – dimensional groups.

3.4.1 Two - Dimensional Roughness Elements

For a cylindrical trip wire in the absence of a streamwise pressure gradient; the experimental results of Tani et al (51) are available . In order to obtain a new correlation following functional relationship can be proposed as was discussed above.

$$R_{x_{T_c}} = f (R_{\delta^*_k})$$
(3.12)

As is shown in Figure 3.6.a when the critical transition Reynolds number, R_{x_T}, is plotted against the displacement thickness Reynolds number , ^{c} $R_{\delta^*_k}$, for the results of Tani et al (51); a good correlation of the results is observed.

Figure 3.6.b represents the least square line fitted to the used experimental results, whose equation was found as

$$\frac{10^6}{R_{x_{T_c}}} = 0.4381 \frac{10^4}{R_{\delta^*_k}} - 1.5889$$
(3.13)

The scatter of the experimental results from the line given above is within $\mp$ 10%.

As can be seen from these figures, increase in $R_{\delta^*_k}$ will cause an increase in Rx_{T_c} indicating the influence of the upstream flow history on the transition characteristics of the trip wire.

The correlation given in equation 3.13 is better than the one proposed by Tani et al ; since

a) It takes the upstream flow effect which was not considered specifically by Tani et al

b) It is a universal relation; due to the reason that the effect of $\frac{x_k}{k}$ which was seen directly in the correlation of Tani et al ; is confined in $R_{\delta^*_k}$; producing relative simplicity in

32

utilization.

The relative location of the roughness to the upper limit of the instabity region may also be an important factor on the up - stream flow history. In order to show this effect on transition characteristics of the roughness element a parameter, ψ , may be defined as $\psi = R_\delta{}^* - R_\delta{}^*_{i_u}$. The parameter seems to be a convenient one because it ^{k} also gives an indication of the closeness of the element to the instability region.

In order to see the effect of ψ on the critical transition Reynolds number, $R_{x_{T_c}}$, Figure 3.7.a and Figure 3.7.b were formed by using the ^{T_c} experimental results of Tani et al for a trip wire again.

As can be seen from these figures there is a direct relation-ship between $R_{x_{T_c}}$ and ψ ; and it is obtained as

$$\frac{10^6}{R_{x_{T_c}}} = 0.1825 \frac{10^4}{\psi} - 0.4384 \qquad (3.14)$$

by the least square line fitting method.

The scatter of the experimental results from the line whose equation is given above is within $\mp$ 6%.

The experimental results of Tani et al used, don't specify the start and the end points of transition. The correlations given in equations 3.13 and 3.14 can be applicable for the transition point, defined by Tani et al. Eqns., 3.13 and 3.14 indicate the importance of the upstream flow history on transition characteristics of a trip wire.

33

3.4.2 Three Dimensional Roughness Elements

It was known that three - dimensional roughness elements exhibit the characteristic of abrupt transition motion. As was discussed previously, their effect was usually represented by the functional relationship between R_{x_T} and R_k .

Since there is still a possibility of representing the experimental data by considering the local flow conditions at the roughness position, it will be worthwhile to see whether there is a functional relationship between $R_{x_{Tc}}$ and $\dfrac{k}{\delta^*_k}$ or not.

It will also be possible to compare the effects of two - dimensional and three - dimensional elements on a common base with the use of these parameters; namely $R_{x_{Tc}}$ and $\dfrac{k}{\delta^*_k}$

In order to determine the functional relationship between $R_{x_{Tc}}$ and $\dfrac{k}{\delta^*_k}$; the available data sets of Hall (31) Göksel (32) , Yeğen (34), Albayrak (35) were used for a spherical roughness element under zero streamwise pressure gradient.

As can be seen from Figure 3.8.a a good correlation of these data which showed that there exists a functional relationship between $R_{x_{Tc}}$ and $\dfrac{k}{\delta^*_k}$, was obtained.

From Figure 3.8.a it is seen that, as $\dfrac{k}{\delta^*_k}$ increases the critical transition Reynolds numbers for the start and the end of transition decrease; and then approach to each other. Finally, the curves representing the start and the end of transition coincide when $R_{x_{Tc}} = R_{x_k} = 6 \times 10^4$ which is the lower limit of the instability region.

The exact form of the functional relationship between $R_{x_{Tc}}$ and $\dfrac{k}{\delta^{*}_{k}}$ was found by the use of a log - log plot of $R_{x_{Tc}}$ versus $\dfrac{k}{\delta^{*}_{k}}$ as was shown in Figure 3.8.b. The following relationships were found by the least square line fitting method.

$$\log_{10} R_{x_{Tcs}} = -3.1228 \; \log_{10} \left(\frac{k}{\delta^{*}_{k}} \right) + 5.5348 \tag{3.15}$$

$$\log_{10} R_{x_{Tce}} = -3.3378 \; \log_{10} \left(\frac{k}{\delta^{*}_{k}} \right) + 5.6638 \tag{3.16}$$

The scatter of experimental results from the relations represented by equations 3.15, 3.16 was found to $\mp 10\%$ and $\mp 5\%$ respectively.

The plots of $R_{x_{Tc}}$ versus $\dfrac{k}{\delta^{*}_{k}}$ seem to be better than the previously used $R_{x_{Tc}}$ versus $R_{k_{c}}$ plots, by Göksel (32) Yeğen (34) and Albayrak (35). In order to represent the transition characteristics of three - dimensional roughness elements; $\dfrac{k}{\delta^{*}_{k}}$ is used. $\dfrac{k}{\delta^{*}_{k}}$ parameter is preferred to R_{k} because it indicates the effect of local flow conditions at the roughness position upon the transition directly. In order to see the difference of the effect of two and three dimensional roughness elements on boundary layer transition Figure 3.9 was formed. This figure shows the plot of $R_{x_{Tc}}$ versus $\dfrac{k}{\delta^{*}_{k}}$ for trip wire and spherical roughness results.

It seems that for the same local flow conditions the movement of the transition towards the roughness element is more slow for a sphere than for a trip wire.

As is seen from Figure 3.10.a and Figure 3.10.b for a spherical roughness the critical transition Reynolds numbers for the start and the end of transition can be represented as a function of $R_{\delta^{*}_{k}}$

Figures 3.11.a and 3.11.b are log - log plots of Figures 3.10.a - 3.10.b. The following relationships can be obtained by fitting lines to the experimental data shown in Figure 3.11.a and Figure 3.11.b.

$$\log_{10} R_{x_{Tcs}} = 1.9415 \quad \log_{10} R_{\delta^*_k} - 0.314 \qquad (3.17)$$

$$\log_{10} R_{x_{Tce}} = 2.0109 \quad \log_{10} R_{\delta^*_k} - 0.500 \qquad (3.18)$$

The scatter of the experimental results from given relations was found to be $\overset{-}{+}$ 6% and $\overset{-}{+}$ 3% for the start and the end of transition respectively. These relationships indicate the influence of upstream flow history upon the transition characteristics of spherical roughness elements.

As can be noticed from Figures 3.11a,3.11b,it is impossible to trip the laminar boundary layer by a spherical roughness element when $R_{\delta^*_k} < 420$. This fact was discussed in section 3.3.

Figure 3.12.a and Figure 3.12.b were plotted to see the relationship between the critical transition Reynolds numbers and ψ for the start and the end of transition respectively.

From these figures the effect of the closeness of the roughness element to the instability region on the transition characteristics of the element can be seen. As is also seen from figures 3.12.a and 3.12.b; when $\psi = 0$, $R_{x_{Tcs}} = 0.09 \times 10^6$ and $R_{x_{Tce}} = 0.1 \times 10^6$.

This means that at the upper limit of the instability region, critical transition length is given as $\left(R_{x_{Tce}} - R_{x_{Tcs}} \right) = 1 \times 10^4$.

Figure 3.13 shows the variation of critical transition Reynolds numbers with $\dfrac{k}{\delta^*_k}$ for the start and the end of transition behind a spherical roughness element for zero and adverse pressure gradients. It is seen that the relationships proposed previously between $R_{x_{Tc}}$ and $\dfrac{k}{\delta^*_k}$ for a zero pressure gradient case can also be applicable for a range of λ_{θ_k} of $-0.052 \leqslant \lambda_{\theta_k} \leqslant -0.02$.

Thus it can be concluded that the presence of an adverse streamwise pressure gradient between the λ_{θ_k} values mentioned above does not

change the dependency of the transition characteristics of the roughness element upon the local flow conditions at the roughness location.

Figures 3.14.a and 3.14.b indicate the variation of critical transition Reynolds numbers with $R_{\delta^*_k}$ in the presence of an adverse streamwise pressure gradient for a spherical roughness element, for the start and the end of transition respectively. Inspection of these figures indicates that the relationships between $R_{x_{T_c}}$ and $R_{\delta^*_k}$ given in equations 3.17 and 3.18 for $\lambda_{\theta_k} = 0$ case can also be applicable for $\lambda_{\theta_k} \geq -0.02$. As λ_{θ_k} assumes values less then -0.02 such as -0.04 and -0.052 experimental results show great deviation from the relationship expressed by equations 3.17 and 3.18.

Thus it can be concluded that for weak adverse pressure gradients the same relationships between R_{x_T} and $R_{\delta^*_k}$ as was given for zero pressure gradient case can be used, with an acceptable error. This may due to the reason that : For stronger pressure gradients the effect of λ_{θ_k} must also be taken into account along with the effect of $R_{\delta^*_k}$.

3.5 CONCLUSIONS

1 - Contrary to the fact of using a single limit of stability ; an instability region concept was introduced. The upper limit of this region corresponds to the theoretical limit of stability i.e. $R_{\delta^*_{i_u}} = 520$; and the lower limit was defined as $R_{\delta^*_{i_L}} = 420$. In this region it is possible to trip a laminar boundary layer with a three - dimensional roughness element, but below the lower the limit of this region tripping seems to be impossible.

2 - It was shown that correlations based on 50% intermittency factor definition for transition point determination give results similar to the ones obtained with the use of surface pitot tubes. This was concluded as; the determination way of the transition region does not influence the transition characteristics of the boundary layer.

3 - It seems that shape of a three - dimensional element is an unimportant factor to be considered providing that , $k < \delta_k$.

4 - It was shown that upstream flow history has a strong effect on transition characteristics of roughness elements. Correlations considering this effect were proposed for trip wires and spherical roughness elements in the form of relationships between $R_{x_{T_c}}$ and $R_{\delta^*_k}$.

5 - The result of previous experiments of Hall (31) , Göksel (32), Albayrak (35), Yeğen (34) were represented by deriving a new form of correlation indicating the importance of local flow conditions at the roughness position. These correlations in the form of relation ships between $R_{x_{T_c}}$ and $\dfrac{k}{\delta^*_k}$ were given in equations 3.15 and 3.16.

6 - The variation of the critical transition Reynolds numbers for the start and the end of transition with parameter,

$$\psi = R_{\delta^*_k} - R_{\delta^*_{iu}}$$ were investigated, for trip wire and spherical roughness element.

7 - The correlations proposed for zero streamwise pressure gradient behind a spherical roughness element between $R_{x_{T_c}}$ and $\dfrac{k}{\delta^*_k}$ were found to be applicable for adverse pressure gradients for the range of λ_{θ_k} of $- 0.052 \leqslant \lambda_{\theta_k} \leqslant - 0.02$.

8 - The correlations between $R_{x_{T_c}}$ and $R_{\delta^*_k}$ proposed for zero pressure gradient case were found to be applicable for only weak adverse pressure gradients.

CHAPTER 4

EFFECTS OF SURFACE ROUGHNESS UPON BOUNDARY LAYER GROWTH

4.1 INTRODUCTION

In this chapter, attention will be given mainly on the recovery length of turbulent boundary layer obtained by tripping a laminar boundary layer with a roughness element; and wake development behind an isolated spherical roughness element placed on a flat plate under zero streamwise pressure gradient.

4.2 BOUNDARY LAYER DEVELOPMENT BEHIND AN ISOLATED ROUGHNESS ELEMENT

Roughness elements have two basic effects on the boundary layer development :

1 - They induce additional disturbances in the boundary layer which may cause transition from laminar to turbulent flow.

2 - Increase in the momentum thickness of the boundary layer occur due to the drag of the roughness elements.

The perturbations induced by roughness elements either decay rapidly or continue to persist even in the developed turbulent boun - dary layer behind the element. The chordwise length measured from the leading edge, of the flat plate at which all of the observable perturbations caused by the roughness element were decayed was defined as the " recovery length " of the turbulent boundary layer by Göksel (32). Thus it is appropriate to consider the boundary layer flow behind the roughness element as composed of two basic regions, namely :

1 - Recovery region in which boundary layer recovers from the roughness - induced perturbations.

39

2 - Perturbation - free region where the boundary layer grows turbulently free from the roughness - induced perturbations.

The disturbances decay asymptotically in the streamwise direction by creating irregularities in the velocity profiles, and also an irregular variation of the integral quantities of the boundary layer is observed in the recovery region. The end of the recovery region is determined as the point where the integral properties of the boundary layer satisfy the following relationship.

$$R_{\delta^*} = A \, R_{\theta} + B \tag{4.1}$$
or
$$H = A + \frac{B}{R_{\theta}}$$

where $H = \dfrac{R_{\delta^*}}{R_{\theta}}$, $\qquad A = 1.35$ and

$B = 83.4 \ (32),$ $\qquad\qquad 103.4 \ (35)$

Through the recovery region, relationship between R_{δ^*} and R_{θ} is irregular showing that the perturbations of the roughness element have not already decayed. After the recovery region, turbulent boundary layer develops regularly. (32) (35).

4.2.1 Recovery Length of the Turbulent Boundary Layer Behind Roughness Elements

Göksel (32) has proposed a correlation for the recovery length of boundary layer behind isolated spherical roughness elements in the following form

$$\frac{X_R - X_k}{k} = f \left(R_k \, \frac{k}{\delta^*_k} \right) \tag{4.2}$$

The exact form of this functional relationship was found later by Göksel (50) as

$$\frac{X_R - X_k}{k} = -1.2 \times 10^{-3} \log R_k \frac{k}{\delta^*_k} + 32 \qquad (4.3)$$

The above equation was found to be applicable for two and three dimensional roughness elements under zero, adverse and favourable pressure gradients provided that $R_k \frac{k}{\delta^*_k} \geqslant 8 \times 10^3$ for spheres and $R_k \frac{k}{\delta^*_k} \geqslant 2 \times 10^3$ for trip wires. Göksel (50) also has found that there is a limiting value of $R_k \frac{k}{\delta^*_k}$ below which a spherical roughness element can't trip a laminar boundary layer; this limit was found to be $R_k \frac{k}{\delta^*_k} = 1 \times 10^3$.

He has also concluded that recovery length of turbulent boundary layer behind a cylindrical trip wire is less than that of behind a sphere for the same $R_k \frac{k}{\delta^*_k}$ value. This indicates that perturbation - free fully turbulent region is closer to the trip wire when it is compared with a spherical roughness element.

Similarly, Yeğen (34) generalized the approach of Göksel for correlating the recovery length of turbulent boundary layer behind an isolated sphere. He obtained the following relationship :

$$\frac{X_R - X_k}{k} = 1.04 \times 10^5 \left(R_k \frac{k}{\delta^*_k} - 595 \right)^{-1} + 20 \qquad (4.4)$$

He also noticed that presence of streamwise pressure gradient does not alter the above relationship. This shows the independency of the recovery length on pressure gradient.

Albayrak (35) proposed a different way for correlating the recovery length behind an isolated spherical roughness element, under variable pressure gradients. He first indicated that the recovery length is decreased with an increase in the roughness Reynolds number, R_k, upto a critical value of it. Above this limiting value, increase in R_k will cause also an increase in the recovery length.

He observed that the flow conditions at the roughness element location
and the roughness height compared with the local boundary layer
thickness determine the recovery length behind the element. He
defined a correlation parameter Δ , as $\Delta = \dfrac{R_k - R_{k \dot cs}}{R_{kce} - R_{kcs}}$ to
incorporate the effect of the transition characteristics of the
roughness element on the recovery length.
He obatined the following correlation :

$$\frac{X_R - X_k}{k} = (\Delta - 9.5) + \frac{441}{\Delta} \qquad (4.5)$$

He found that within a particular range of $\lambda \theta_k$ of $- 0.052 \leqslant \lambda \theta_k \leqslant$
$+ 0.053$,there is no parametric effect of streamwise pressure
gradient on the recovery length of turbulent boundary layer.
Albayrak also concluded that $\Delta = 21$ is the critical value above which reco-
very; length increases with an increase in Δ and observable minimum reco-
very length corresponding to this limit is $\dfrac{X_R - X_k}{k} = 32.5$.

Under the light of the above mentioned studies on the recovery
length; following results can be derived:

1 - The recovery length seems to be independent of streamwise
pressure gradient.

2 - Since critical transition Reynolds numbers $R_{x_{Tc}}$ are
functions of $\dfrac{k}{\delta^*_k}$, the non - dimensional recovery length
$\dfrac{X_R - X_k}{k}$ seems to be a function of $R_k \dfrac{k}{\delta^*_k}$ only.

3 - The main factors influencing the recovery length of turbu-
lent boundary layer seem to be

i)   type and dimensions of the roughness element.

ii)   transition characteristics of the roughness element.

iii)   local flow conditions at the roughness position .

4 - Since determination of recovery lengths behind a roughness element is not very accurate, experimentally found recovery lengths show a large scatter from the proposed correlations.

4.2.2 New Attempts for Correlating Recovery Length of Turbulent Boundary Layer

Since $R_{\delta^*_k}$ represents the upstream flow history effect in the absence of a streamwise pressure gradient; it will be worthwhile to see its effect which has not been done by other investigators on the recovery length.

The recovery length of a turbulent boundary layer behind a roughness element can be represented in a functional relationship as follows

$$X_R = f (X_k , U , \nu , k, \lambda_{\Theta_k}) \tag{4.6}$$

The above relation may also be expressed as

$$\frac{X_R}{X_k} = f (R_{X_k} , R_k , \lambda_{\Theta_k}) \tag{4.7}$$

where $R_{X_k} = \dfrac{U x_k}{\nu}$ and $R_k = \dfrac{Uk}{\nu}$

In reference (50) it was shown that

$$R_{\delta^*_k} = f (R_{X_k} , R_k, \lambda_{\Theta_k}) \tag{4.8}$$

and for $\lambda_{\Theta_k} = 0$

$$R_{\delta^*_k} = f (R_{X_k} , R_k)$$

thus

$$\frac{X_R}{X_k} = f (R_{\delta^*_k}) \tag{4.9}$$

43

Figure 4.1 shows the variation of $\dfrac{X_R}{X_k}$ with $R_{\delta^*_k}$ behind a spherical roughness element under zero pressure gradient. As is seen from this figure there is a direct relationship between $\dfrac{X_R}{X_k}$ $R_{\delta^*_k}$; as $R_{\delta^*_k}$ increases $\dfrac{X_R}{X_k}$ decreases.

Figure 4.2 shows the same plot of $\dfrac{X_R}{X_k}$ versus $R_{\delta^*_k}$ by taking the variable pressure gradient data into account. Since λ_{θ_k} does not have a parametric effect on the recovery length, the functional relationship given above as equation 4.9 can be used in $-0.040 \leqslant \lambda_{\theta_k} \leqslant +0.053$ range. As can be seen from Figure 4.2; when $R_{\delta^*_k}$ increases , $\dfrac{X_R}{X_k}$ decreases upto $R_{\delta^*_k}$ becomes 1200. When this limit is exceeded, further increase in $R_{\delta^*_k}$ does not affect $\dfrac{X_R}{X_k}$. Thus minimum value of $\dfrac{X_R}{X_k}$ seems to be about 1.15. It is also interesting to note that when $R_{\delta^*_k}$ tends to $R_{\delta^*_{iL}}$ =420; $\dfrac{X_R}{X_k}$ approaches to ∞ indicating the impossibility of tripping the laminar boundary layer below the lower limit of the instability region. If the errors in determination of the recovery length are taken into account, the scatter of the experimental results from the drawn line in figure 4.2 is meaningful.

The plots of $\dfrac{X_R}{X_k}$ versus $R_{\delta^*_k}$ are better than the ones of $\dfrac{X_R - X_k}{k}$ versus R_k $\dfrac{k}{\delta^*_k}$, since :

1 - $\dfrac{X_R}{X_k}$ is simpler than $\dfrac{X_R - X_k}{k}$ and provides direct information about the relative position of the fully turbulent region behind the roughness element .

2 - $R_{\delta^*_k}$ represents the flow history effect

The recovery length of a turbulent boundary layer can be non - dimensionalized in a somewhat different way than it is presented in Reference (32) . The distance behind the element in which perturbations were decayed can be given in a Reynolds number defined as

44

$$R_{x_L} = \frac{U(X_R - X_k)}{\nu} \quad ; \quad X_L = X_R - X_k$$

It may be given as

$$R_{x_L} = f\left(R_k \; \frac{k}{\delta^*_k} \right) \tag{4.10}$$

Figures 4.3, 4.4, 4.5 were formed to see the variation of R_{x_L} with $R_k \; \frac{k}{\delta^*_k}$, for spherical roughness elements and trip wires. As can be seen from these figures the limiting values of $R_k \; \frac{k}{\delta^*_k}$ are 8×10^3 and 2×10^3 for spheres and trip wires respectively. Upto these limits, increase in $R_k \; \frac{k}{\delta^*_k}$ causes a decrease in R_{x_L}.

Decrease in R_{x_L} indicates faster decay of perturbation behind roughness elements. It seems also that the minimum R_{x_L} values are about 0.45×10^5 and 0.50×10^5 for trip wires and spherical roughness elements respectively. Inspection of Figure 4.3 and Figure 4.5 indicates that the relationship between R_{x_L} and $R_k \; \frac{k}{\delta^*_k}$ is independent of the pressure gradient for the range of λ_{θ_k} of $-0.052 \leqslant \lambda_{\theta_k} \leqslant +0.045$.

Since the local flow conditions at the roughness element determine the recovery length behind the element (50), the following functional relationship can be proposed :

$$R_{x_L} = \frac{U(X_R - X_k)}{\nu} = f\left(\frac{k}{\delta^*_k} \right) \tag{4.11}$$

Figure 4.6 shows the variation of R_{x_L} with $\frac{k}{\delta^*_k}$ behind a spherical roughness element without a pressure gradient while in Figure 4.7 it is seen that λ_{θ_k} does not have a significant effect on R_{x_L}.

As can be seen from these figures $\frac{k}{\delta^*_k}$ may be taken as a correlation parameter for the recovery length. Figure 4.7 shows that R_{x_L} decreases with an increase in $\frac{k}{\delta^*_k}$. It is seen that when $\frac{k}{\delta^*_k} = 1$ R_{x_L} tends to infinity and when $\frac{k}{\delta^*_k} = 3.5$ R_{x_L}

takes its minimum value for λ_{θ_k} range of $-0.04 \leq \lambda_{\theta_k} \leq +0.045$. The minimum value of R_{x_L} indicates that fully turbulent region can't start at the roughness element. Thus $\dfrac{k}{\delta^*_k} = 3.5$ seems to represent the critical roughness height which causes ; MRL, minimum recovery distance behind the element. Similarly tolerable roughness size to trip a laminar boundary layer is seen to be given with the condition $\dfrac{k}{\delta^*_k} = 1$ at which R_{x_L} tends to infinity.

Therefore following relationships were proposed.

$$\left(\frac{k}{\delta^*_k} \right)_{MRL} = 3.5 \tag{4.12}$$

$$\left(\frac{k}{\delta^*_k} \right)_{tolerable} = 1.0 \tag{4.13}$$

These relationships can also be given as

$$k_{MRL} = 6.02 \; \frac{x_k}{(R_{x_k})^{1/2}} \tag{4.14}$$

$$k_{tolerable} = 1.72 \; \frac{x_k}{(R_{x_k})^{1/2}} \tag{4.15}$$

Schiller (48) had defined the critical roughness size for a trip wire as

$$R_k = \frac{u_k \, k}{\nu} = 170 \tag{4.16}$$

Equation 4.16 may also be written as

$$k_{critical} = 22.6 \; \frac{x_k}{(R_{x_k})^{3/4}} \tag{4.17}$$

Equation 4.17 is similar to the form proposed for a spherical roughness element given in equation 4.14.

Thus, similar to the criteria developed by Schiller for trip wires, roughness height giving minimum recovery length, and the

tolerable roughness height, for a spherical roughness element in the $\lambda\theta_k$ range of $-0.04 \leqslant \lambda\theta_k \leqslant +0.045$ can now be determined from equations 4.14 and 4.15.

4.3 WAKE DEVELOPMENT

Gregory - Walker (26) suggested that the angle of spread of the wake behind an isolated cylindrical element increases downstream of the element.

Göksel (32) observed the same wake growth pattern behind an isolated spherical roughness element as Gregory - Walker did previously. He has shown that only if the roughness element is large or the flow velocity is high enough, straight edges of the wakes can be seen with a constant spread angle; otherwise spread angle of the wake increases downstream of the element and edges are curved.

Göksel defined the turbulent wake width Reynolds number as $R_{w_T} = \dfrac{U w_T}{\nu}$ where w_T is the width of the turbulent wake. He proposed that growth of R_{w_T} behind an isolated sphere can be given as a function of momentum thickness Reynolds number behind the center - line of the roughness element, $R_{\theta_{c_L}} = \dfrac{U\theta}{\nu}$. As can be seen from Figure 4.8; R_{w_T} seems to be a function of R_θ and $\dfrac{x_k}{k}$ for $R_{\theta_{c_L}} < 2000$, and only of $R_{\theta_{c_L}}$ for $R_{\theta_{c_L}} > 2000$. Unfortunately, Göksel was not able to obtain a sound correlation due to the great scatter of experimental data. He also correlated the transitional wake growth Reynolds number $R_{w_T} = \dfrac{U w_t}{\nu}$ with $(R_x - R_{x_k})^{1/2}$ and concluded that R_{w_t} seems to be a function of $(Rx - Rx_k)$ and R_k. The transitional wake width was seen to increase with R_k for a given $(R_x - R_{x_k})$ for $R_{w_t} < 1.5 \times 10^5$; and the dependency of R_{w_t} on R_k was seen to vanish for values of $R_{w_t} > 1.5 \times 10^5$.

The dimensionless starting distance of the turbulent wake $\dfrac{x_{w_T} - x_k}{k}$ was found to decrease with increasing roughness Reynolds number, R_k, Göksel has also shown that this distance is dependent on x_k. Thus

47

a single exact form of the relationship to determine $\dfrac{X_{W_T} - x_k}{k}$ couldn't be determined.

4.3.1 Correlations of the Wake Development Behind an Isolated Spherical Roughness Element Under Zero Streamwise Pressure Gradient

The approach of Göksel for cerrelating the wake development behind an isolated spherical element was the only one in the available literature. As was suggested by Göksel (32) the turbulent wake width Reynolds number, R_{W_T}, is strongly dependent on the variation of the momentum thickness Reynolds number, $R\Theta_{\zeta}$, behind the centerline of the element.

A functional relationship as

$$R_{W_T} = f (R\Theta_{\zeta}) \tag{4.18}$$

may be taken .

However, it is known that

$$R\Theta = f (R_x, R_{x_k}, R_k, \lambda\Theta_k) \tag{4.19}$$

and for $\lambda\Theta_k = 0$

$$R\Theta = f (R_x, R_{x_k}, R_k) \tag{4.20}$$

The functional relationship given by equation 4.20 shows that the flow conditions over the solid boundary are taken into account if $R\Theta$ is used as a dependent variable.

In order to find the exact form of the above relationship between R_{W_T} and $R\Theta$; R_{W_T} is plotted against $R\Theta_{\zeta}$; and this is shown in Figure 4.9. As can be seen from this figure experimental results fall in a band indicating the dependency of R_{W_T} on $R\Theta_{\zeta}$. Turbulent wake width increases as $R\Theta_{\zeta}$ increases. It's seen that the greatest deviation from the mean of the experimental results belongs to the

an isolated spherical roughness element. There seems to be no dependency of $\left(R_{x_{W_T}} - R_{x_k} \right)$ on $\dfrac{X_k}{k}$ for the proposed relationship.

As can be seen from Figure 4.12 when $R_k \dfrac{k}{\delta^*_k}$ increases, turbulent wake moves towards the roughness element, but there is always a finite distance behind the element and the apex of the turbulent wedge.

If the straight portion of the curve shown in Figure 4.12 is extrapolated by the dashed lines, the hypothetical condition of $R_{x_{W_T}} = R_{x_k}$ is obtained when $R_k \dfrac{k}{\delta^*_k} = 2 \times 10^3$. This finding is in accordance with Göksel's (32) results. In other words for both two and three dimensional roughness elements short transition and recovery lengths can be obtained for $R_k \dfrac{k}{\delta^*_k} \geqslant 2 \times 10^3$.

Also from Figure 4.12 for the covered range of experimental results the minimum possible distance behind the element to the apex of the turbulent wake is seen to be $\left(R_{x_{W_T}} - R_{x_k} \right) = 0.25 \times 10^5$. Furthermore increase in $R_k \dfrac{k}{\delta^*_k}$ does not change the distance behind the element to the apex of the turbulent wake providing that $R_k \dfrac{k}{\delta^*_k} \geqslant 9 \times 10^3$.

In order to obtain a unique relationship between the previously used parameter by Göksel (32), $\dfrac{X_{W_T} - X_k}{k}$ and R_k, the effect of local flow conditions at the roughness position must again be considered. This can be done by plotting $\dfrac{X_{W_T} - X_k}{k}$ against $R_k \dfrac{k}{\delta^*_k}$. As can be seen from Figure 4.13, the minimum possible value for $\dfrac{X_{W_T} - X_k}{k}$ is found to be 10, and the limiting value for $R_k \dfrac{k}{\delta^*_k}$ is seen to be 9×10^3 as was previously observed.

As is shown in Figure 4.14 the relationship between $\dfrac{X_{W_T} - X_k}{k}$ and $R_k \dfrac{k}{\delta^*_k}$ is plotted on a log - log scale and a least square line whose equation is given below may be fitted to the experimental results.

$$\log_{10} \dfrac{X_{W_T} - X_k}{k} = 1.3846 \ \log_{10} \left(R_k \dfrac{k}{\delta^*_k} \right) + 6.613 \qquad (4.23)$$

case of $k = 1/32$ ", $x_k = 24$ ". In order to eliminate this deviation and to narrow this band R_{W_T} versus $(R\Theta_{C_L} - R\Theta_k)$ plot was formed as shown in Figure 4.10. The choice of this new parameter, namely $(R\Theta_{C_L} - R\Theta_k)$ is reasonable; since the momentum thickness at the roughness location represents the upstream flow effects and strongly influence the downstream momentum thickness development.

As is seen from Figure 4.10 the experimental results fall in a smaller band than they were in the previous plot. As is seen in Figure 4.11 when Figure 4.10 is plotted on a log - log scale, a least square line now can be fitted to the experimental results, giving the following relationship between R_{W_T} and $(R\Theta_{C_L} - R\Theta_k)$

$$\log_{10} R_{W_T} = 1.2414 \ \log_{10} (R\Theta_{C_L} - R\Theta_k) + 1.2449 \qquad (4.21)$$

As was shown in Reference 32, the use of non - dimensional turbulent wake starting distance, $\dfrac{X_{W_T} - X_k}{k}$ showed dependency on $\dfrac{x_k}{k}$ which makes impossible to obtain a unique correlation for

$\dfrac{X_{W_T} - X_k}{k}$. Thus a somewhat different non - dimensional group can be determined for correlation purposes. For this reason, Reynolds number for the turbulent wake starting distance was defined as $R_{X_{W_T}} = \dfrac{U x_{W_T}}{V}$; and the distance behind the roughness element upto the turbulent wake starting position may be given as the difference $(R_{X_{W_T}} - R_{X_k})$. In order to obtain a sound correlation for $(R_{X_{W_T}} - R_{X_k})$, because as was pointed out earlier R_k and $\dfrac{k}{\delta^*_k}$ is a good measure of the perturbations fed into the flow by the roughness element; the following functional relationship may be proposed :

$$R_{X_{W_T}} - R_{X_k} = f \left(R_k \ \dfrac{k}{\delta^*_k} \right) \qquad (4.22)$$

As can be seen from Figure 4.12, there exists a relationship between, $(R_{X_{W_T}} - R_{X_k})$ and $R_k \ \dfrac{k}{\delta^*_k}$ for the turbulent wake observed behind

49

Since for a zero pressure gradient case $R_{\delta^*_k}$ represents the upstream flow effects; it will be interesting to see the variation of $R_{x_{W_T}}$ with $R_{\delta^*_k}$. As is seen in Figure 4.15 as $R_{\delta^*_k}$ increases $R_{x_{W_T}}$ increases also. When a least square line is fitted to the experimental results shown in Figure 4.16, the following relationship is obtained.

$$\log_{10} R_{x_{W_T}} = 1.6906 \ \log_{10} R_{\delta^*_k} + 0.6137 \qquad (4.24)$$

Thus, it is also possible to find the distance to the apex of the turbulent wedge from the leading edge of the   plate.

4.4 CONCLUSIONS

1 – The recovery length behind an isolated spherical element can be represented in a form which shows the upstream flow effects in variable streamwise pressure gradients $- 0.04 \leqslant \lambda_{\theta_k} \leqslant + 0.053$

2– It was found that when $R_{\delta^*_k}$ attains the value of 1200; further increase in $R_{\delta^*_k}$ does not change $\dfrac{X_R}{X_k}$. Minimum value of $\dfrac{X_R}{X_k}$ was found to be 1.15.

3– The distance behind the roughness element to the fully tur- bulent region was defined as $R_{x_L} = \dfrac{U(X_R - X_k)}{v}$. Minimum R_{x_L} values were determined for spheres and trip wires using the plots of R_{x_L} versus $R_k \dfrac{k}{\delta^*_k}$.

4– It was found that the relationship between R_{x_L} and $R_k \dfrac{k}{\delta^*_k}$ is independent of the pressure gradient for the range of λ_{θ_k} of $- 0.052 \leqslant \lambda_{\theta_k} \leqslant + 0.045$.

5– A correlation between R_{x_L} and $\dfrac{k}{\delta^*_k}$ was proposed for λ_{θ_k} range of $- 0.04 \leqslant \lambda_{\theta_k} \leqslant + 0.045$. Two relationships which define the critical dimensions of the spherical roughness elements were

proposed. These relationships were given in equations 4.14 and 4.15.

6- Turbulent wake growth behind a spherical roughness element was investigated. A correlation between R_{W_T} and ($R\Theta_{c} - R\Theta_{k}$) was proposed. This correlation was given in equation 4.21.

7- It was found that $R_{X_{W_T}} = R_{X_k}$ when $R_k \dfrac{k}{\delta^{*}_{k}} = 2 \times 10^{3}$

8- It was found that turbulent wake starts at a fixed distance behind the spherical roughness element. This minimum possible distance can be given either as $R_{X_{W_T}} - R_{X_k} = 0.25 \times 10^{5}$; or as

$$\dfrac{X_{W_T} - X_k}{k} = 10.$$

9- Correlation given in equation 4.24 also describes the starting distance of the turbulent wake, considering the upstream flow effects.

TRANSITION CHARACTERISTICS, AND BOUNDARY LAYER DEVELOPMENT BEHIND A ROW
OF SPHERICAL ROUGHNESS ELEMENTS ON A FLAT PLATE UNDER ZERO STREAMWISE
PRESSURE GRADIENT

5.1 INTRODUCTION

In practice, not only single isolated roughness elements but
also multiple roughness elements occur on real surfaces such as wings,
blades of turbomachinery e.t.c. It is thus vital to investigate the
effects of multiple roughness elements on boundary layer transition
and on the growth of boundary layer behind the elements.

The results of previous investigations about the effects of
row of spherical roughness elements were reviewed. New and different
representations were formed for row of spherical roughness elements
as was done in Chapters 3 and 4 for an isolated element.

The study is confined to flow with a zero streamwise pressure
gradient due to the reason that available data in the literature
belongs to the zero pressure gradient case.

5.2 BRIEF REVIEW OF THE PREVIOUS WORK ON TRANSITION CHARACTERISTICS
OF A SPANWISE ROW OF SPHERICAL ROUGHNESS ELEMENTS

As was shown in Reference 32 , the position of transition ,
x_T , behind the centerline of a row of roughness elements under zero
streamwise pressure gradient may be given as

$$x_T = f (U, \nu , k , x_k , S , n)$$

or

$$R_{x_T} = f (R_k, R_{x_k} , \frac{S}{k} , n) \tag{5.1}$$

For a fixed $\frac{S}{k}$ and n above functional relationship takes a similar

form as for the single element case.

Göksel (32) has observed that the relationship between $\frac{1}{R_k}$ and $\frac{x_T}{x_k}$ for a spanwise row of spanwise row of spherical roughness elements is similar to that of an isolated element. He has also noticed that the variation of $R_{x_{Tc}}$ with R_{k_c} for the start and the end of transition shows the same behaviour as was seen for a single element case. Contrary to the single element case, he noticed that it is possible to trip the laminar boundary layer at the position corresponding to the lower limit of the instability region with a spanwise row of spherical elements. This is shown in Figure 5.1. He has also studied the effect of spanwise spacing of the elements in the row on the critical roughness Reynolds numbers for the start and the end of transition. He concluded that the ratio of $\frac{R_{k_c row}}{R_{k_c single}}$ is reduced for $\frac{S}{k} < 2$, and for $\frac{S}{k} > 2$ the ratio of $\frac{R_{k_c row}}{R_{k_c single}}$ attains approximately the value of unity. This is shown in Figure 5.2. Carmichael (39) suggested a $\frac{S}{k}$ value of 4; and Tani et al (41) suggested a value of 6 for cylindrical elements for the same criterion.

The second effective parameter, n, number of the elements in the row, was also considered in his study. He showed that the ratio of $\frac{R_{k_c row}}{R_{k_c single}}$ decreases with increasing n for a constant $\frac{S}{k}$, upto n = 9. When n $\geq$ 9 , $\frac{R_{k_c row}}{R_{k_c single}}$ increases and at the condition of n = 11, this ratio takes the same value for the start and the end of transition. This can be seen in Figure 5.3.

Under the light of these observations following results can be deduced.

1- The effect of a row of spherical roughness elements upon boundary layer transition is similar to that of an isolated sphere. Since the correlations between $R_{x_{To}}$ and R_{k_c} ; and those between

54

$\dfrac{1}{R_k}$ and $\dfrac{x_T}{x_k}$ were almost identical for the row of spherical elements and an isolated element case.

2- It seems that it is possible to trip a laminar boundary layer by a row of spherical elements at even the lower limit of the instability region. As was understood from results of Göksel, if the spacing of the elements in the row is decreased; in the limit $s = 0$ or at least $s = k$, the row of spherical elements behaves as a two - dimensional trip wire for which there is no dependency on the instability region.

3- It was also unterstood that increasing the number of elements in the row or decreasing the spacing between the elements produces almost the same effect.

5.3 NEW CORRELATION ATTEMPTS ABOUT THE TRANSITION CHARACTERISTICS OF A ROW OF SPHERICAL ELEMENTS

The same approach as was given for an isolated spherical roughness element mentioned in chapter 3 can also be used for a row of spheres to obtain new forms of correlations. So that the upstream flow history is incorporated in the correlations.

Figure 5.4.a and Figure 5.5.a indicates that $R_{x_{T_c}}$ for a spanwise row of spherical roughness elements can be correlated with the ratio of $\dfrac{k}{\delta^*_k}$.

Figure 5.4.b and Figure 5.5.b are the log - log plots of Rx_{T_c} versus $\dfrac{k}{\delta^*_k}$ for the corresponding figures, 5.4.a, 5.5.a. As can be seen from these logarithmic plots least square lines can be fitted to the experimental results producing the following relationships.

$$\log_{10} R_{x_{Tcs}} = -3.7402 \; \log_{10} \dfrac{k}{\delta^*_k} + 5.3434 \qquad (5.2)$$

$$\log_{10} R_{x_{Tce}} = -3.7909 \ \log_{10} \frac{k}{\delta^*_k} + 5.4432 \qquad (5.3)$$

for $s = \frac{1}{32}$ "

and

$$\log_{10} R_{x_{Tcs}} = -3.3568 \ \log_{10} \frac{k}{\delta^*_k} + 5.4385 \qquad (5.4)$$

$$\log_{10} R_{x_{Tce}} = -3.5064 \ \log_{10} \frac{k}{\delta^*_k} + 5.5211 \qquad (5.5)$$

for $s = \frac{5}{32}$ "

The comparison of the above equations with corresponding ones for an isolated spherical roughness element shows that when $s = k = \frac{1}{32}$ " the correlations proposed for row deviate a lot from those of a single element case for the start and the end of transition, while as the spacing between the elements is increased from $\frac{1}{32}$ " to $\frac{5}{32}$ " the correlations given for an isolated element can also be used for the row as well. These results indicate that : When the spacing of the elements in the row attains the value of $s = 5k$ the row acts as an isolated element. When $s = k$, on the other hand row behaves as a two - dimensional trip wire as was mentioned previously in this chapter.

Figure 5.6.a and Figure 5.7.a indicate the variation of $R_{x_{Tc}}$ with $R_{\delta^*_k}$ for a spanwise row of spherical roughness elements with $s = k$ and $s = 5k$ respectively. The following relationships were obtained in log - log plots of $R_{x_{Tc}}$ vs $R_{\delta^*_k}$ by fitting least square lines to the experimental results.

$$\log_{10} R_{x_{Tcs}} = 1.9984 \ \log_{10} R_{\delta^*_k} - 0.4669 \qquad (5.6)$$

$$\log_{10} R_{x_{Tce}} = 1.9561 \ \log_{10} R_{\delta^*_k} - 0.3488 \qquad (5.7)$$

for $s = \frac{1}{32}$ "

56

and

$$\log_{10} R_{x_{Tcs}} = 1.9983 \log_{10} R_{\delta^*_k} - 0.4668 \tag{5.8}$$

$$\log_{10} R_{x_{Tce}} = 2.0118 \log_{10} R_{\delta^*_k} - 0.5091 \tag{5.9}$$

for $s = \frac{5}{32}$."

These are given in Figure 5.6.b and Figure 5.7.b

The comparison of the above relationships with those obtained for a single element case indicates that the effect of upstream flow history on the critical transition Reynolds numbers for the start and the end of transition can be represented by the same relationships for isolated and row of spherical roughness elements, irrespective of the spacing of the elements in the row.

5.4 CORRELATION OF THE RECOVERY LENGTH OF TURBULENT BOUNDARY LAYER BEHIND A ROW OF SPHERICAL ROUGHNESS ELEMENTS

Göksel (32) has shown that the recovery length behind a row of spherical roughness elements ($s = \frac{5}{32}$," $k = \frac{1}{32}$ ", $n = 11 \frac{x_k}{k} = 3$ ") can be correlated as was done previously for an isolated element. The recovery length behind a row of spheres is also a function of roughness Reynolds number, R_k , and the same correlation between $\frac{x_R - x_k}{k}$ and $R_k \frac{k}{\delta^*_k}$ given in chapter 4 can also be used for the row of spheres. Göksel also noted that the difference in the behaviour of recovery length behind the row measured at the centerline of the row and along a line midway between two elements may be due to the presence of horseshoe vortices and the sense of their rotation.

In order to represent the recovery length behind a row of spheres in a form where the upstream flow history is considered, the approach taken in chapter 4, must be used. Figure 5.8.a and Figure 5.8.b shows the variation of $\frac{x_R}{x_k}$ against $R_{\delta^*_k}$ behind

57

a row of spherical roughness elements at $Z = 0''$ and $Z = -\frac{15}{32}''$

respectively. Inspection of Figure 5.8.a, - 5.8.b indicates

that due to the above mentioned difference in the horseshoe vortices

behind the row; for $Z = -\frac{15}{32}''$ case $\frac{x_R}{x_k}$ decreases suddenly at

$R_{\delta_k^*} = 460$ while for $Z = 0''$, decrease in $\frac{x_R}{x_k}$ covers a wide

range. The critical $R_{\delta_k^*}$ value upon which no influence of it on

the recovery length is seen, was found to be about 600 which was

lower than the value of 1.2×10^3, given for an isolated element

previously. The minimum $\frac{x_R}{x_k}$ value was seen to be about 1.35 ,

while it was found to be 1.15 for a single element.

Figure 5.9.a, Figure 5.9.b indicates the variation of

$R_{x_L} = U \left(\frac{x_R - x_k}{\nu} \right)$ with $R_k \frac{k}{\delta_k^*}$ for $Z = 0''$ and

$Z = -\frac{15}{32}''$ respectively. As is seen from these figures, $U \left(\frac{x_R - x_k}{\nu} \right)$

decreases with an increase in $R_k \frac{k}{\delta_k^*}$, upto a limit of

$R_k \frac{k}{\delta_k^*}$ above which either $U \left(\frac{x_R - x_k}{\nu} \right)$ increases

or stays approximately constant with an increase in $R_k \frac{k}{\delta_k^*}$.

It was seen from these figures that, the limiting value of $R_k \frac{k}{\delta_k^*}$

was about 2500. As it is seen from Figure 5.9.a the minimum

R_{x_L} value is found to be 0.4×10^5 behind the centerline of the

row. This value is similar to that of an isolated element case.

Thus it is again apparent that when $s = 5k$, row acts as an isolated

roughness element.

As can be seen from Figure 5.10.a and Figure 5.10.b, R_{x_L} can

be correlated with $\frac{k}{\delta_k^*}$ behind a row of spherical elements.

It is also seen that R_{x_L} tends to infinity as $\frac{k}{\delta_k^*}$ attains

approximately a value of 1.70. This is found by extending the

straight portion of the R_{x_L} versus $\frac{k}{\delta_k^*}$ curve to the abcissa .

It is also seen that minimum R_{x_L} value is obtained when $\frac{k}{\delta_k^*}$

attains the value of 2.1. Thus $\frac{k}{\delta_k^*} = 2.1$ seems to repre-

sent the critical condition which causes, MRL, minimum recovery

distance behind the row. Similarly tolerable roughness size to trip

the laminar boundary layer is seen to be given with the condition,

$\dfrac{k}{\delta^{*}_{k}} = 1.70$ at which R_{x_L} tends to infinity. Therefore following

relationships are proposed.

$$\left(\dfrac{k}{\delta^{*}_{k}}\right)_{MRL} = 2.1 \tag{5.10}$$

$$\left(\dfrac{k}{\delta^{*}_{k}}\right)_{tolerable} = 1.7 \tag{5.11}$$

5.5 WAKE DEVELOPMENT BEHIND A ROW OF ROUGHNESS ELEMENTS

It was known that every element in the row forms its own wake

and these wakes are separated from each other by the horseshoe var-

tices. The wakes start to interact with each other, and form a turbulent

wake at increasing roughness Reynolds numbers at a certain distance

behind the roughness, or at a constant roughness Reynolds number with

increasing distance from the row. Göksel has observed this fact, and

concluded that wake interaction length is completely dependent on

the roughness Reynolds number.

He also investigated the growth of turbulent wake behind a row

of spheres ($k = \dfrac{1}{32}$ '', $s = \dfrac{5}{32}$ '', $n = 11$, $x_k = 3$ '') and found that

R_{w_T} is a function of $R\theta_{c_L}$. However, he couldn't obtain an exact

form of the relationship between $R\theta_{c_L}$ and R_{w_T}, but he noticed

that when $R_{\theta_{c_L}} > 2000$ R_{w_T} is a function of $R_{\theta_{c_L}}$ only as

he had observed previously for an isolated roughness element.

In order to find a better correlation for turbulent wake growth

behind row of spherical roughness elements, R_{w_T} was plotted against

$(R_{\theta_{c_L}} - R_{\theta_k})$ and is shown in Figure 5.11. As can be seen from this

figure, the dependency of R_{w_T} upon R_k can be neglected for a

certain band of results. The greatest deviation is seen to be due

to the results belonging to $R_k = 848$ and $R_k = 759$, because at these

R_k values the interaction of the individual wakes have not been completed.

The comparison of the result obtained for an isolated sphere with this one, showed that the correlation between R_{w_m} and $(R\theta_{c_L} - R\theta_k)$ proposed for an isolated sphere can't be used for the row of spheres. This is due to the reason that the wake formation behind an isolated element is completely different from that of the wake formation behind the row roughness elements.

5.6 CONCLUSIONS

1 - For $s \leqslant k$, Laminar boundary layer can be tripped by a row of spherical roughness elements at even the lower limit of the instability region; since row behaves as a two - dimensional element.

2 - Increasing the number of the elements in the row or decreasing the spacing between them produces almost the same effect.

3 - For $s = 5k$ the correlations given for an isolated element, between $R_{x_{Tc}}$ and $\dfrac{k}{\delta^*_k}$, can be used for the row of spherical elements as well.

4 - The spacing of the elements is ineffective on the correlations between $R_{x_{Tc}}$ and $R_{\delta^*_k}$.

5 - Two relationships decribing MRL and tolerable roughness height to trip the laminar boundary layer with a row of spherical roughness elements for $s = 5k$ were given in equations (5.10) and (5.11).

6 - Turbulent wake development behind a row of roughness elements was seen to be different from that of an isolated element case contrary to the previously proposed fact in Reference 32.

60

CHAPTER 6

SUGGESTIONS FOR FURTHER WORK

The effects of isolated and row of roughness elements upon boundary layer transition and boundary layer development were investigated.

New correlations were formed to represent the upstream flow history effect upon transition characteristics of roughness elements and boundary layer development, with the special emphasis on recovery length of turbulent boundary layer.

Simple relationships which define the critical dimensions of a spherical roughness element were proposed in terms of $\dfrac{k}{\dfrac{\delta^*}{k}}$.

Wake growth characteristics of single and row of roughness elements were analyzed. A correlation describing the turbulent wake development behind an isolated spherical roughness element was proposed.

Thus it seems that the picture which describes the effects of roughness upon boundary layer development on a flat plate is almost completed.

Wake development behind a row of roughness elements and transition characteristics of roughness elements of distributed nature needs further experimental investigation.

Table 3.1 Comparison of the Correlations Proposed by Göksel and Tani et al.

$R_{x_{T_{cs}}} \, 10^{-5}$ (1)	$R_{x_{T_{ce}}} \, 10^{-5}$ (1)	$R_{x_{T_{cs}}} \, 10^{-5}$ (2)	$R_{x_{T_{ce}}} \, 10^{-5}$ (2)	$\dfrac{X_k}{k}$	Experiment
9.837	11.35	10.52	11.320	799.7	
6.475	7.281	6.46	7.260	576	
4.091	4.494	4.077	4.479	384	Göksel
1.432	1.520	1.426	1.514	159.9	
0.591	0.615	0.589	0.612	79.	
6.584	7.546	6.575	7.52	576	
3.972	4.456	4.340	4.44	384	
1.742	1.886	1.73	1.875	191	Hall
0.707	0.793	0.708	0.794	96	
0.588	0.640	0.582	0.634	80	
5.37	6.202	5.35	6.18	504	Yeğen
1.87	2.038	1.86	2.03	210	Albayrak

(1) Experimental results which correspond to correlations of Göksel given by Equations 3.6, 3.7.

(2) Tani et al correlation results given by Equation 3.5

Based on experimental data of Göksel - Hall - Yeğen - Albayrak, obtained behind a spherical roughness - element on a flat plate with $\lambda_\Theta = 0$.

Table 3.2 Reduced Data Set for the Experimental Results of Tani et al (51)

$\dfrac{X_k}{k}$	$\dfrac{k}{\delta^*_k}$	R_k	$R_{\delta^*_k}$	$R_{\delta^*_k} - R_{\delta^*_{i_u}}$	$R_{x_{T_G}} 10^{-6}$
956	0.562	897	1596	1076	0.944
319	0.903	771	853	333	0.27
498	0.754	847	1123	603	0.447
699	0.744	1158.1	1556	1036	0.833
922	0.580	918	1582	1062	0.880
1162	0.559	1073	1919	1399	1.289
478	1.015	1461	1439	919	0.719
747	0.692	1067	1541	1021	0.825
1048	0.653	1292	1978	1458	1.415
1211	0.548	1084	1923	1403	1.345
1383	0.490	984	2008	1488	1.415
655	0.673	877	1303	783	0.610
1023	0.546	914	1673	1153	0.992
1292	0.503	980	1948	1428	1.305
1659	0.483	927	1919	1399	1.557

Table 3.3 Calculation results for $\dfrac{k}{\delta^*_k}$ behind a spherical roughness element.

$\dfrac{k}{mm}$	$\dfrac{x}{mm}$	$R_{x_{kcs}} 10^{-5}$	$\dfrac{k}{\delta^*_k}$	$R_{x_{kce}} 10^{-5}$	$\dfrac{k}{\delta^*_k}$	$\dfrac{X_k}{k}$	Experiment
0.794	635	9.837	0.72	11.356	0.77	799.7	
0.794	457	6.475	0.81	7.281	0.86	576	
0.794	305	4.091	0.96	4.494	1.01	384	Göksel
0.794	127	1.432	1.37	1.520	1.41	159.9	
0.794	63	0.591	1.78	0.615	1.81	79.3	
0.794	457	6.584	0.819	7.546	0.877	576	
0.794	305	3.972	0.953	4.456	1.010	384	
0.794	152	1.742	1.267	1.886	1.318	191	Hall
1.59	152	0.707	1.61	0.793	1.71	96	
0.794	64	0.588	1.74	0.640	1.82	80	
1.19	600	5.370	0.84	6.202	0.908	504	Yeğen
1.19	250	1.87	1.19	2.038	1.24	210	Albayrak

Table 3.4 Calculation results for parameters $R_\delta{}^*$ and $\psi = R_{\delta^*{}_k} - R_{\delta^*{}_{i_u}}$ behind a spherical roughness element

$\dfrac{k}{\delta^*{}_k}$ START	R_{kcs}	ψ	$R_{\delta^*{}_k}$ START	$\dfrac{k}{\delta^*{}_k}$ END	R_{kce}	$R_{\delta^*{}_k}$ END	ψ	Experiment
0.72	1320	1313	1833	0.77	1420	1844	1324	
0.81	1125	868	1388	0.86	1265	1470	950	
0.96	1065	589	1109	1.01	1170	1158	638	Göksel
1.37	895	133	653	1.41	950	673.7	153	
1.78	745	—101.5	418.5	1.81	775	428	−92	
0.82	1145	876	1396	0.877	1310	1493.7	973	
0.95	1135	674	1194	1.01	1160	1148.5	628	
1.267	910	198	718	1.32	985	746	226	Hall
1.61	740	−61	459	1.71	830	485	−34	
1.74	730	−100.5	419.5	1.82	795	436.8	−83	
0.84	1065	747	1267	0.908	1230	1354	834	Yeğen
1.19	890	227	747	1.24	970	782	262	Albayrak

Table 3.5 Reduced data set for the Experimental results obtained Under Varible Pressure Gradients Behind a Spherical Roughness Element

$R_{x_{Tcs}} 10^{-5}$	$\dfrac{x_k}{k}$	$\lambda\Theta_k$	$R_{\delta^*}k_{st.}$	$R_{\delta^*}k_{en.}$	$\dfrac{k}{\delta^*k}_{st.}$	$\dfrac{k}{\delta^*k}_{end.}$	$R_{x_{Tce}}10^{-5}$
4.015	377	−0.02	1100	1155	0.96	1.021	4.448
2.532	252	−0.02	875	890	1.14	1.168	2.6208
1.61687	188	−0.02	700	725	1.22	1.365	1.8612
2.4521	251.5	−0.04	915	1005	1.065	1.134	2.8671
1.4196	168	−0.04	700	770	1.207	1.32	1.71361
3.6156	314.4	−0.052	1220	1305	0.942	1.015	4.1658
2.079	210	−0.052	910	965	1.087	1.139	2.3100
4.074	420	+0.027	895	925	1.083	1.124	4.3680
2.8574	314	+0.027	750	780	1.213	1.262	3.0929
1.8488	213	+0.026	606	976	1.43		
4.1025	426.9	+0.0525	800	1090	1.201		

Table 4.1 Reduced data Set for the Experimental Results of Göksel and Yeğen for the Recovery Length Behind a Spherical Roughness Element.

$\lambda\Theta_k$	$\dfrac{x_k}{k}$	$\dfrac{10^3}{R_k}$	$\dfrac{X_R}{X_k}$	$R_{\delta^*_k}$	Experiment
0	768	0.74	1.37	1745	
		0.65	1.16	1865	
		0.59	1.24	1884	Göksel
		0.51	1.20	2095	
		0.45	1.12	2223	
0	94.4	1.17	2.69	487	
		0.83	1.50	585	
0	63	1.09	2.35	417	
		0.77	1.84	495	
		0.54	1.33	594	
		0.85	2.0	466	
0	32		1.66	699	
0	32	0.546	1.66	583	
			2.35	418	
			1.73	493	
-0.02	377	0.84	1.5	1113	Yeğen
-0.02	252	0.80	1.66	938	
		0.56	1.33	1119	
-0.02	188	0.94	1.67	746	
		0.60	1.34	938	
		0.42	1.16	1114	
-0.04	252	0.95	1.75	955	
		0.61	1.25	1196	
		0.43	1.18	1425	

Table 4.2 Reduced Data Set for the Experimental Result of Albayrak for the Recovery Length Behind a Spherical Roughness Element.

λ_{θ_k}	$\dfrac{X_k}{k}$	$\dfrac{10^3}{R_k}$	$\dfrac{X_R}{X_k}$	$R_{\delta^*_k}$
+0.030	105	0.94	1.99	474
		0.66	1.39	566
		0.49	1.36	652
		0.39	1.38	730
		0.33	1.42	812
		0.30	1.47	839
+0.053	252	0.44	1.198	961
		0.35	1.158	1072
		0.32	1.150	1127
		0.29	1.150	1178
		0.27	1.119	1225
+0.030	157	1.03	2.59	550
		0.74	1.59	653
		0.59	1.40	731
		0.49	1.25	808
		0.45	1.32	837
+0.045	252	0.83	1.32	657
		0.54	1.25	910
		0.47	1.17	970
+0.030	210	0.88	2.59	695
		0.79	1.60	733
		0.72	1.48	769
		0.66	1.40	799
		0.61	1.32	839

Table 4.3 Calculation Results for R_{X_L} for the Experimental Data of Albayrak

$R_{\delta}*_k$	$\dfrac{U(X_B - X_k)}{V} \; 10^{-5}$
474	1.1109
566	0.634
652	0.765
730	1.007
812	1.329
839	1.636
550	2.40
653	1.26
731	1.059
808	0.808
837	1.093
657	0.967
910	1.152
970	0.93
695	3.79
733	1.57
769	1.385
799	1.268
839	1.096

Table 4.4 Calculation Results for R_{X_L} for the Experimental Data of Göksel and Yeğen

$R \, \delta^*_k$	$\dfrac{U(X_R - X_k)}{v} \, 10^{-5}$	$\dfrac{X_k}{k}$
1113	2.23	377
938	2.096	252
1119	1.485	
746	1.33	188
938	1.045	
1114	0.744	
955	1.98	
1196	1.032	252
1425	1.091	
1745	3.8448	768
1865	1.9532	
1884	3.2072	
2095	2.9675	
2223	2.1216	
417	0.78	
495	0.68	
594	0.39	64
701	0.55	
800	0.71	
417	0.77	
493	0.602	32
583	0.78141	
699.3	1.104	

Table 4.5 Reduced Data Set for the Wake Development Behind a Spherical
Roughness Element with $\lambda_\theta = 0$ Based on the Results of Göksel (32)

$R_{x_k} \cdot 10^{-5}$	$\dfrac{X_{W_T} U}{\nu}$	$\dfrac{X_{W_T} - X_k}{k}$	$R_{\delta^*_k}$	$R_k \dfrac{k}{\delta^*_k}$	$(R_{X_{W_T}} - R_{x_k}) \cdot 10^{-5}$
11.71	14.64×10^5	192	1865.5	1248.3	2.93
12.96	15.12×10^5	128	1883.9	1512.4	2.15
14.79	17.26×10^5	128	2094.5	1772.8	2.47
16.97	19.8×10^5	128	2223.3	2196.7	2.83
0.814	2.71×10^5	224	497.3	1475.5	1.895
1.170	2.3×10^5	96	585.3	2460	1.147
0.82368	1.36×10^5	42	495.0	3346.2	0.54
1.17056	1.57×10^5	22	593.83	5633.3	0.40
1.65632	1.91×10^5	10	701.35	9549.7	0.26
2.1504	2.48×10^5	10	800.0	1411.2	0.330

Table 4.6 Deduced Data Set From the Experimental Results of Göksel, Which Were Taken From Figure 4.74 of Rèference 32.

$\dfrac{k}{\delta^*_k}$	k (inch)	X_k (inch)	R_k	R_θ	$\dfrac{10^5}{R_{W_T}}$	Symbol
	$\dfrac{3}{64}$	3	3366	440	13.5	O
				530	5.6	
				790	2.8	
				1300	1.0	
				1680	0.5	
				3020	0.3	
3.69	$\dfrac{3}{64}$	3	2588	454	10	X
				640	4	
				1170	0.85	
				2460	0.40	
				2980	0.25	
3.08	$\dfrac{3}{64}$	3	1829	370	12.8	Δ
				500	8	
				890	1.8	
				2330	0.4	
2.6	$\dfrac{3}{64}$		1287	390	14.5	+
				870	2.4	
				1260	1	
				1720	0.6	
2.19	$\dfrac{3}{64}$	3	914	650	5.7	⊡
				930	2	
				1300	1.3	
7.4	$\dfrac{3}{32}$	3	5175	380	6	⊘
				510	3.6	
				560	2.2	
				880	1.5	
				1340	0.85	
				1800	0.5	
				2660	0.25	
				3220	0.20	
6.27	$\dfrac{3}{32}$	3	3660	400	6.4	⊿
				480	4.2	
				710	2.5	
				1040	1.2	
				1380	0.8	
				1970	0.5	

Table 4.6 Cont.

$\frac{k}{\delta^*_k}$	k (inch)	X_k (inch)	R_k	R_Θ	$\frac{10^5}{R_{W_T}}$	Symbol
6.27	$\frac{3}{32}$	3	3660	400 480 710 1040 1380 1970	6.4 4.2 2.5 1.2 0.8 0.5	⟋
5.21	$\frac{3}{32}$	3	2570	350 340 520 800 1040 1410 1770	10.3 6 3.6 2.4 1.8 0.8 0.5	⊠
4.38	$\frac{3}{32}$	3	1830	380 600 1040 1300	8.5 4.3 1.35 1	V
2.05	$\frac{1}{32}$	3	1200	440 510 680 1020 1330 1820 2260	12.8 12.75 3.1 1.65 1.2 0.8 0.5	●
1.74	$\frac{1}{32}$	3	848	700 960 1300 1620	7.2 3.6 0.8 0.6	Y
0.994	$\frac{1}{32}$	24	2210	1250 1580 1920	3.4 1.4 0.55	U
0.92	$\frac{1}{32}$	24	1927	1120 1360 1700	4 1.6 0.9	∩
0.8.69	$\frac{1}{32}$	24	1688	1000 1320 1520	9.1 2 1.4	⊔
0.818	$\frac{1}{32}$	24	1526	1140 1320	2.5 7.5	▽

Table 4.7 Calculation Results for $\left(R_{\theta_{\mathcal{L}}} - R_{\theta_k}\right)$, for the Experimental results of Göksel (32)

$R_{\theta_{\mathcal{L}}} - R_{\theta_k}$	$R_{W_T} \, 10^{-5}$	Symbol	$R_{\theta_{\mathcal{L}}} - R_{\theta_k}$	$R_{W_T} \, 10^{-5}$	Symbol	$R_{\theta_{\mathcal{L}}} - R_{\theta_k}$	$R_{W_T} \, 10^{-5}$	Symbol
172.65	0.156		384.9	0.29		488.73	0.175	
252.65	0.238		714.9	0.71	u	768.73	0.175	□
482.65	0.4	Å	1054.9	1.81		1138.73	0.76	
812.65	0.83							
1152.65	1.25		312.1	0.25		109.3	0.166	
1742.65	2		552.1	0.625	∧	239.3	0.27	∅
159.54	0.097		892.1	1.11		289.3	0.454	
149.54	0.16		383.9	0.4		609.3	0.666	
329.54	0.27		563.9	0.66	▽	1069.3	1.17	
609.54	0.416	⊄	280.9	0.109		1529.3	2.0	
849.54	0.55		600.9	0.5	⊔	2329.3	4.0	
1219.54	1.25		800.9	0.71		2949.3	5.0	
1579.54	2		132.07	0.074				
219.24	0.117		222.07	0.17				
439.24	0.23	V	482.07	0.35	O			
878.24	0.74		992.07	1.0				
1139.24	1		1372.07	2.0				
214.44	0.078		2712.07	3.3				
284.44	0.078		183.25	0.1				
454.44	0.32	●	369.25	0.25				
794.44	0.606		899.25	1.17	X			
1104.44	0.83		2189.25	2.5				
1594.44	1.25		2709.25	4				
2034.44	2		142.77	0.078				
510.54	0.138		272.77	0.125	Δ			
770.54	0.27	Y	662.77	0.555				
1110.54	1.25		2102.77	2.5				
1430.54	1.66		199.01	0.068				
			679.01	0.416	+			
			069.01	1				
			529.01	1.6				

Table 5.1 Calculation Results of $R_{x_{Tcs}}$, $R_{x_{Tce}}$ and $\dfrac{k}{\delta^{*}_{k}}$ for a Row of Spherical Roughness Elements ($k = \dfrac{1}{32}$ ", $s = \dfrac{2}{32}$ ", $n = 11$, $x_k = 12$ ")

$\dfrac{k}{\delta^{*}_{k}}$ START	$R_{x_{Tcs}}$	$\dfrac{k}{\delta^{*}_{k}}$ END	$R_{x_{Tce}}$
0.781	5.99×10^{5}	0.816	6.54×10^{5}
0.723	9.14×10^{5}	0.755	9.97×10^{5}
1.112	1.35×10^{5}	1.149	1.44×10^{5}
1.585	0.685×10^{5}	1.626	0.72×10^{5}
0.938	3.84×10^{5}	0.971	4.12×10^{5}

Table 5.2 Calculation Results of $R_{x_{Tcs}}$, $R_{x_{Tce}}$ and $\dfrac{k}{\delta^{*}_{k}}$ for Row of Spherical Roughness Elements ($k = \dfrac{1}{32}$ ", $s = \dfrac{1}{32}$ ", $n = 11$, $x_k = 12$ ")

$\dfrac{k}{\delta^{*}_{k}}$ START	$R_{x_{Tcs}}$	$\dfrac{k}{\delta^{*}_{k}}$ END	$R_{x_{Tce}}$
1.438	0.564×10^{5}	1.492	0.607×10^{5}
1.121	1.37×10^{5}	1.154	1.454×10^{5}
0.914	3.65×10^{5}	0.962	4.04×10^{5}
0.747	5.48×10^{5}	0.785	6.06×10^{5}
0.706	8.72×10^{5}	0.719	9.84×10^{5}

73

Table 5.3 Calculation Results of $R_{x_{Tcs}}$, $R_{x_{Tce}}$ and $R_{\delta}*$ for Row of Spherical Roughness Elements$_k$ ($k = \frac{1}{32}$", $s = \frac{1}{32}$", $n = 11$, $x_k = 12$)

$R_{\delta}*_k$ START	$R_{x_{Tcs}}$	$R_{\delta}*_k$ END	$R_{x_{Tce}}$
1333.7	5.99×10^5	1392.5	6.54×10^5
1646.5	9.14×10^5	1720.1	9.97×10^5
633.2	1.35×10^5	654.3	1.44×10^5
450.6	0.685×10^5	562.4	0.721×10^5
1066	3.84×10^5	1107.3	4.12×10^5

Table 5.4 Calculation Results of $R_{x_{Tcs}}$, $R_{x_{Tce}}$ and $R_{\delta}*_k$ for a Row of Spherical Roughness Elements ($k = \frac{1}{32}$", $s = \frac{1}{32}$", $n = 11$, $x_k = 12$")

$R_{\delta}*_k$ START	$R_{x_{Tcs}}$	$R_{\delta}*_k$ END	$R_{x_{Tce}}$
409.0	0.564×10^5	424.1	0.607×10^5
637.1	1.371×10^5	656.5	1.454×10^5
1041.9	3.65×10^5	1094.1	4.04×10^5
1274.8	5.48×10^5	1340.8	6.06×10^5
1609.4	8.72×10^5	1783.0	9.84×10^5

Table 5.5 Reduced Data Set for the Results of Göksel taken from Table 5.1 of Reference (32)

$$k = \frac{1}{32}'' , \quad X_k = 3'' , \quad s = \frac{5}{32}'' , \quad n = 11, \quad z = 0''$$

$\dfrac{U(X_R - X_k)}{V}$	$R_k \quad \dfrac{k}{\mathfrak{6}^*_k}$
291456	1244.76
108544	1475.52
38400	2460.0
54016	4118.72
92820	6188.0

$$k = \frac{1}{32}''' , \quad X_k = 3'' , \quad s = \frac{5}{32}''' , \quad n = 11, \quad z = \frac{15}{32}'''$$

432630	1244.76
101760	1475.52
61785.6	2460.0
70004.73	4118.72
66300	6188.0

Table 5.6 Reduced Data Set for the Results of Göksel Taken From Figure 5.32 of Reference 32 for the Turbulent Wake Development Behind a Row of Spherical Roughness Elements

$R_k = 2210$		$R_k = 1688$	
$R_{\theta_{\mathcal{C}}} - R_{\theta_k}$	$R_{W_T} \, 10^{-5}$	$R_{\theta_{\mathcal{C}}} - R_{\theta_k}$	$R_{W_T} \, 10^{-5}$
128.84	0.8475	100	0.7246
308.84	1.000	230	0.7576
638.84	0.9434	490	0.7576
1388.84	1.4286	1090	1.0417
2688.84	2.6316	1590	1.5152
3278.84	2.500	2140	1.9231
3878.84	4.1667	2970	2.2727
		3930	2.500

$R_k = 1200$		$R_k = 848$	
$R_{\theta_{\mathcal{C}}} - R_{\theta_k}$	$R_{W_T} \, 10^{-5}$	$R_{\theta_{\mathcal{C}}} - R_{\theta_k}$	$R_{W_T} \, 10^{-5}$
177.28	0.3906	510.048	0.2075
377.28	0.5814	820.048	0.4132
837.28	0.8929	1180.048	0.8333
1607.28	1.5625	1500.048	1.250
1977.28	1.5152	1670.048	1.111
2317.28	1.4925		

$R_k = 759$	
$R_{\theta_{\mathcal{C}}} - R_{\theta_k}$	$R_{W_T} \, 10^{-5}$
590.2688	0.1852
910.2688	0.6098
1170.2688	0.6250
1370.2688	0.8621
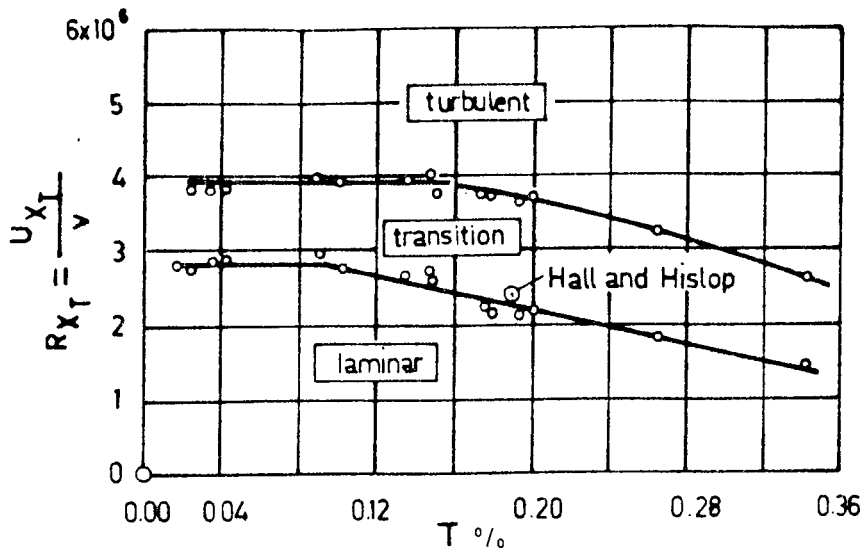
Fig.2.1 Influence of Turbulence Intensity, T, on Transition Reynolds
Number, R_{X_T}, on Flate Plate Under Zero Streamwise Pressure
Gradient, as Measured by Schubauer - Scramstad (2)
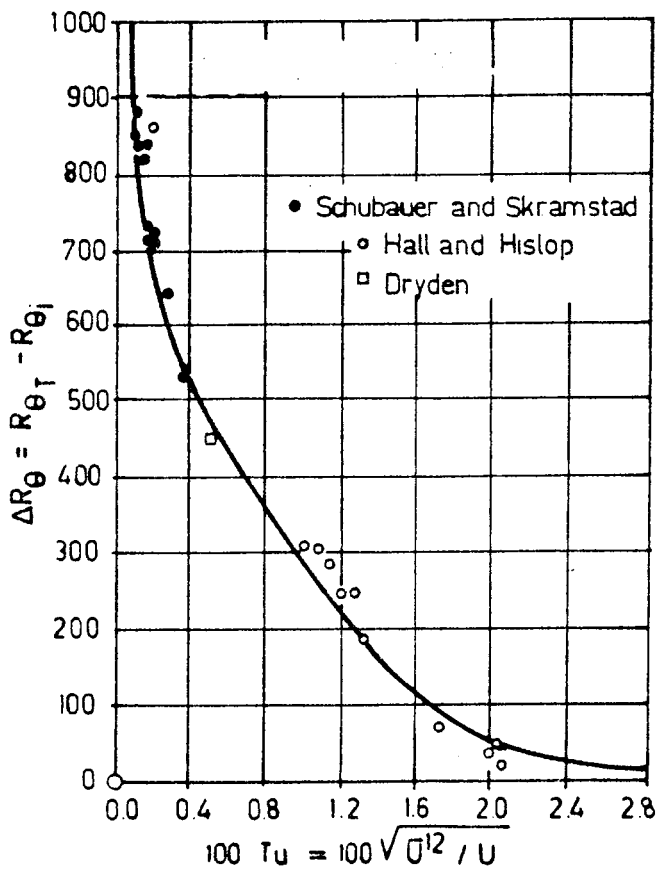
Fig.2.2 Influence of Turbulence Intensity, T, on the Distance Between
the Points of Instability and Transition

77
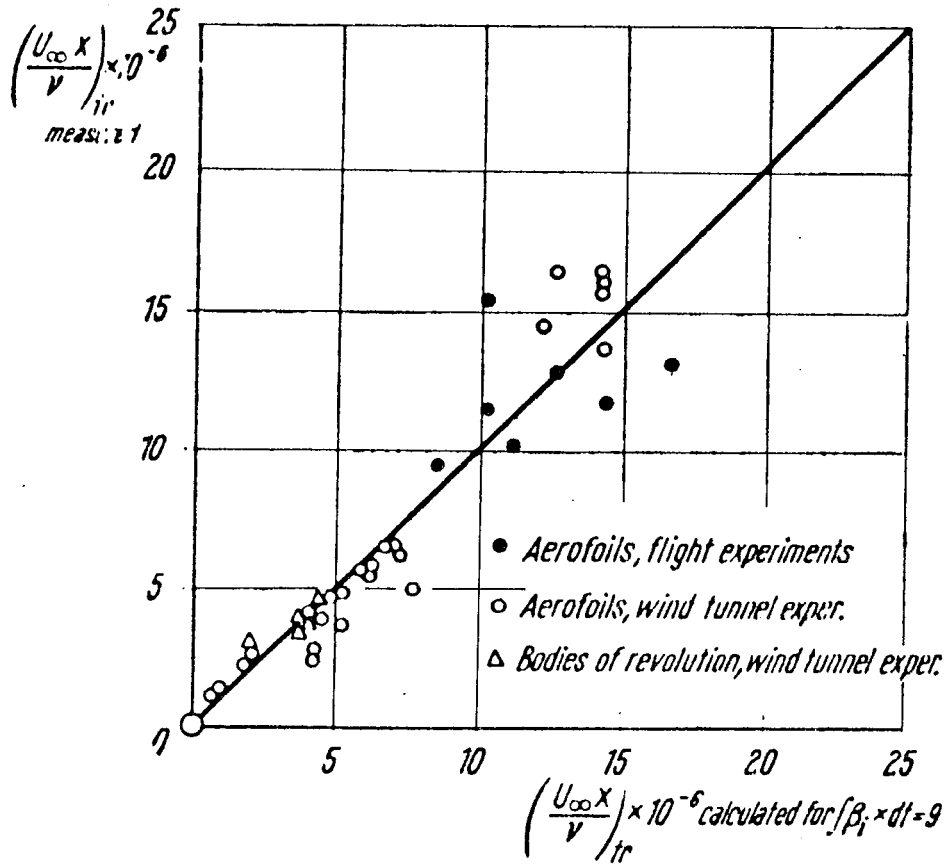
Fig.2.3 Determination of the Amplification Rate Exponential (β_i dt)
for Unstable Disturbances Extended Over the Path From the
Limit of Stability to the Point of Transition,After Smith (24)
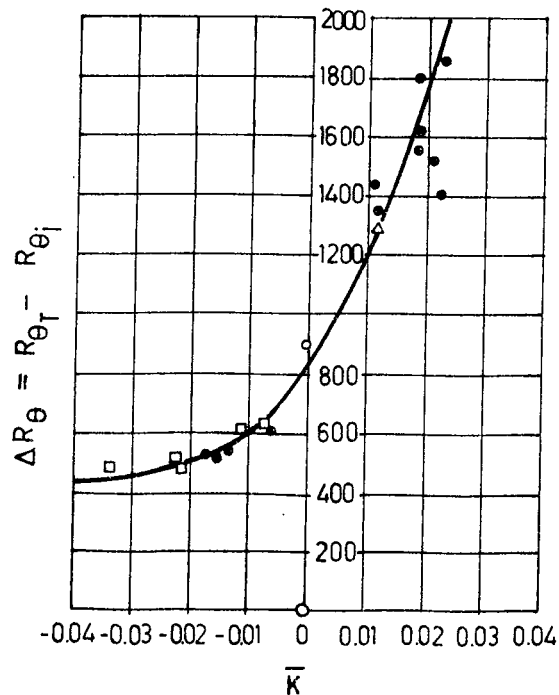
Fig.2.4 Influence of Pressure Gradient on ΔR_θ , After Granville (20)
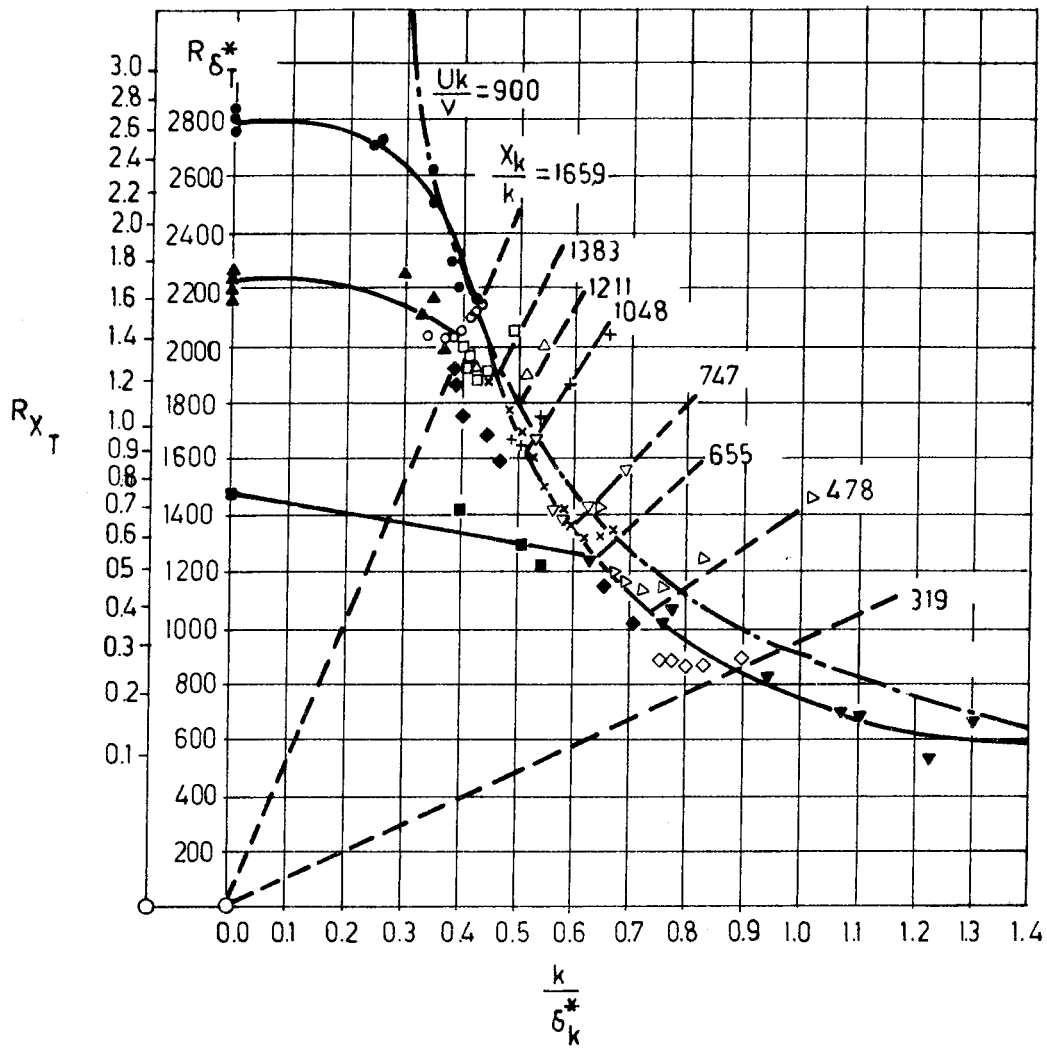
Fig. 3.1 Critical Transition Reynolds Number as a Function of $\dfrac{k}{\delta^*_k}$

for single Two - Dimensional Roughness Element on a Flat
Plate Under Zero Streamwise Pressure Gradient, After Dryden.
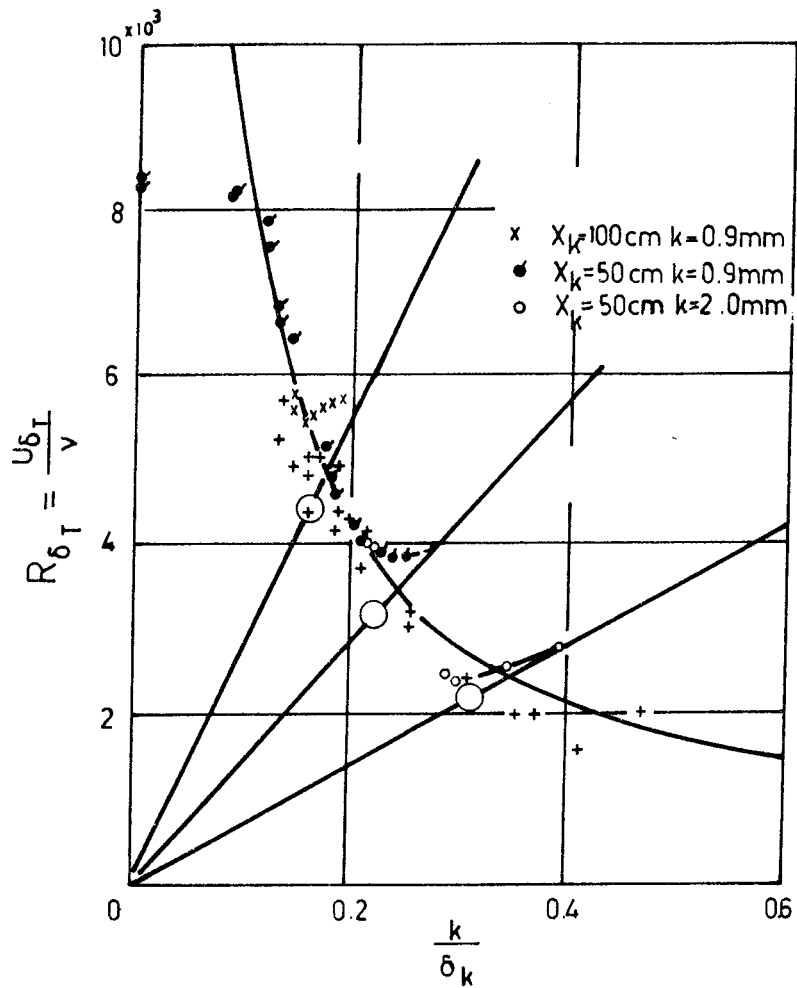
Fig.3.2   Transition   Reynolds Number, R_{δ_T},   Change With $\dfrac{k}{\delta_k}$,

Tani - Sato (11).
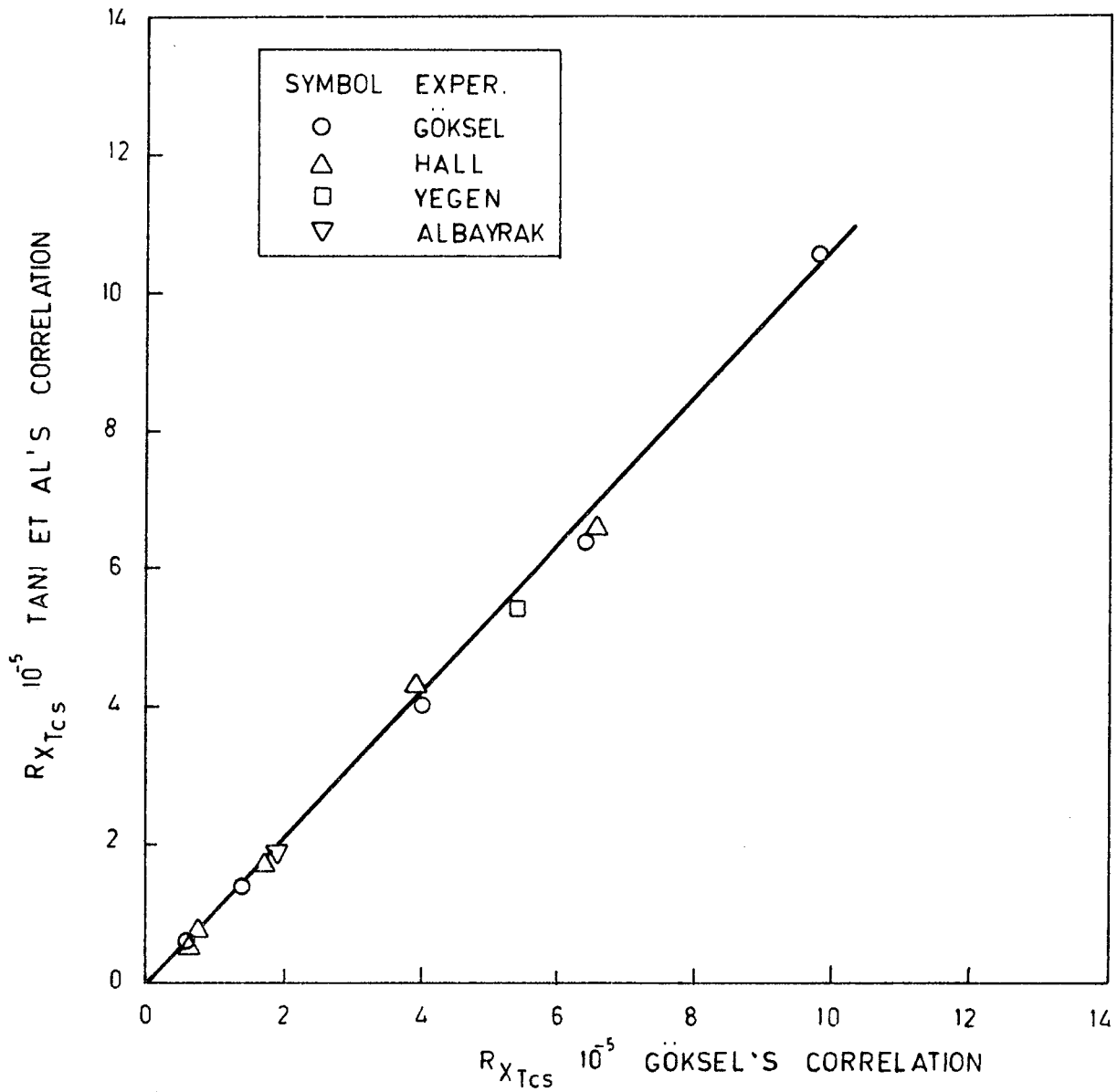
Fig.3.3 Relation Between the Proposed Correlations of Göksel and Tani et al for the Start of Transition, Based on the Experimental Results Behind a Spherical Roughness Element.
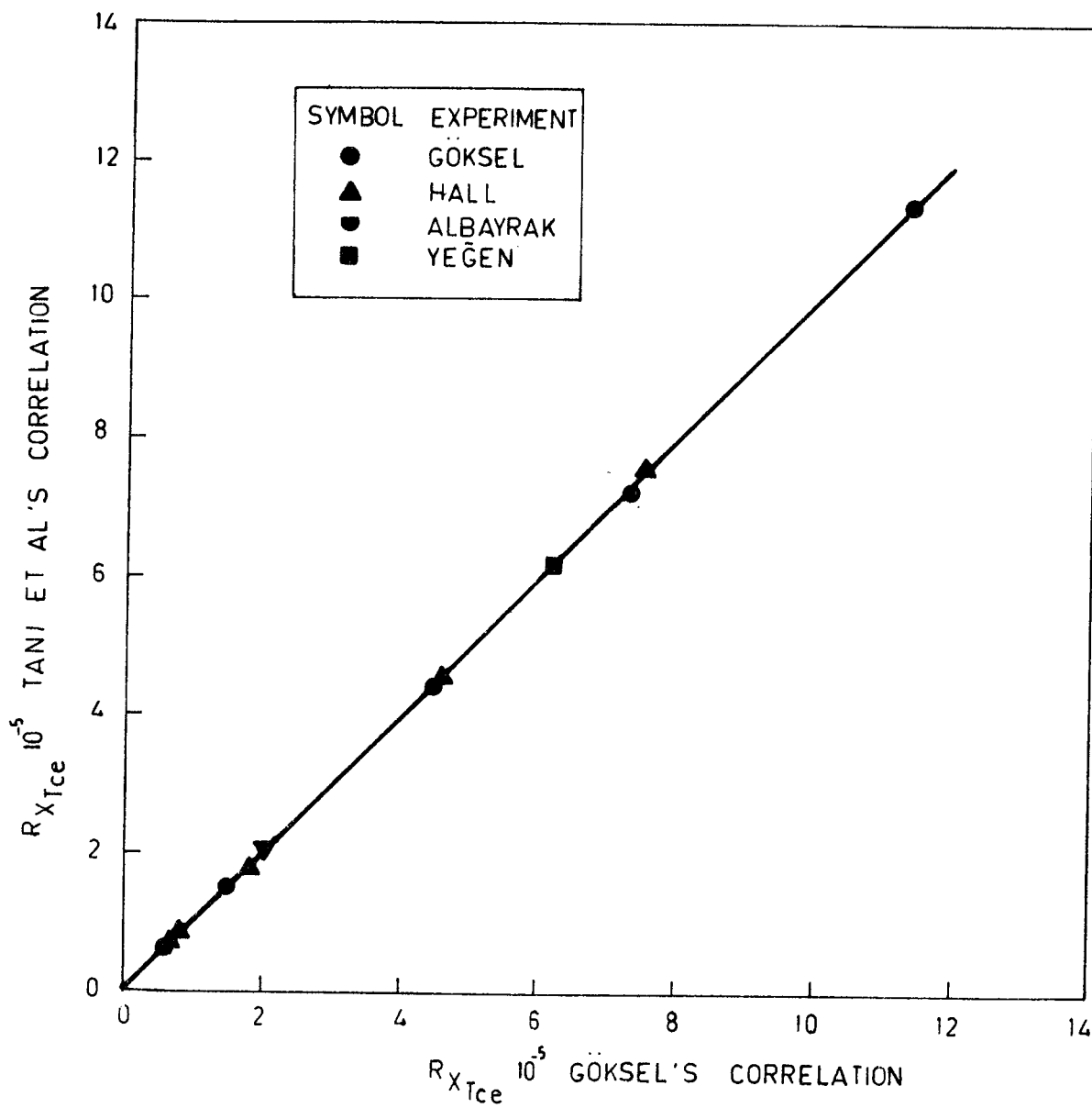
Fig.3.4 Relation Between the Proposed Correlations of Göksel and Tani
et al for the end of Transition, Based on the Experimental
Results Behind a Spherical Roughness Elements.
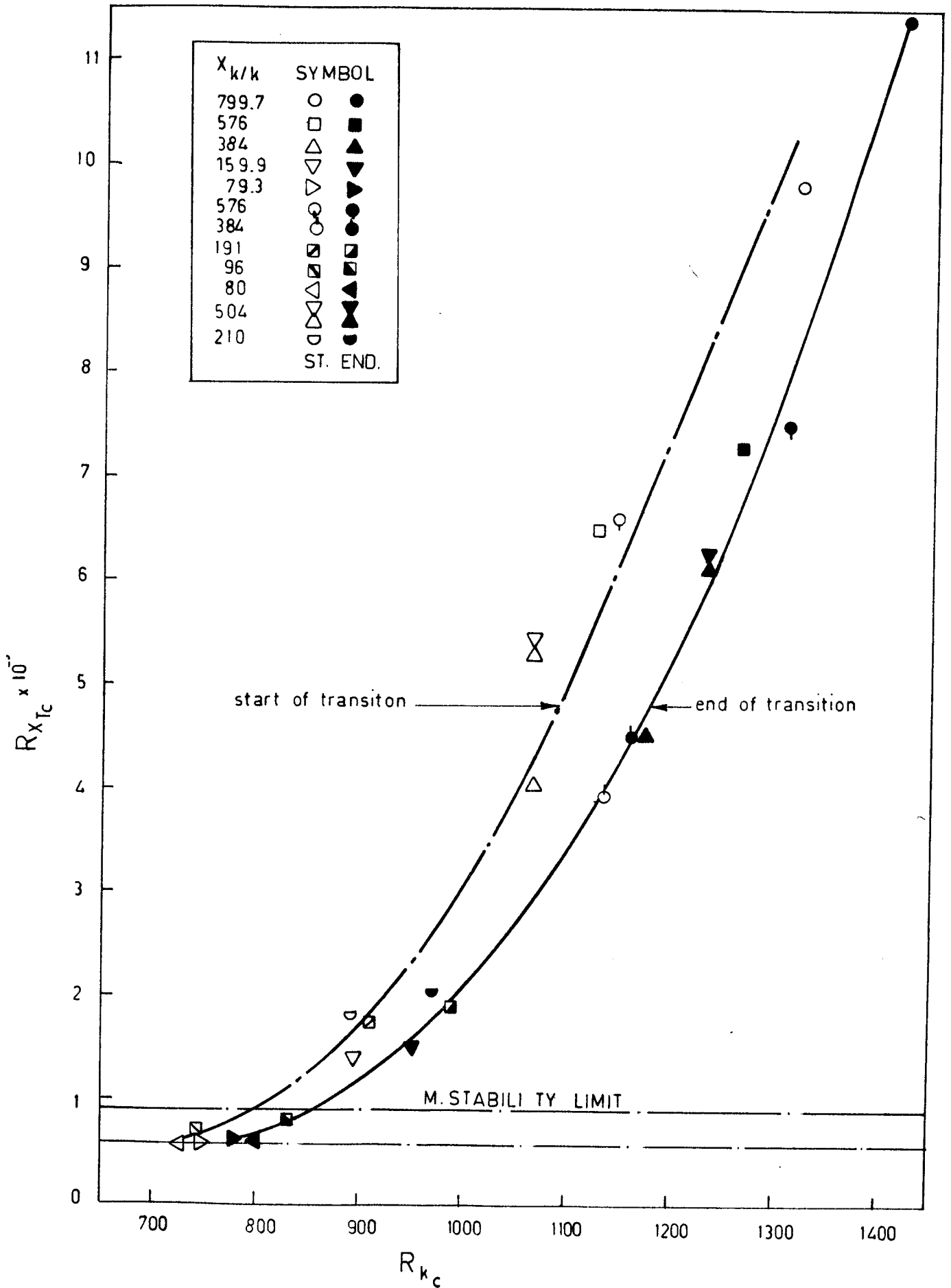
Fig. 3.5 Variation of $R_{x_{T_c}}$ With R_{k_c} for a Spherical Roughness Element on a Flat Plate Under Zero Pressure Gradient.

83
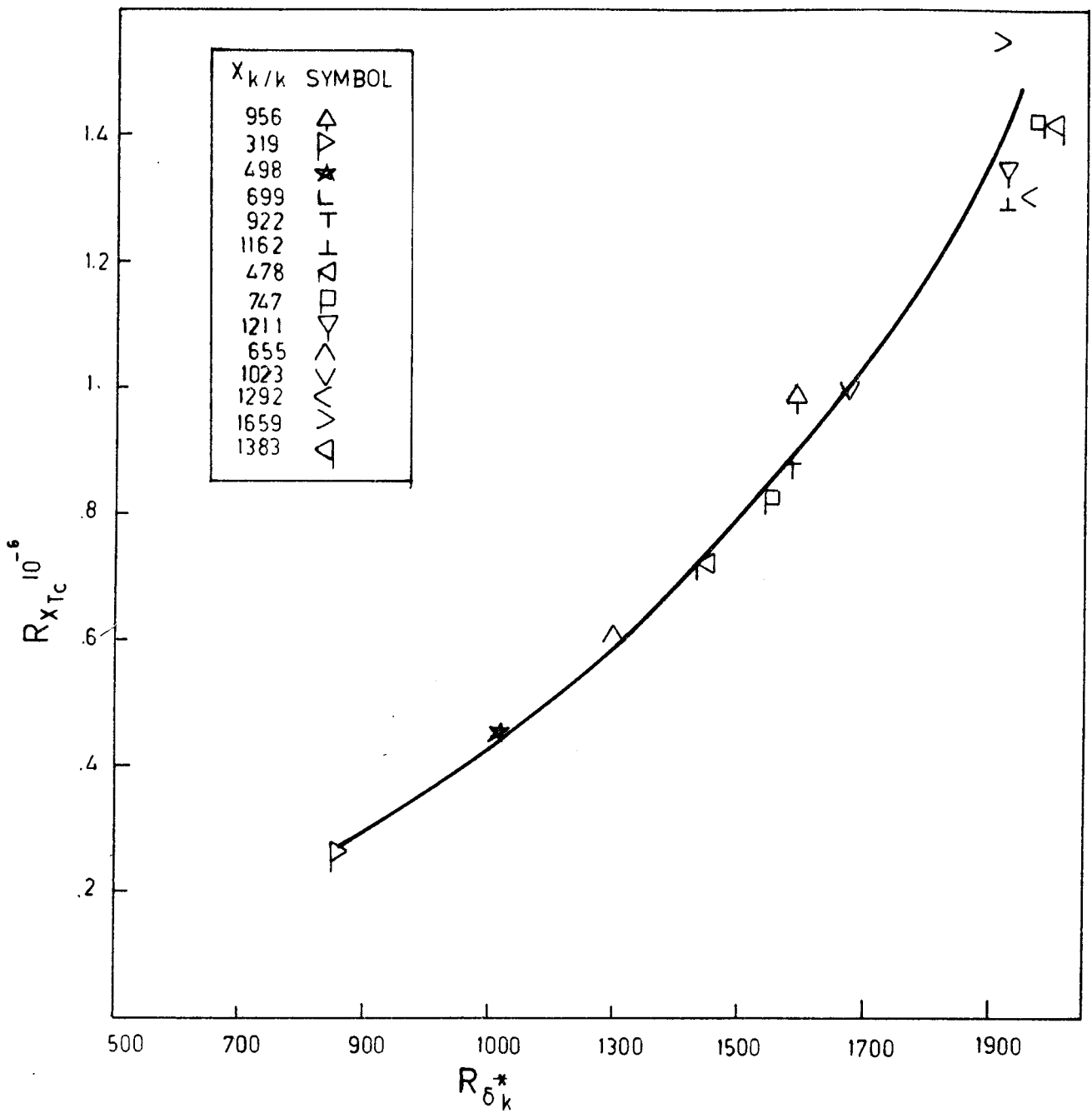
Fig.3.6.a Variation of $R_{x_{Tc}}$ With $R_{\delta^*_k}$ for a Trip Wire on a Flat
Under Zero Pressure Gradient, Based on the Experimental
Results of Tani et al (51).
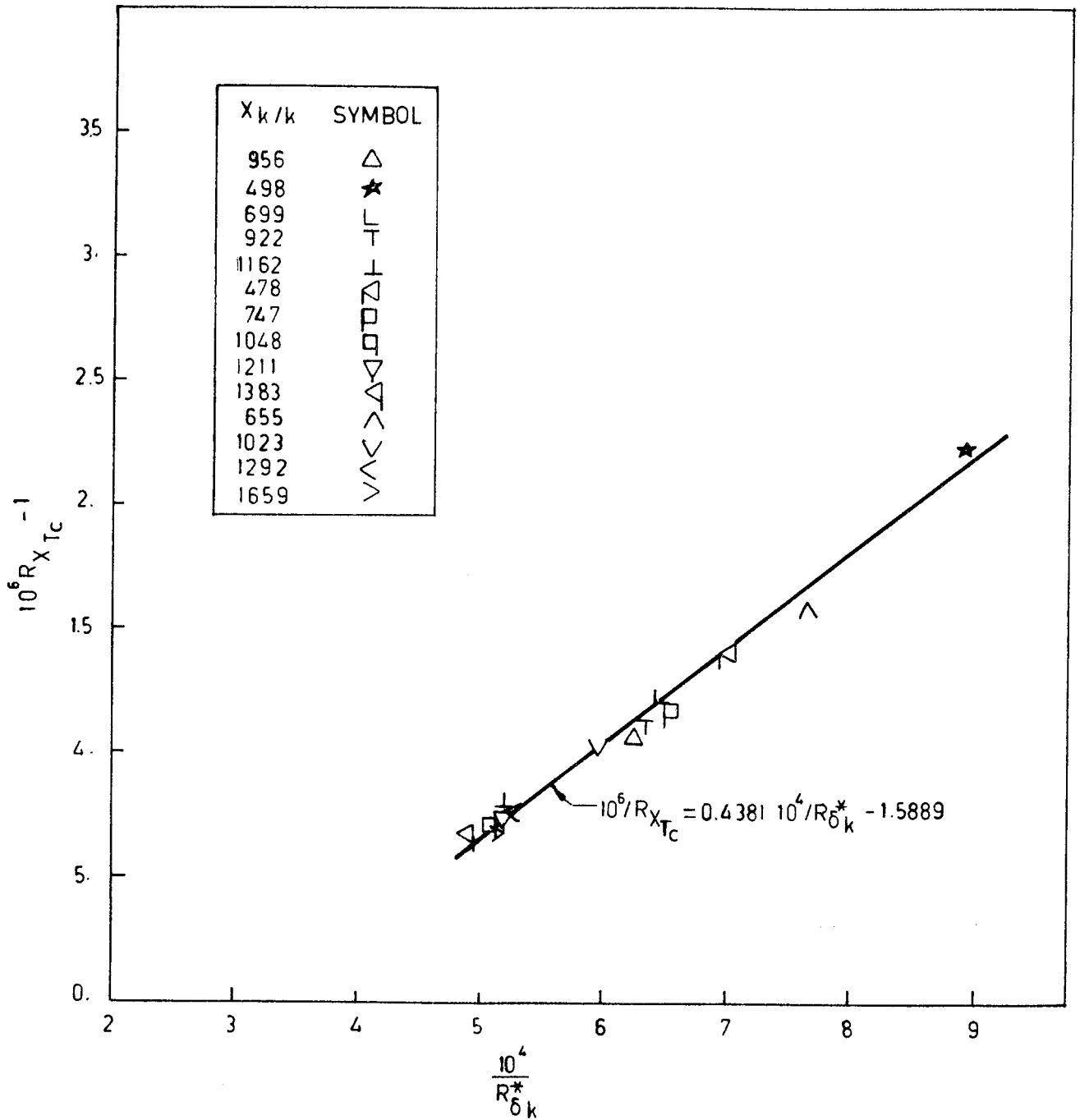
Fig.3.6.b Correlation Between $R_{x_{Tc}}$ and $R_{\delta^*_k}$ for the Trip Wire Data
of Tani et al (51).
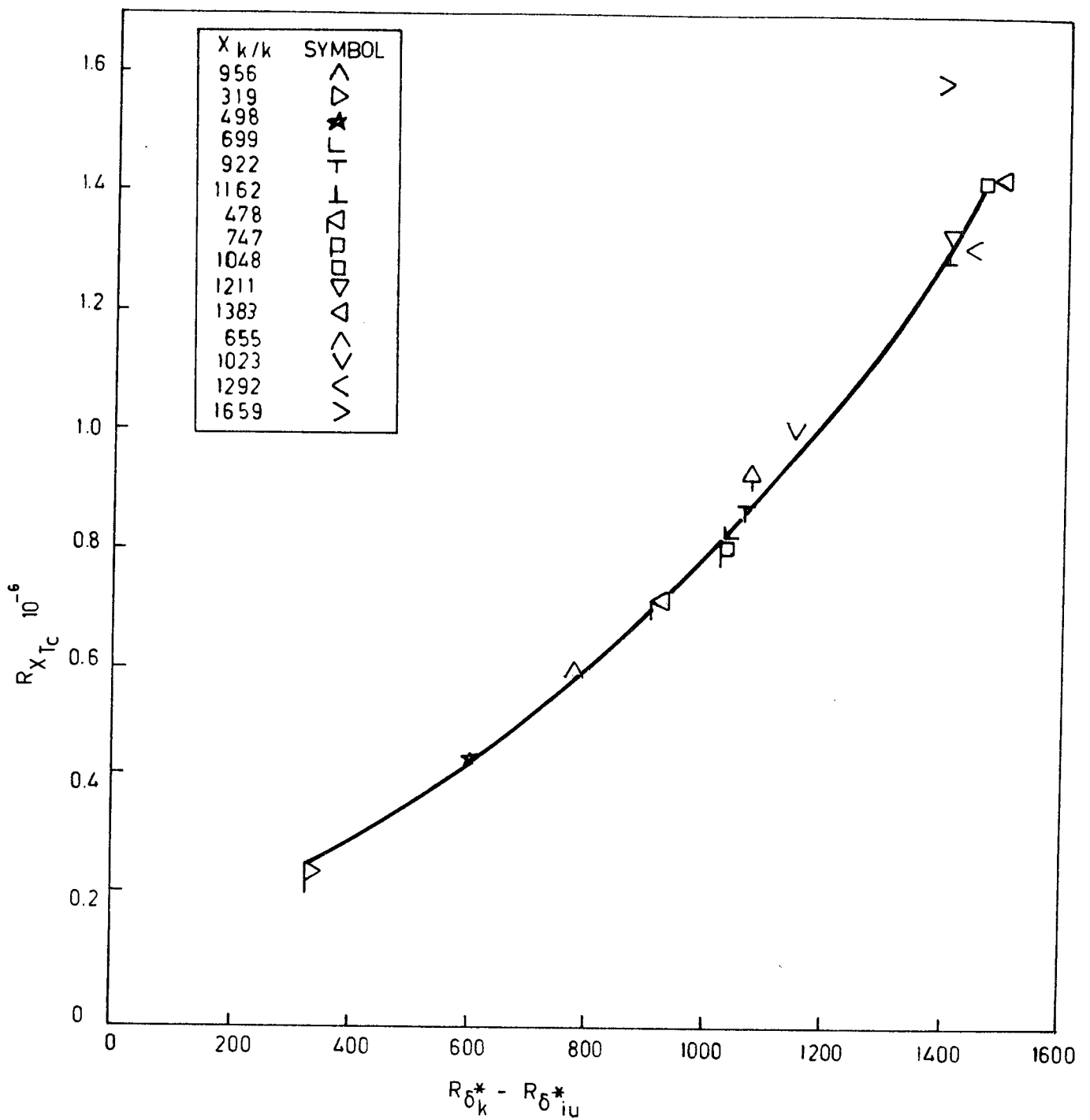
Fig.3.7.a Variation of $R_{x_{T_c}}$ With $\psi = R_{\delta^*_k} - R_{\delta^*_{i_u}}$ for a Trip Wire on a Flat Plate Under Zero Pressure Gradient, Based on the Experimental Results of Tani et al (51).

$X_{k/k}$	SYMBOL
956	∧
498	☆
699	L
922	T
1162	⊥
478	◁
747	□
1048	□
1211	▽
1383	◁
655	∧
1023	<
1292	<
1659	>

$$\frac{10^6}{R_{X_{Tc}}} = 0.1825 \ \frac{10^4}{\psi} - 0.4384$$

Vertical axis: $10^6 (R_{X_{Tc}})^{-1}$

Horizontal axis: $\dfrac{10^4}{R_{\delta_k^*} - R_{\delta_{iu}^*}}$
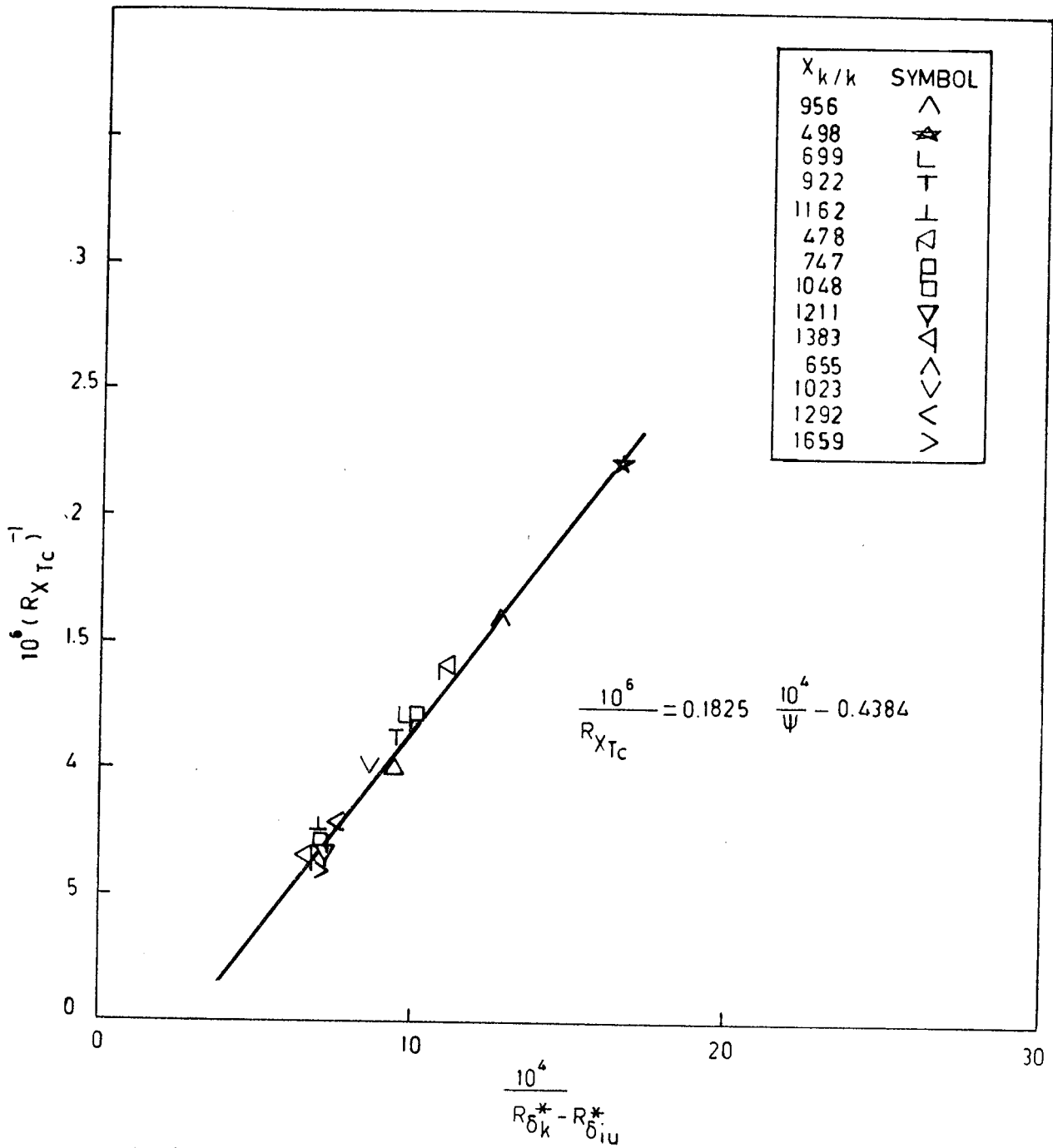
Fig.3.7.b Correlation Between $R_{X_{Tc}}$ and ψ for the Trip Wire Data of Tani et al (51).
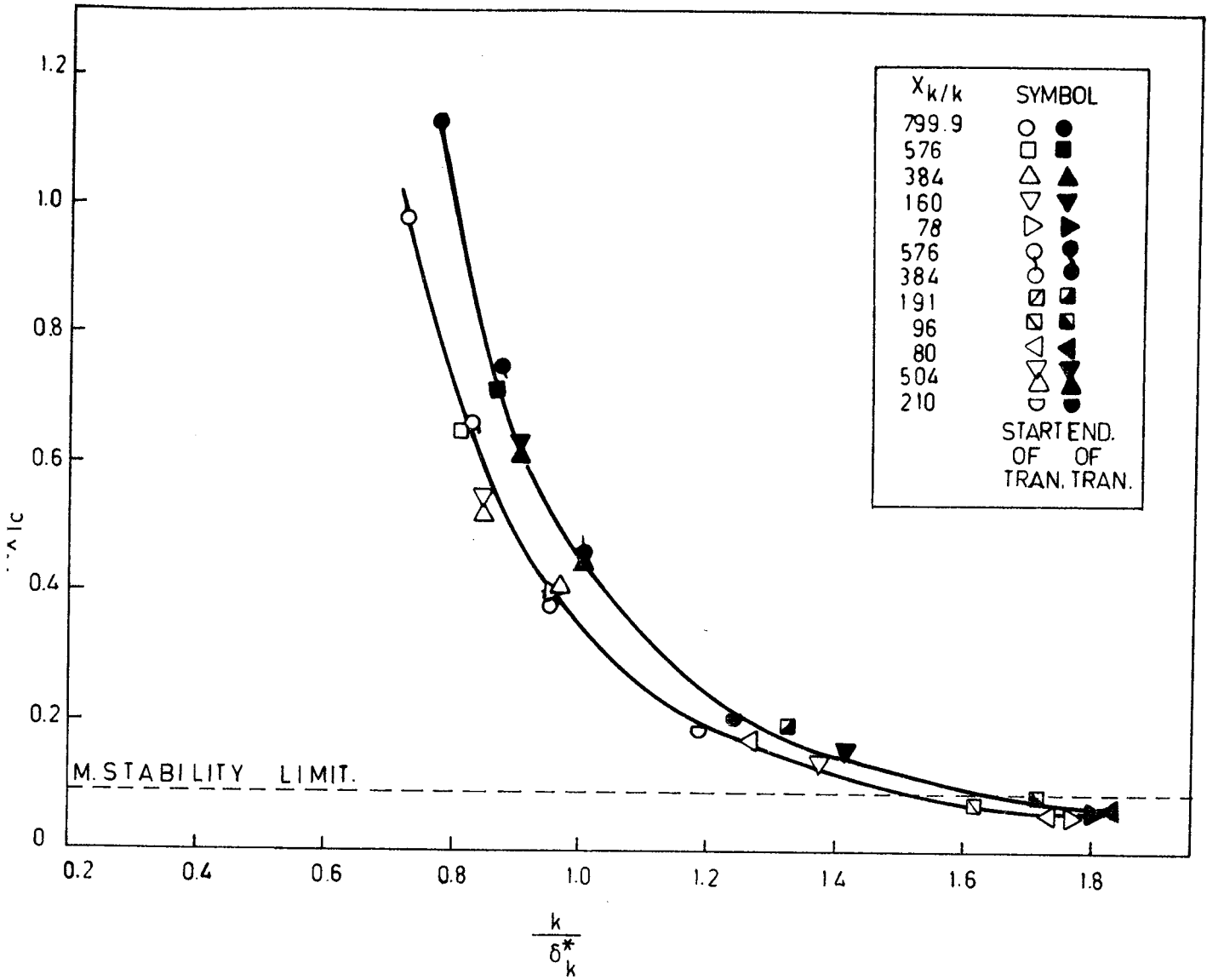
Fig. 3.8.a Variation of $R_{x_{Tcs}}$ and $R_{x_{Tce}}$ With $\dfrac{k}{\delta^*_k}$ for a Sphere

on a Flat Plate With $\lambda_{\theta} = 0$, Based on the Experimental Results

of Hall, Göksel, Yeğen, Albayrak.

$X_{k/k}$	SYMBOL	
799.9	○	●
576	□	■
384	△	▲
160	▽	▼
78	▷	◀
576	◐	●
384	▣	▣
191	▤	▣
96	◁	◀
80	⋈	◪
504		
210	▽	●

START END.
OF OF
TRAN. TRAN.

$\log_{10} R_{X_{Tce}} = -3.3378 \log_{10}(\frac{k}{\delta_k^*}) + 5.6638$

$\log_{10} R_{X_{Tcs}} = -3.1228 \log_{10}(\frac{k}{\delta_k^*}) + 5.5348$
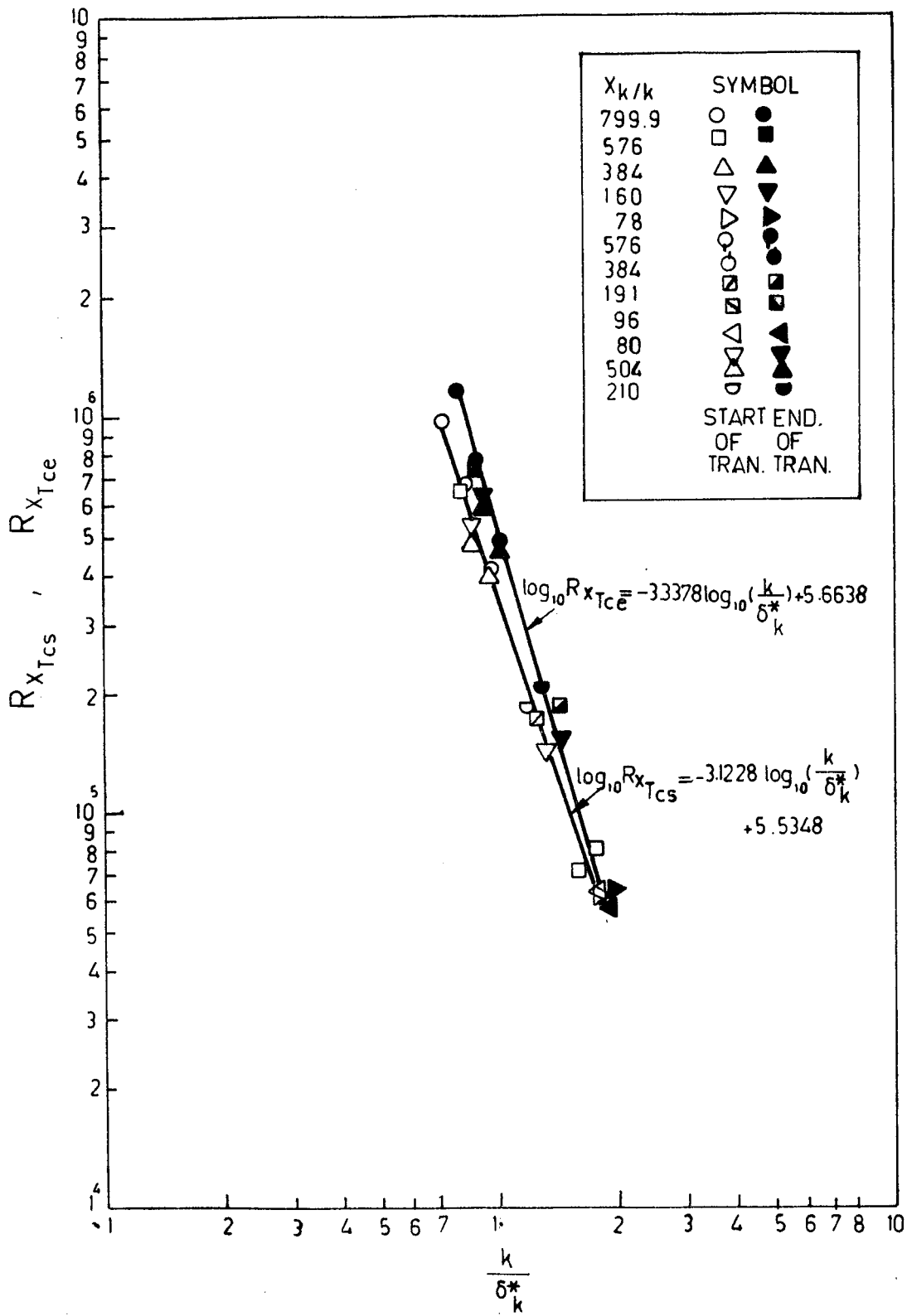
Fig.3.8.b Correlations Between $R_{X_{Tcs}}$, $R_{X_{Tce}}$ and $\frac{k}{\delta_k^*}$ for a Sphere on a Flat Plate With $\lambda_\theta = 0$,

$X_{k/k}$	SYM.	$X_{k/k}$	SYMBOL	
		799	○	●
		576	□	■
956	△	384	△	▲
319	▷	159.9	▽	▼
498	☆	79	▷	▶
922	T	576	○	●
1162	⊥	384	○	●
1383	◁	191	▨	▨
1211	▽	96	▨	▨
655	∧	80	◁	◀
1023	∨	504	⊠	▼
1292	<	210	○	●
1659	>		ST.	EN.
WIRE		SPHERE		

vertical axis: $R_{x_{Tc}} 10^{-5}$

horizontal axis: $\dfrac{k}{\delta^*_k}$
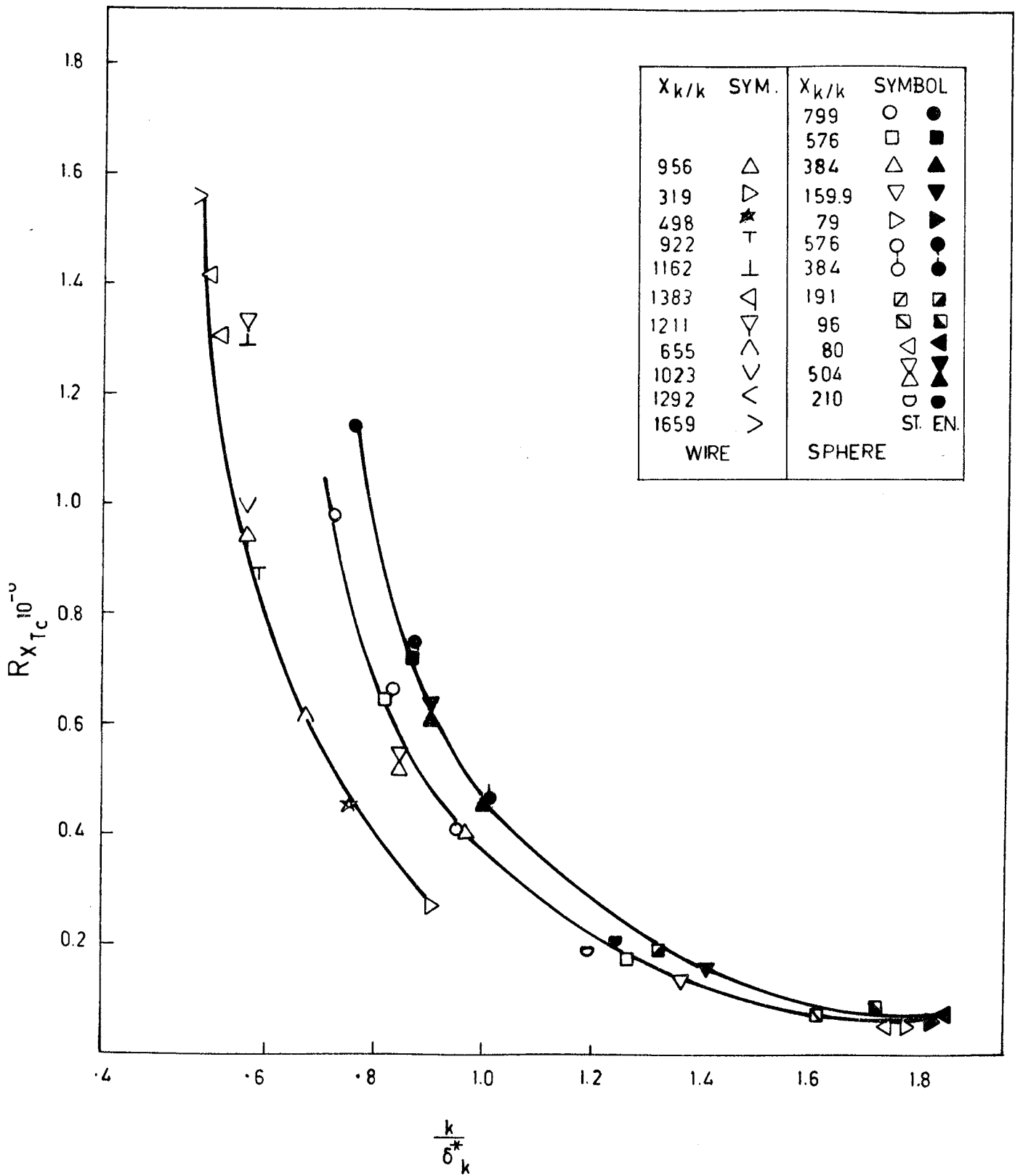
Fig. 3.9 Variation of $R_{x_{Tc}}$ With $\dfrac{k}{\delta^*_k}$ for Trip Wire and Sphere Results, Based on the Experiments of Tani et al and Göksel, Hall, Yeğen, Albayrak.

90
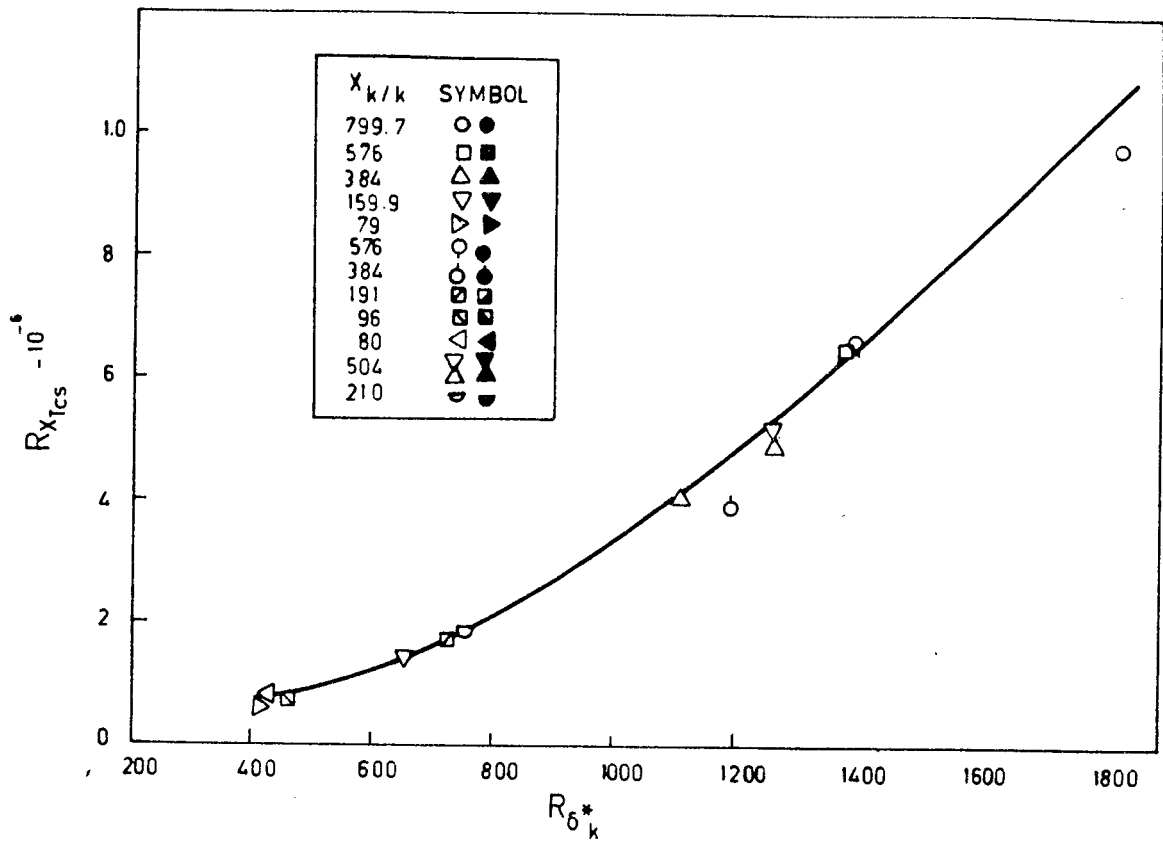
Fig.3.10.a Variation of $R_{x_{Tcs}}$ With $R_{\delta^*_k}$ for a Spherical Roughness Element on a Flat Plate With $\lambda_\theta = 0$, Based on the Results of Göksel, Hall, Yeğen, Albayrak.
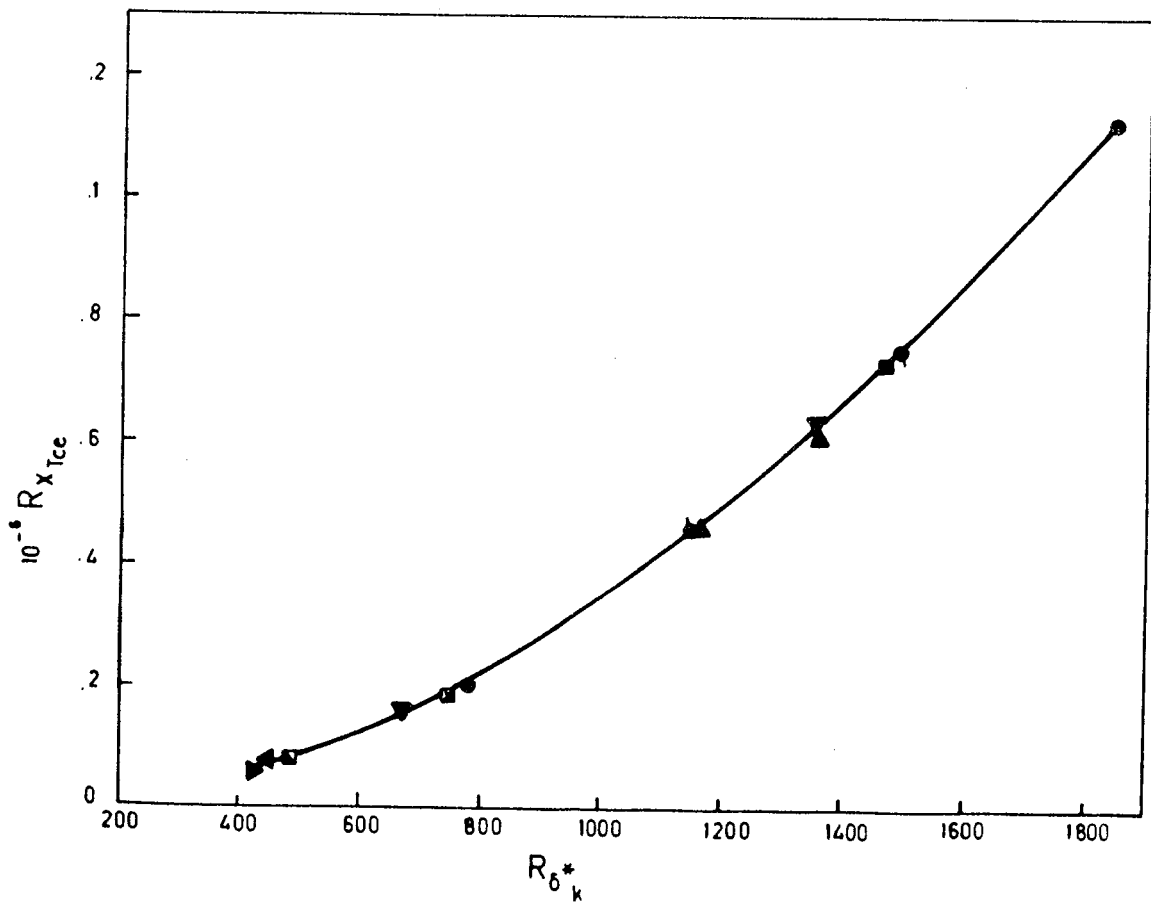
Fig.3.10.b Variation of $R_{x_{Tce}}$ With $R_{\delta^*_k}$ for a Spherical Roughness Element on a Flat Plate With $\lambda_\theta = 0$, Based on Results of Göksel, Hall, Yeğen, Albayrak

91
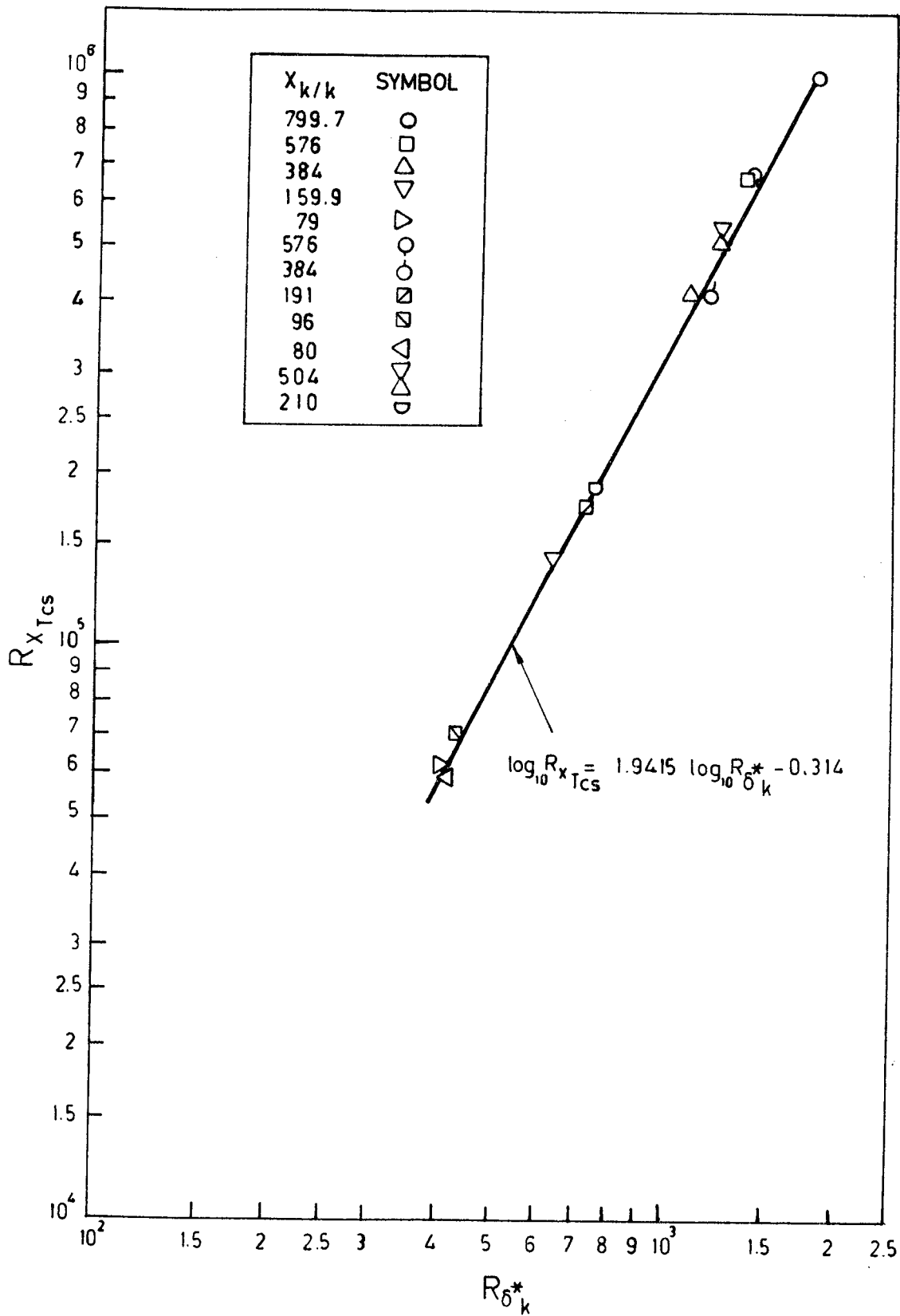
Fig.3.11.a Correlation Between $R_{x_{Tcs}}$ and $R_{\delta^*_k}$ for a Spherical Roughness Element on a Flat Plate With $\lambda_\theta = 0$.

92
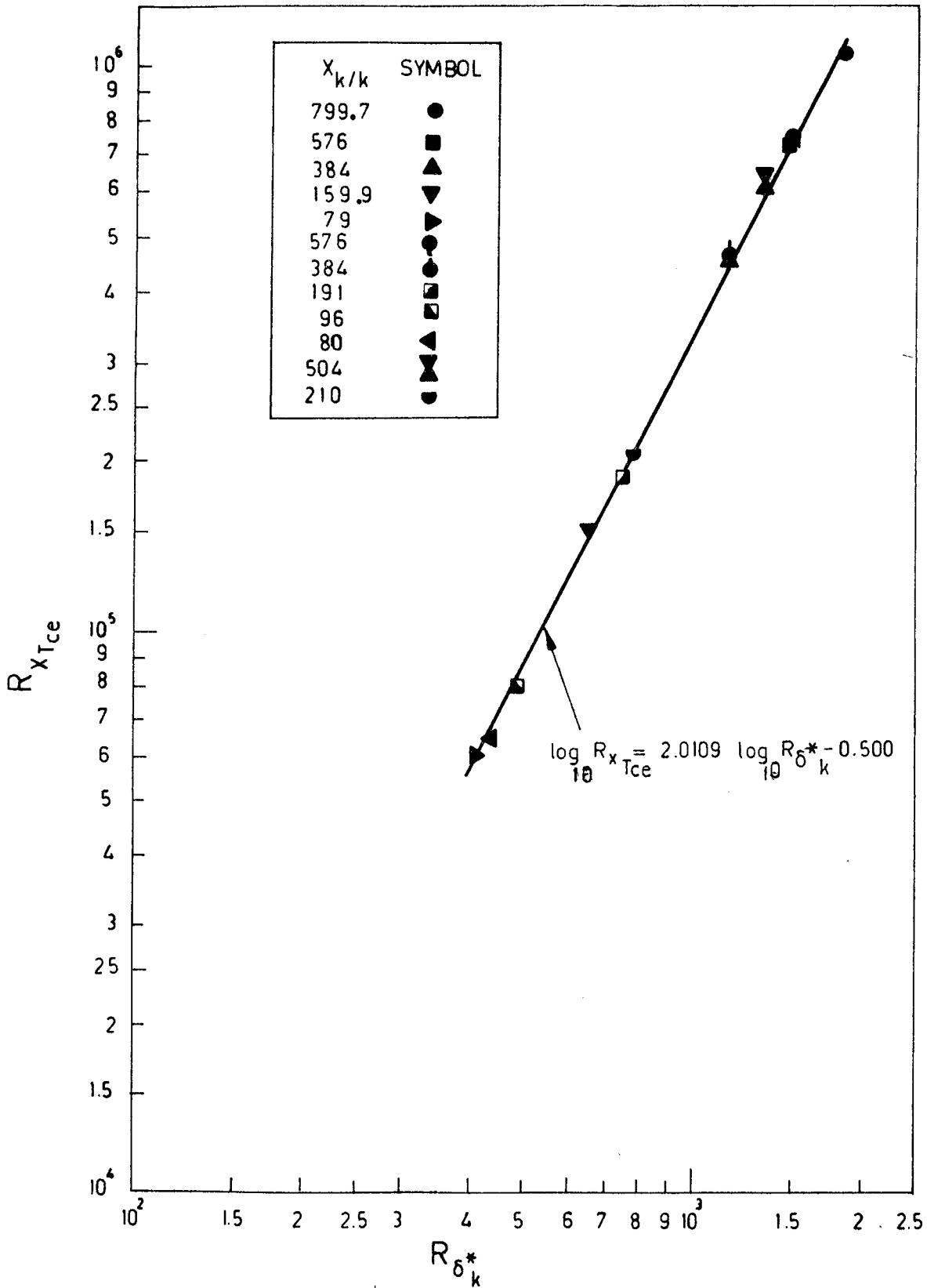
Fig.3.11.b Correlation Between $R_{x_{Tce}}$ and $R_{\delta^*_k}$ for a Spherical Roughness Element on a Flat Plate With $\lambda_\theta = 0$.
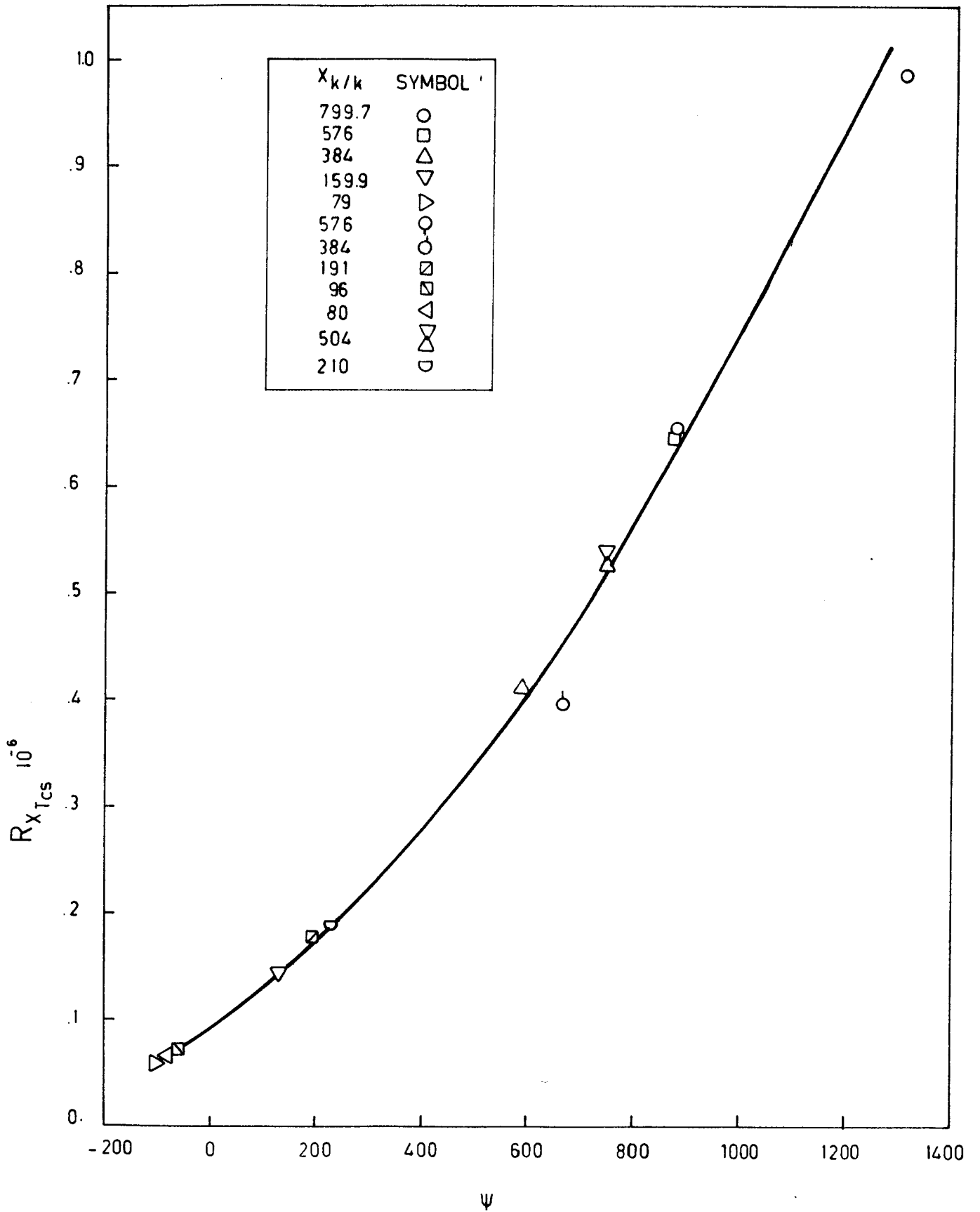
Fig.3.12.a The Influence of ψ on $R_{x_{Tcs}}$ for a Sphere on a Flat Plate

With $\lambda_{\Theta} = 0$, Based on the Results of Göksel, Hall, Yeğen, Albayrak.
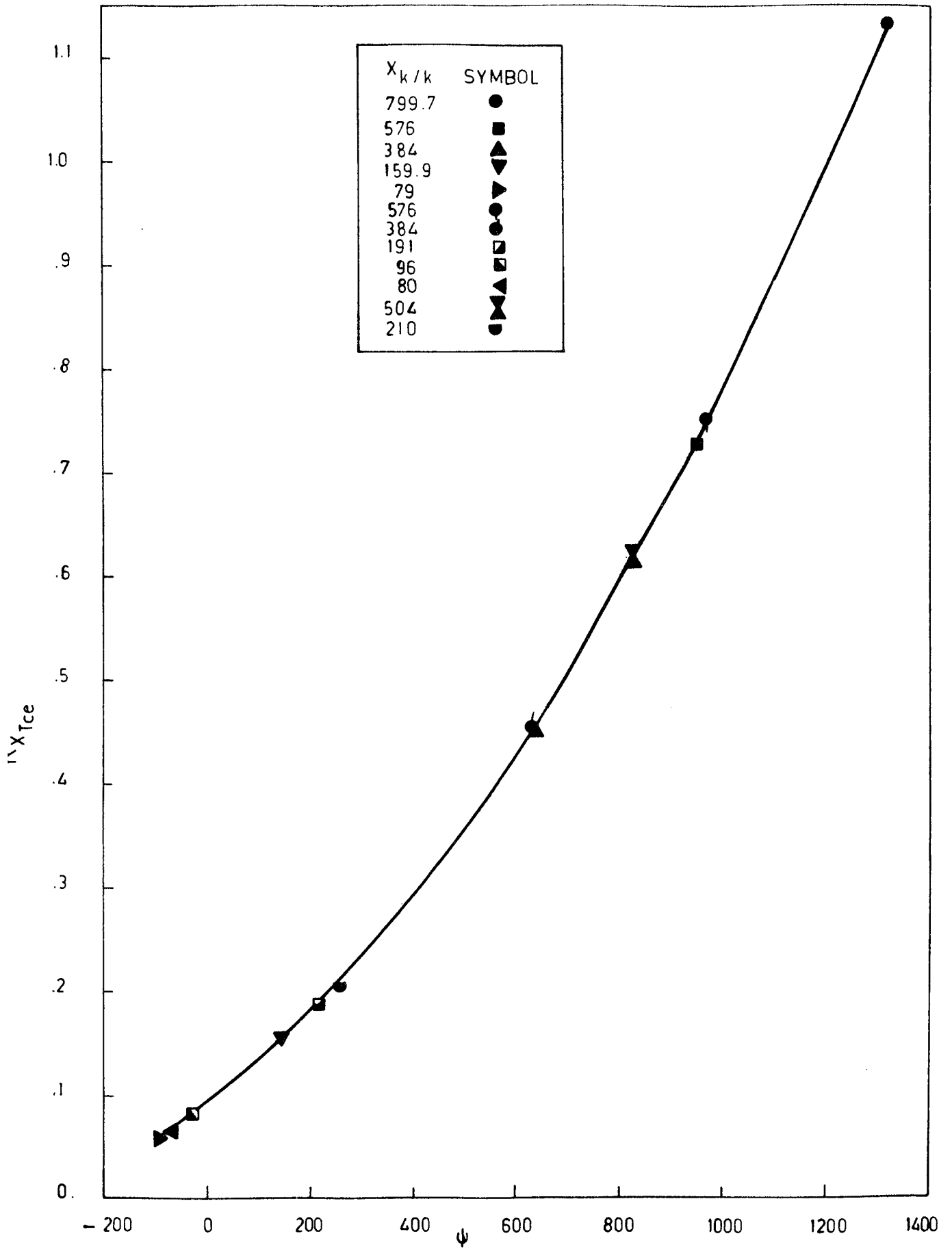
Fig.3.12.b The Influence of ψ on $R_{x_{Tce}}$ for a Sphere on a Flat Plate
With $\lambda_Q = 0$, Based on the Results of Göksel, Hall, Yeğen, Albayrak.

95
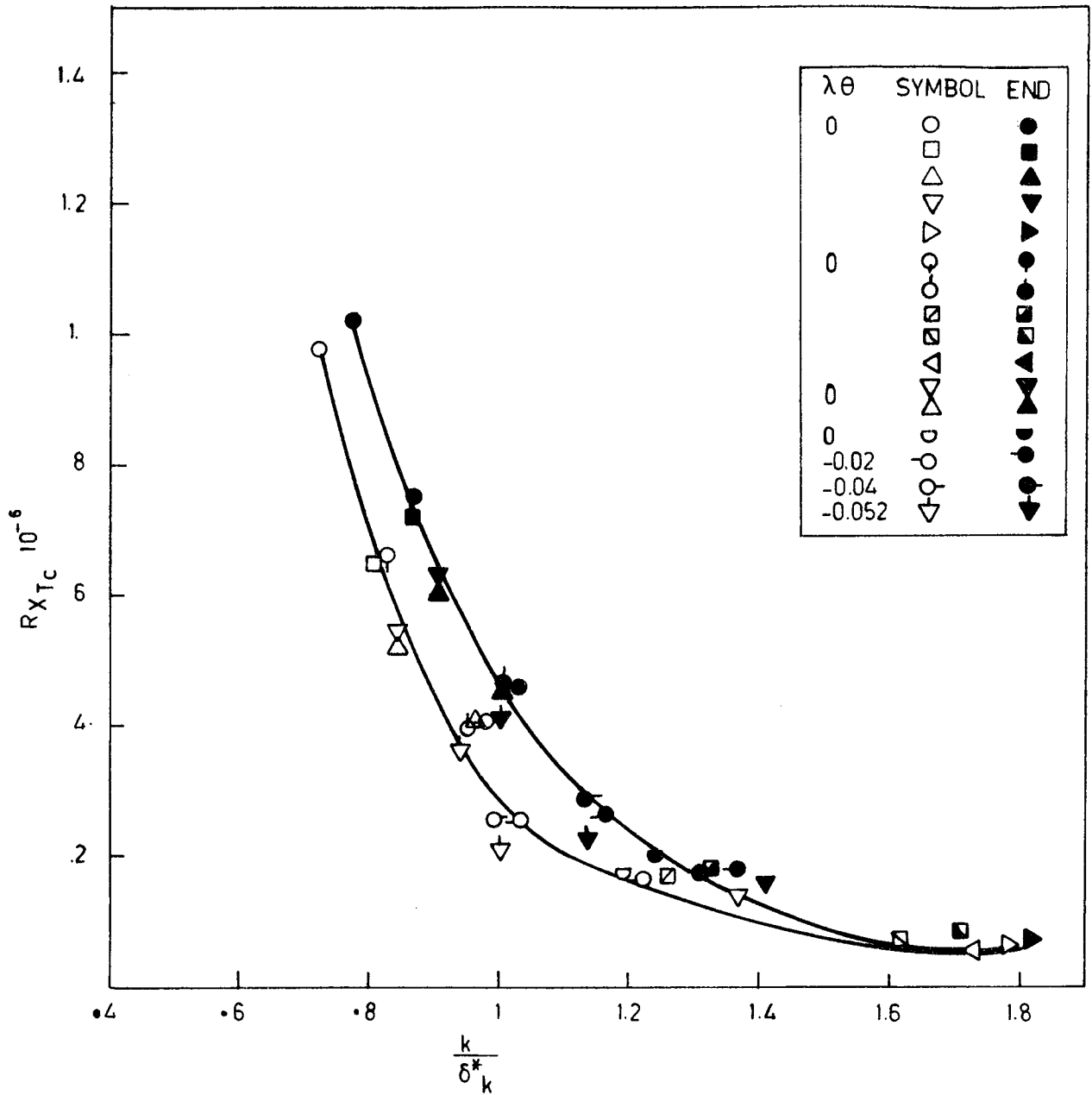
Fig. 3.13   Variation of $R_{x_{Tcs}}$, $R_{x_{Tce}}$ With $\dfrac{k}{\delta^*_k}$ Behind a Sphere

on a Flat Plate Under Zero and Adverse Pressure Gradients,

Based on the Experimental Results of Göksel, Yeǧen.
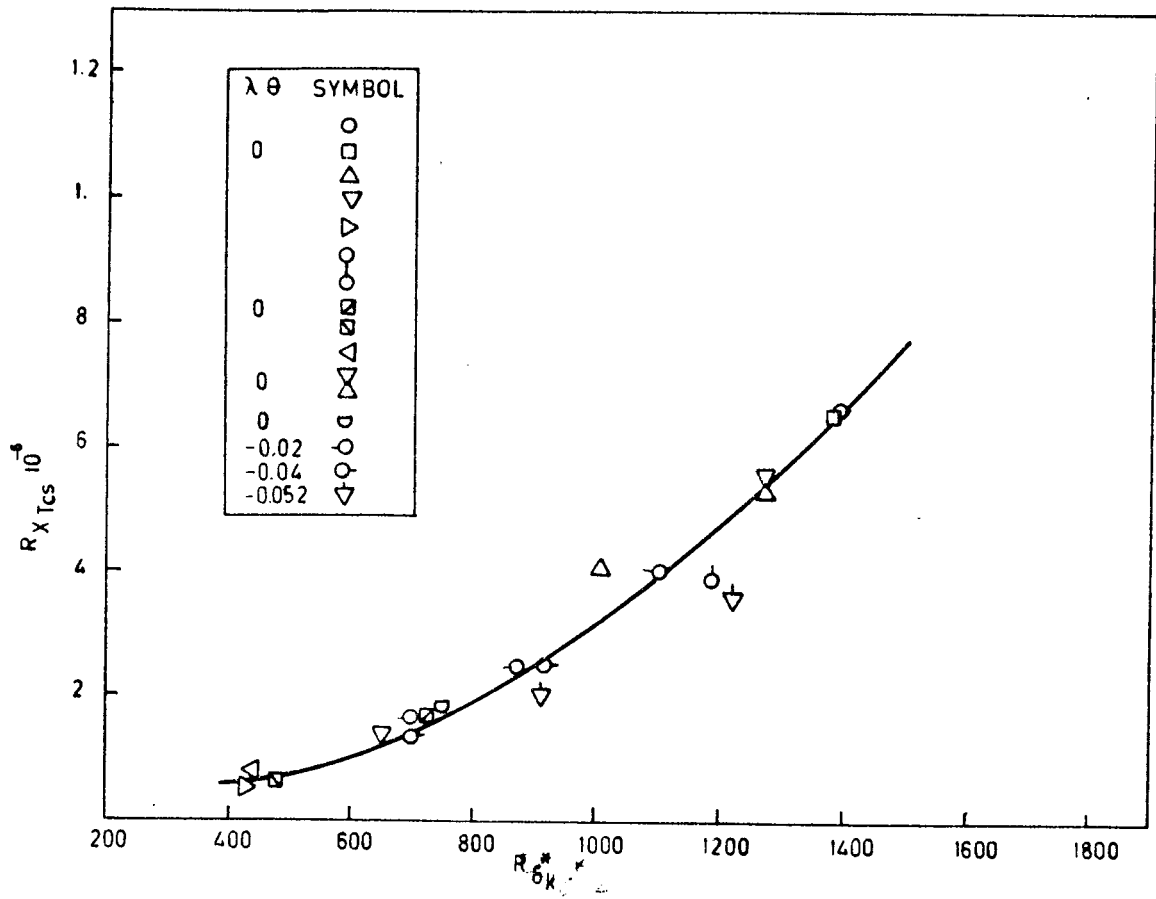
Fig.3.14.a   Variation of $R_{x_{Tcs}}$ With $R_{\delta^*_k}$ for a Spherical Roughness Element on a Flat Under Zero and Adverse Pressure Gradients, Based on the Experimental Results of Göksel, Yeğen.
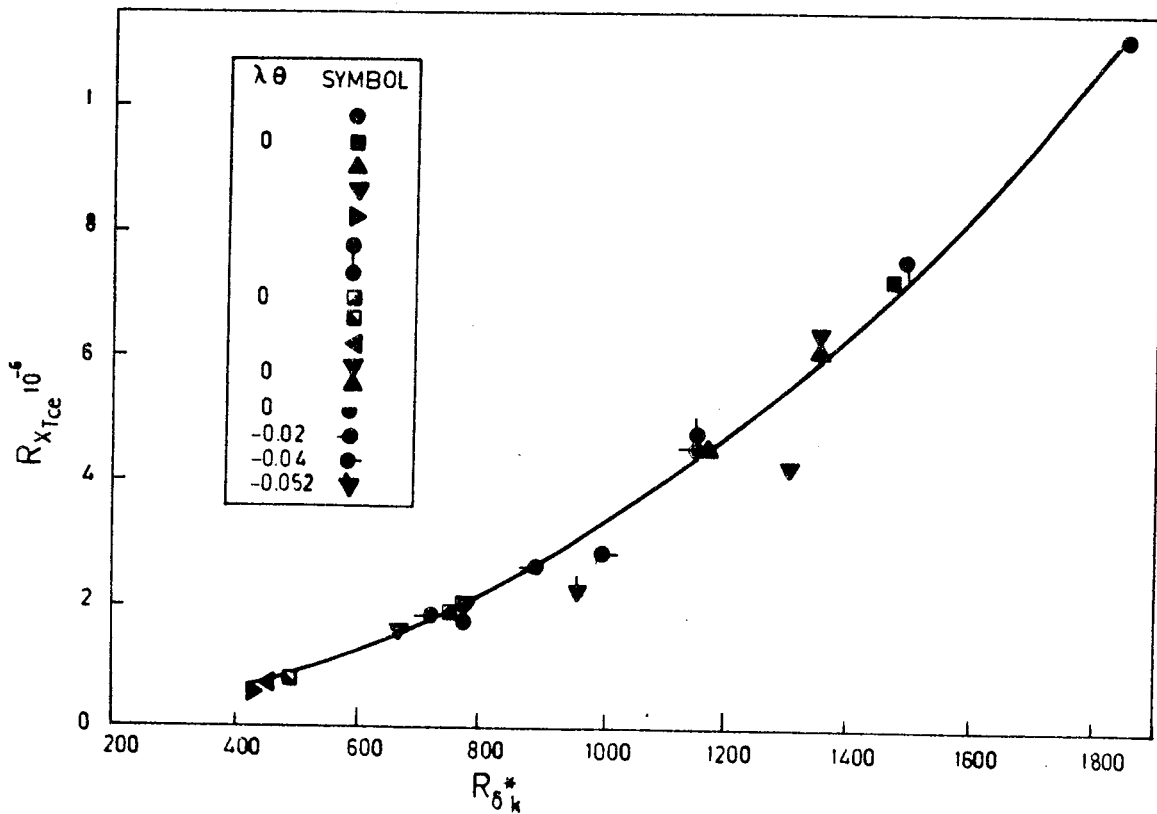
Fig.3.14.b   Variation of $R_{x_{Tce}}$ With $R_{\delta^*_k}$ for a Spherical Roughness Element on a Flat Plate Under Zero and Adverse Pressure Gradients, Based on the Experimental Results of Göksel, Yeğen.

97
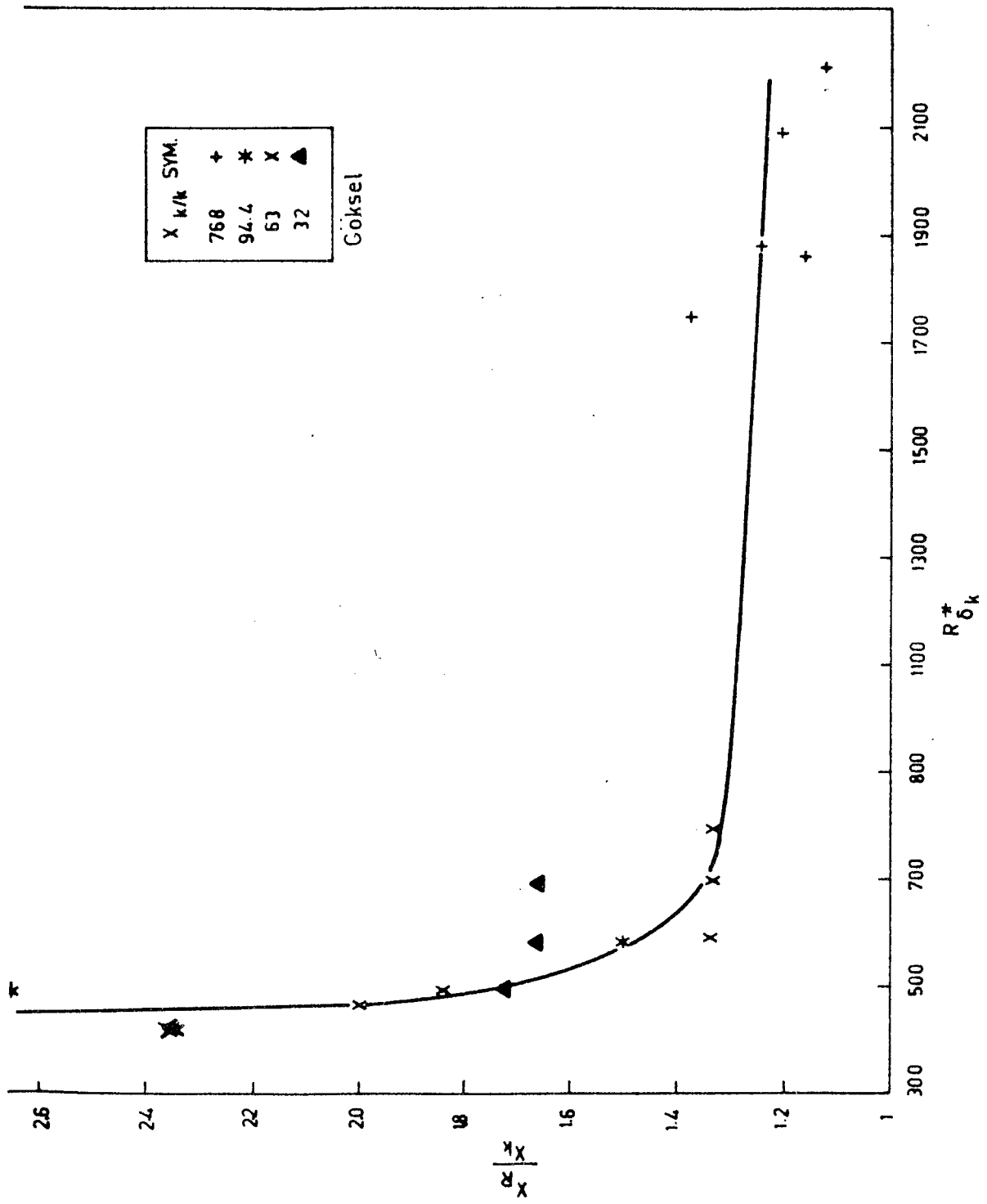
Fig. 4.1 Variation of $\dfrac{X_R}{X_k}$ With $R_{\delta_k}^*$ Behind a Spherical Roughness
Element on a Flat Plate With $\lambda_\Theta = 0$.
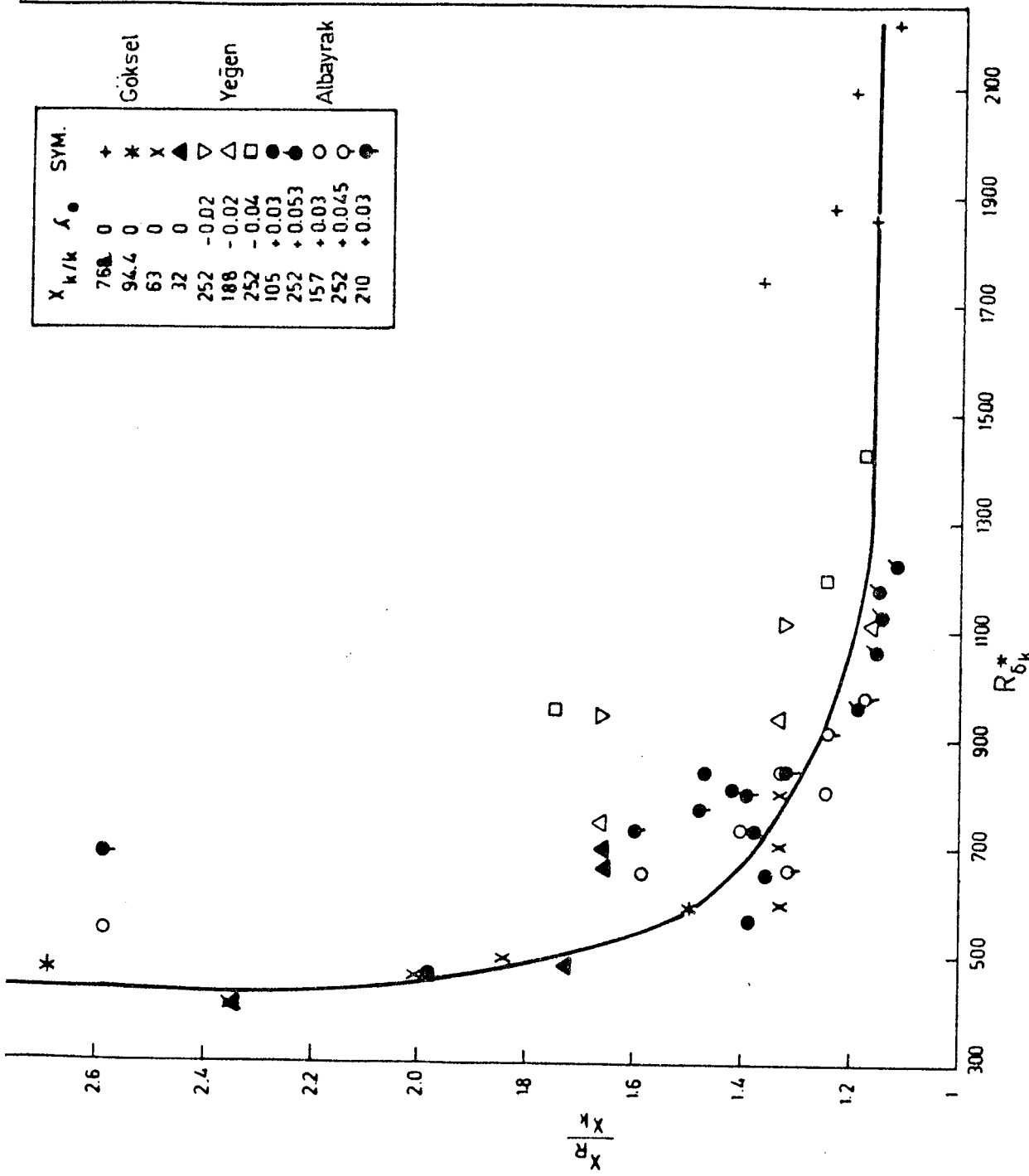
Fig.4.2 Variation of $\dfrac{X_R}{X_k}$ With $R_{\delta_k}^*$ Behind a Spherical Roughness Element on a Flat Plate With $-0.04 \leq \lambda_0 \leq +0.053$.
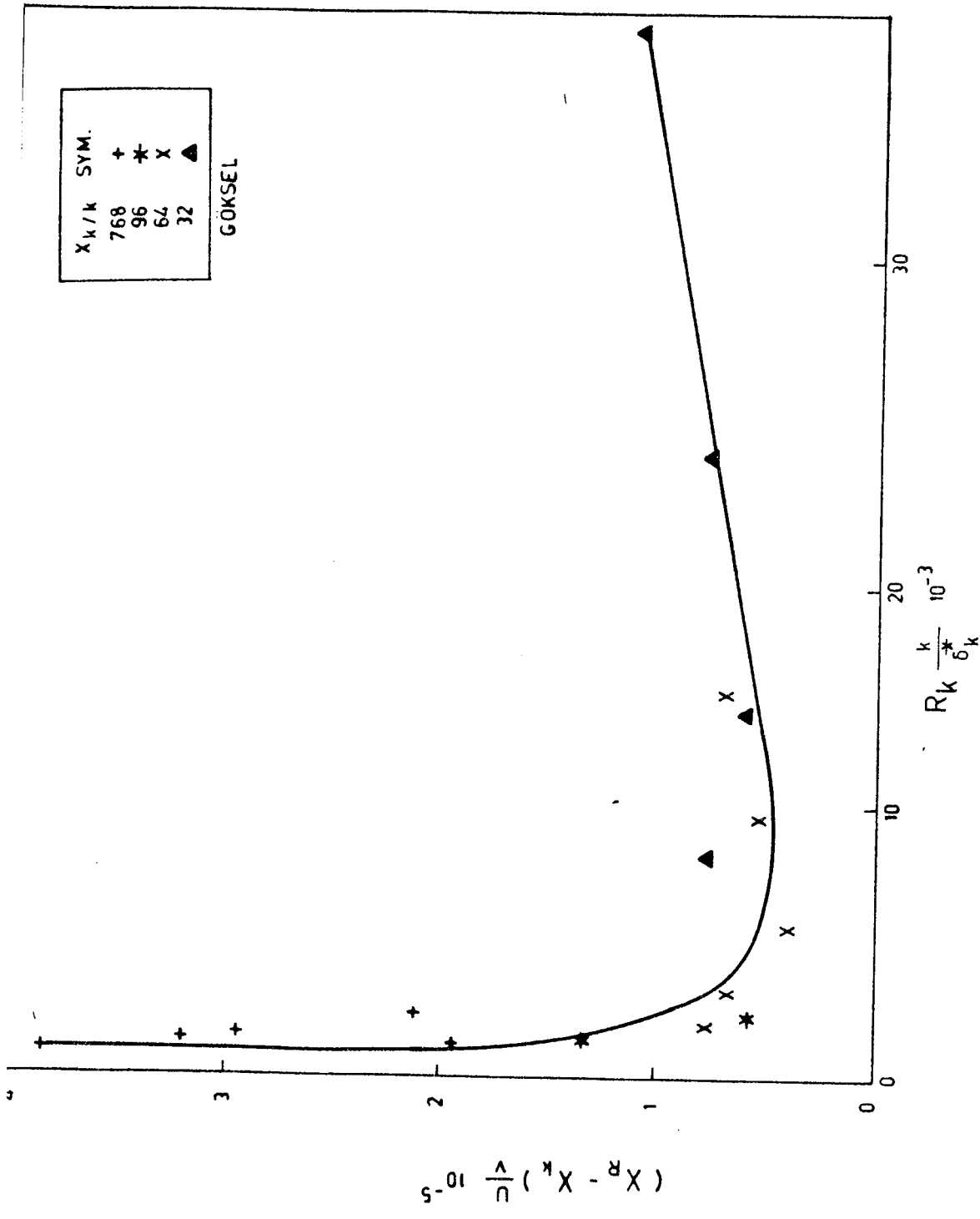
Fig.4.3 Variation of R_{X_L} With R_k $\dfrac{k}{\delta^*_k}$ Behind a Spherical Roughness Element on a Flat Plate
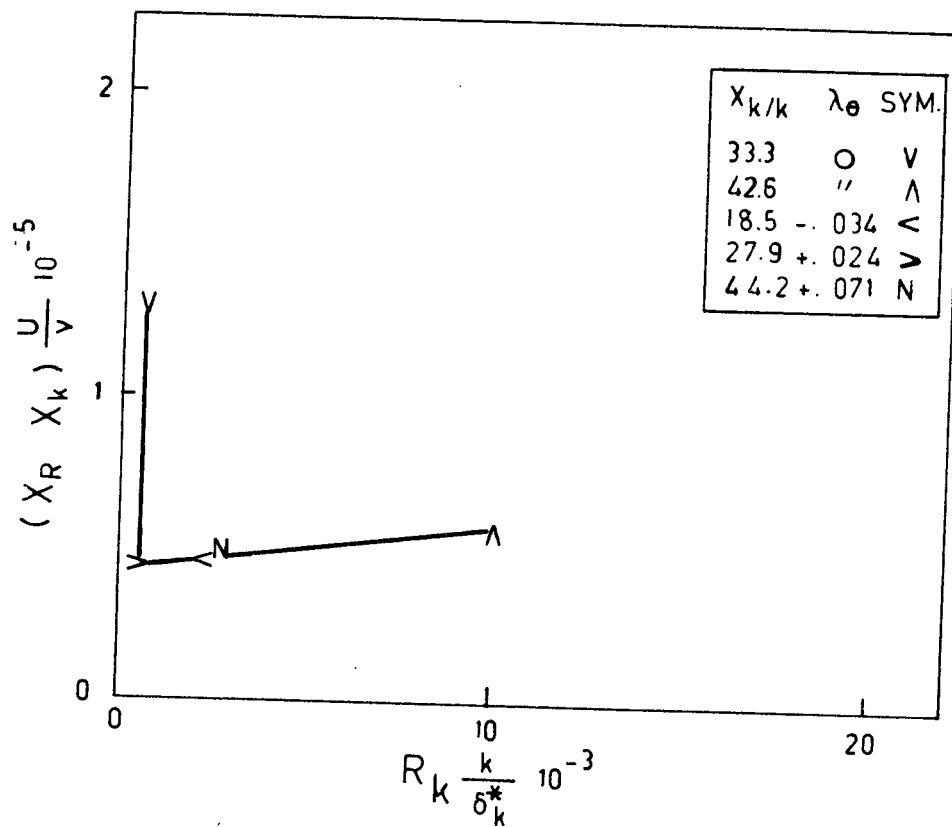
Fig.4.4   Variation of $^R X_L$ With $R_k \dfrac{k}{\delta_k^*}$ Behind a Trip Wire on a Flat Plate Under Variable Pressure Gradients, Based on Hall's Results.
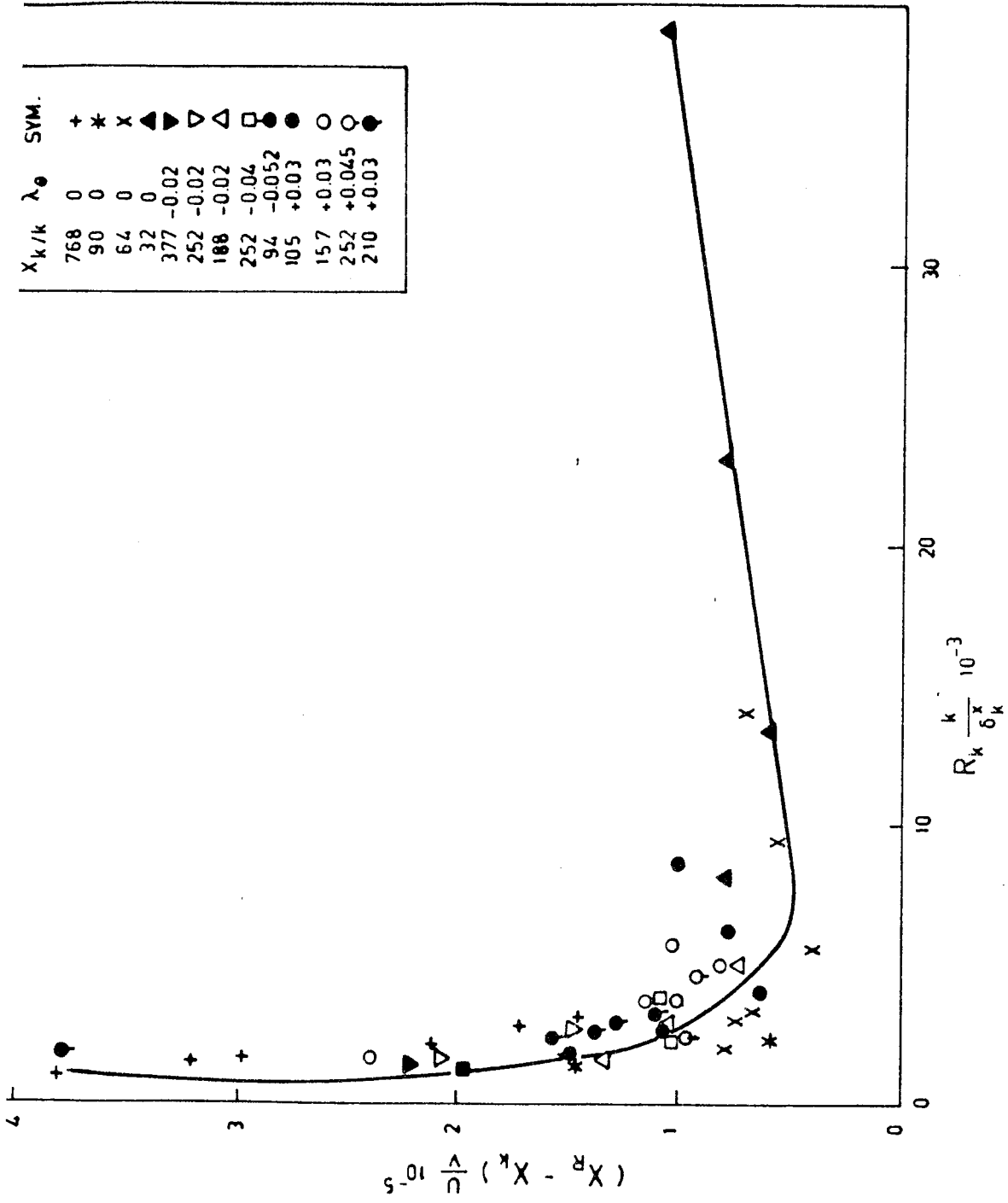
Fig.4.5 Variation of R_{X_L} With $R_k \dfrac{k}{\delta_k^*}$ Behind a Spherical Roughness

Element on a Flat Plate With $-0.052 \leqslant \lambda_{\theta_k} \leqslant +0.045$. Based
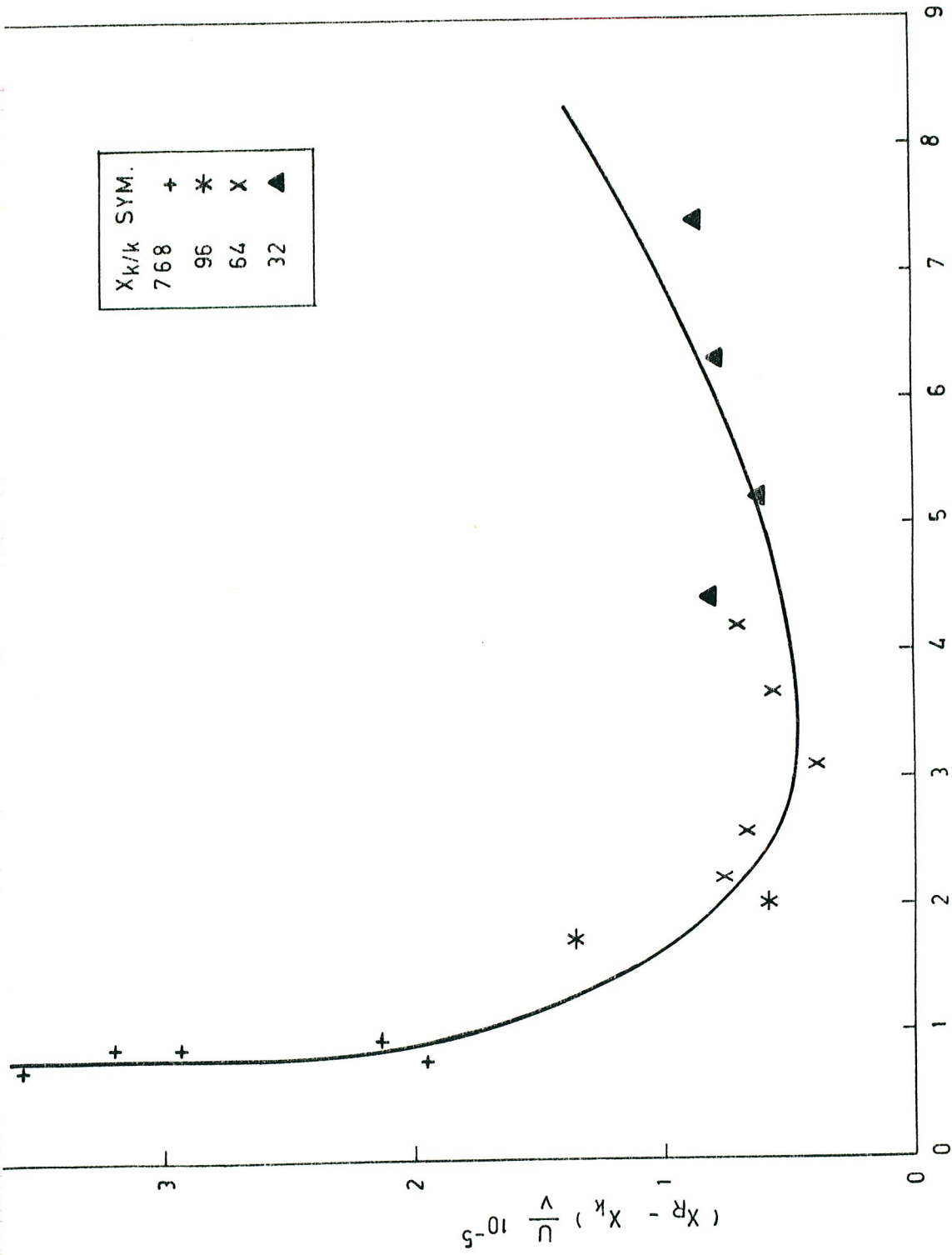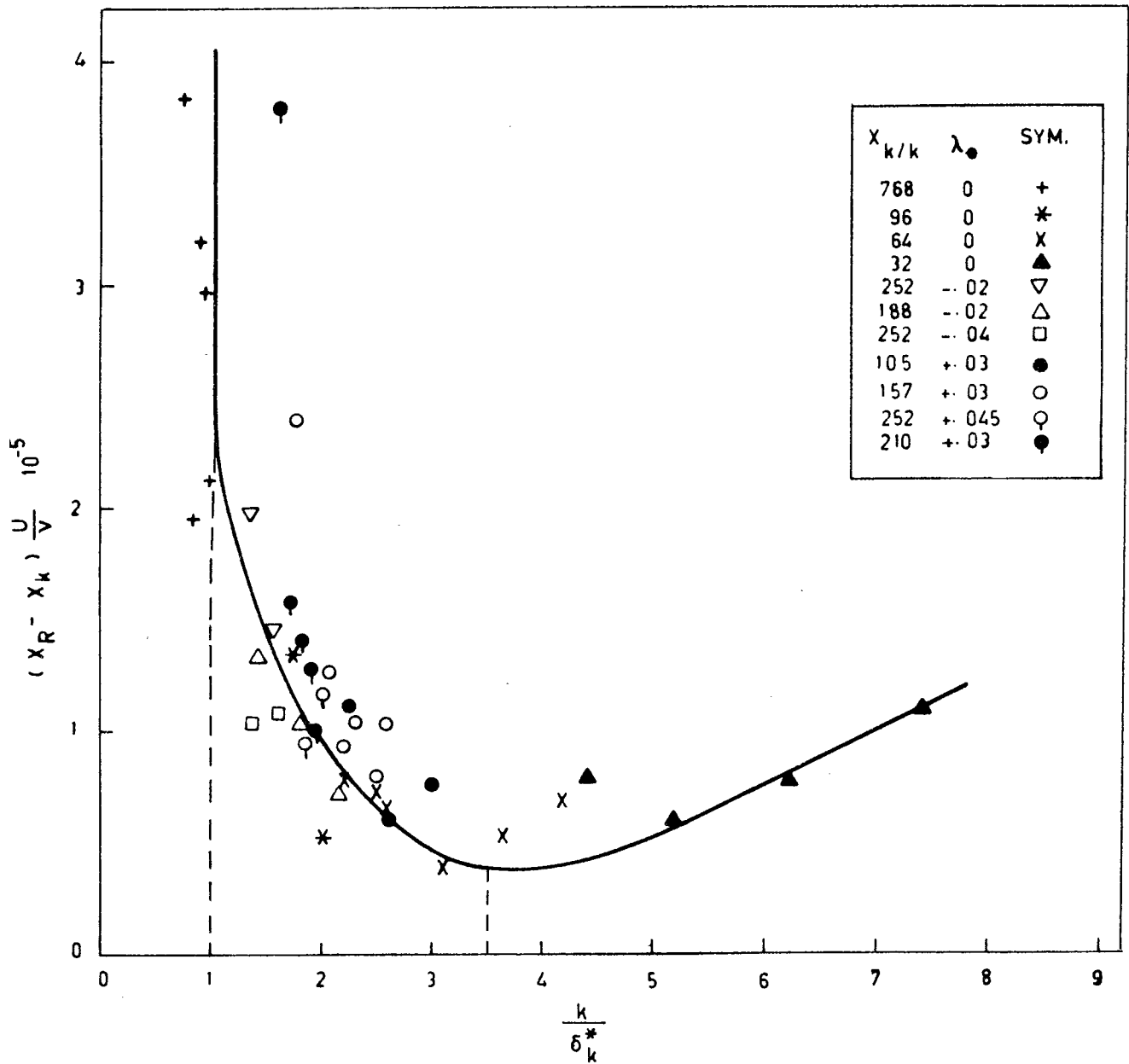
on Experimental Results of Göksel, Yeğen, Albayrak.

Fig.4.6 Variation of R_{X_L} with $\frac{k}{\delta_k^*}$ Behind a Spherical Roughness

Element on a Flat Plate With $\lambda_\theta = 0$

$X_{k/k}$	$\lambda_\bullet$	SYM.
768	0	+
96	0	✱
64	0	✗
32	0	▲
252	-.02	▽
188	-.02	△
252	-.04	□
105	+.03	●
157	+.03	○
252	+.045	○
210	+.03	◐

Fig.4.7 Variation of R_{X_L} With $\dfrac{k}{\delta^*_k}$ Behind a Spherical Roughness

Element on a Flat Plate With $- 0.04 \leqslant \lambda_{\theta_k} \leqslant + 0.045$, Based on
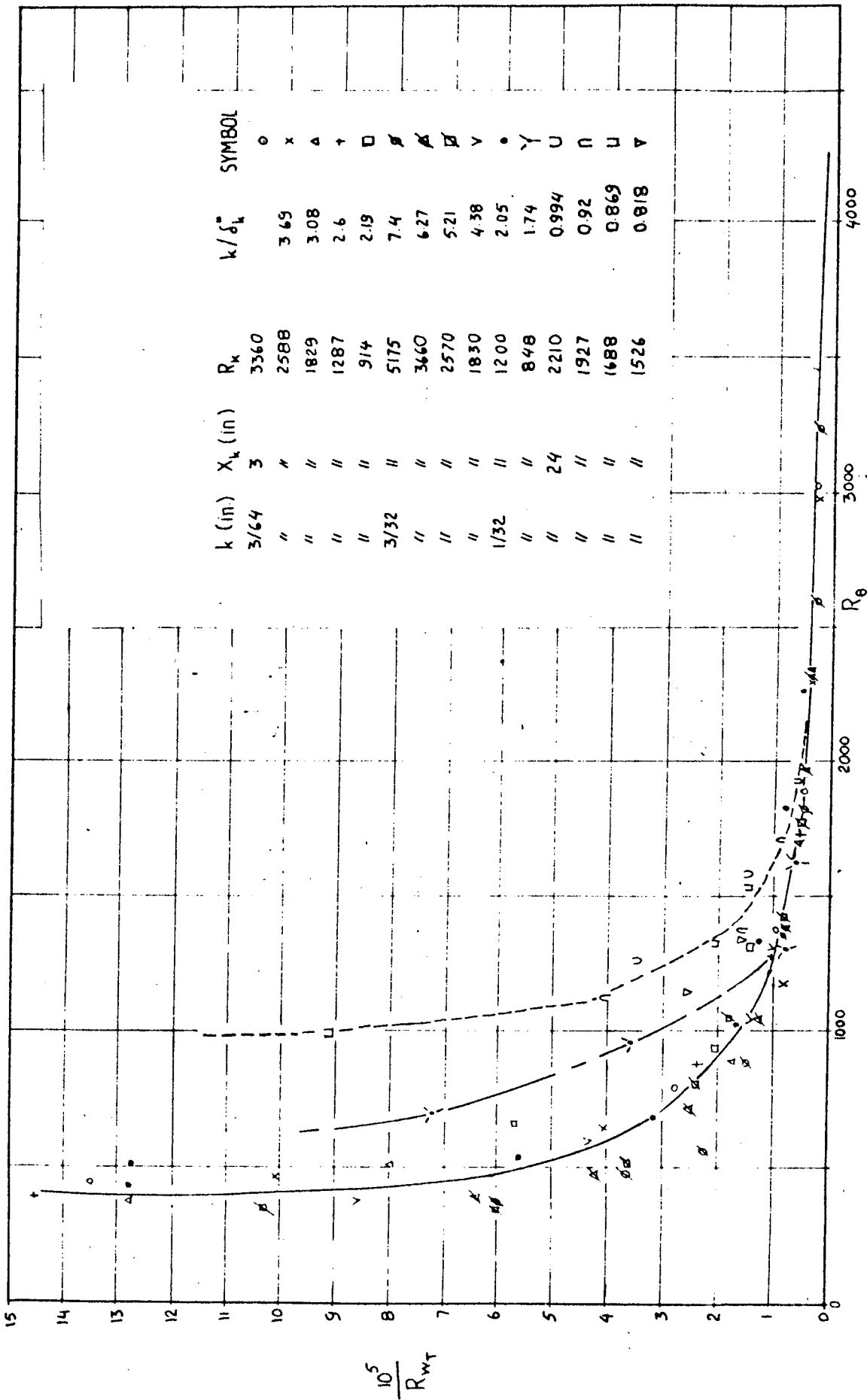
the Experimental Results of Göksel, Yeğen, Albayrak.

k (in)	X_k (in)	R_x	k/δ_k^*	SYMBOL
3/64	3	3360	3.69	o
"	"	2588	3.08	x
"	"	1829	2.6	Δ
"	"	1287	2.19	+
3/32	"	914	7.4	□
"	"	5175	6.27	Ø
"	"	3660	5.21	⋈
1/32	"	2570	4.38	⊠
"	"	1830	2.05	v
"	24	1200	1.74	•
"	"	848	0.994	Y
"	"	2210	0.92	∪
"	"	1927	0.869	∩
"	"	1688	0.818	⊐
"	"	1526		▷

$\dfrac{10^5}{R_{w_T}}$

R_θ

Fig. 4.8 Turbulent Wake Growth Behind an Isolated Spherical Roughness
Element From Reference 32.

105

k_{in}	xk_{in}	xk/k	R_k	SYMB
3/64	3	64	3360	○
			2588	X
			1829	△
			1287	+
			914	□
1/32	3	32	5175	∅
			3660	△
			2570	⊠
			1830	∨
1/32	3	96	1200	●
			848	Y
1/32	24	768	2210	∪
			1927	∩
			1688	⊔
			1526	▽
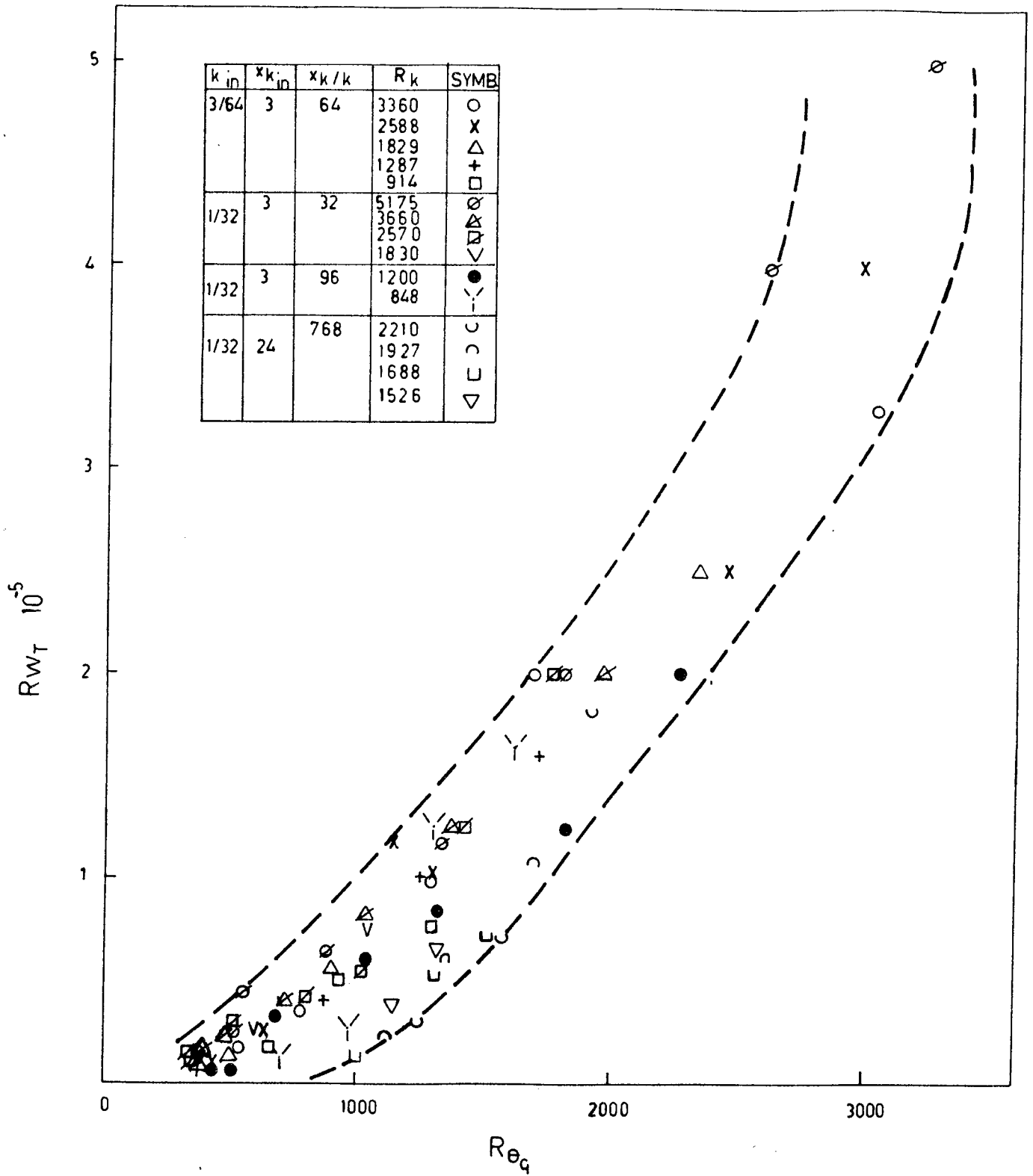
Fig. 4.9 Variation of R_{w_T} With R_{θ_q} Behind a Spherical Roughness

Element, Based on the Experimental Results of Göksel (32) .

k_{in}	$X_{k_{in}}$	$X_{k/k}$	R_k	SYM.
3/64	3	64	3360	◯
			2588	X
			1829	△
			1287	+
			914	□
3/32	3	32	5176	⌀
			3660	◬
			2570	⊠
			1830	V
1/32	3	96	1200	●
			848	⩗
1/32	24	768	2210	⋃
			1927	⋂
			1688	⊔
			1526	▽
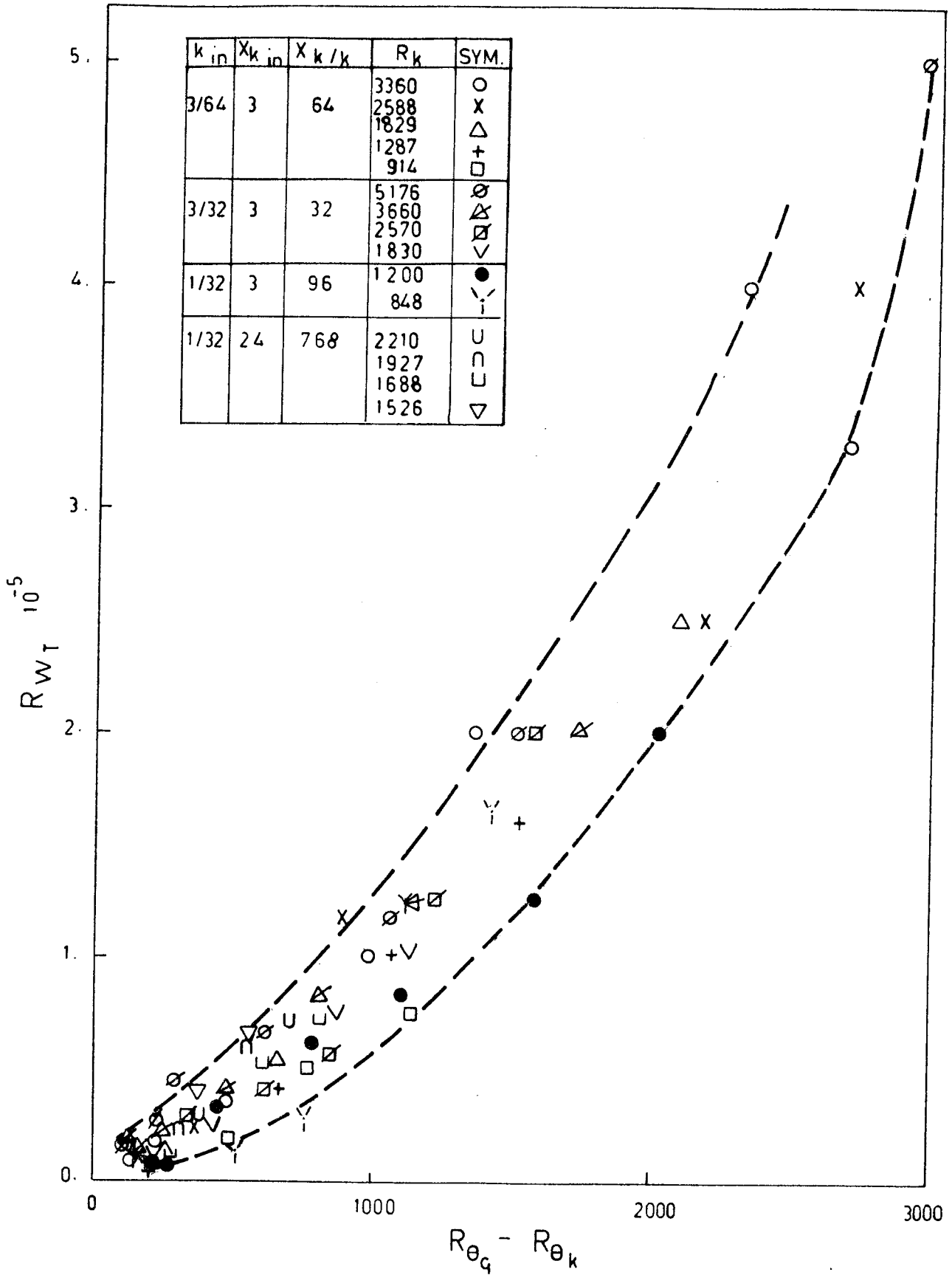
Fig.4.10 Variation of R_{W_T} With $(R_{\theta_q} - R_{\theta_k})$ Behind a Spherical Roughness Element.

The figure contains a log-log plot with the y-axis labeled R_{W_T} ranging from 10^1 to 10^6, and the x-axis labeled $(R_{\theta_q} - R_{\theta_k})$ ranging from 10^4 to beyond.

The fitted line equation shown:

$$\log_{10} R_{W_T} = 1.2414 \log_{10} (R_{\theta_q} - R_{\theta_k}) + 1.2449$$

k_{in}	$X_{k_{in}}$	$X_{k/k}$	R_k	SYM.
3/64	3	64	3360 2588 1829 1287 914	O X △ + □
3/32	3	32	5176 3660 2570 1830	∅ ⋈ ⊠ V
1/32	3	96	1200 848	● Ÿ
1/32	24	768	2210 1927 1688 1526	U ∩ ⊔ ▽
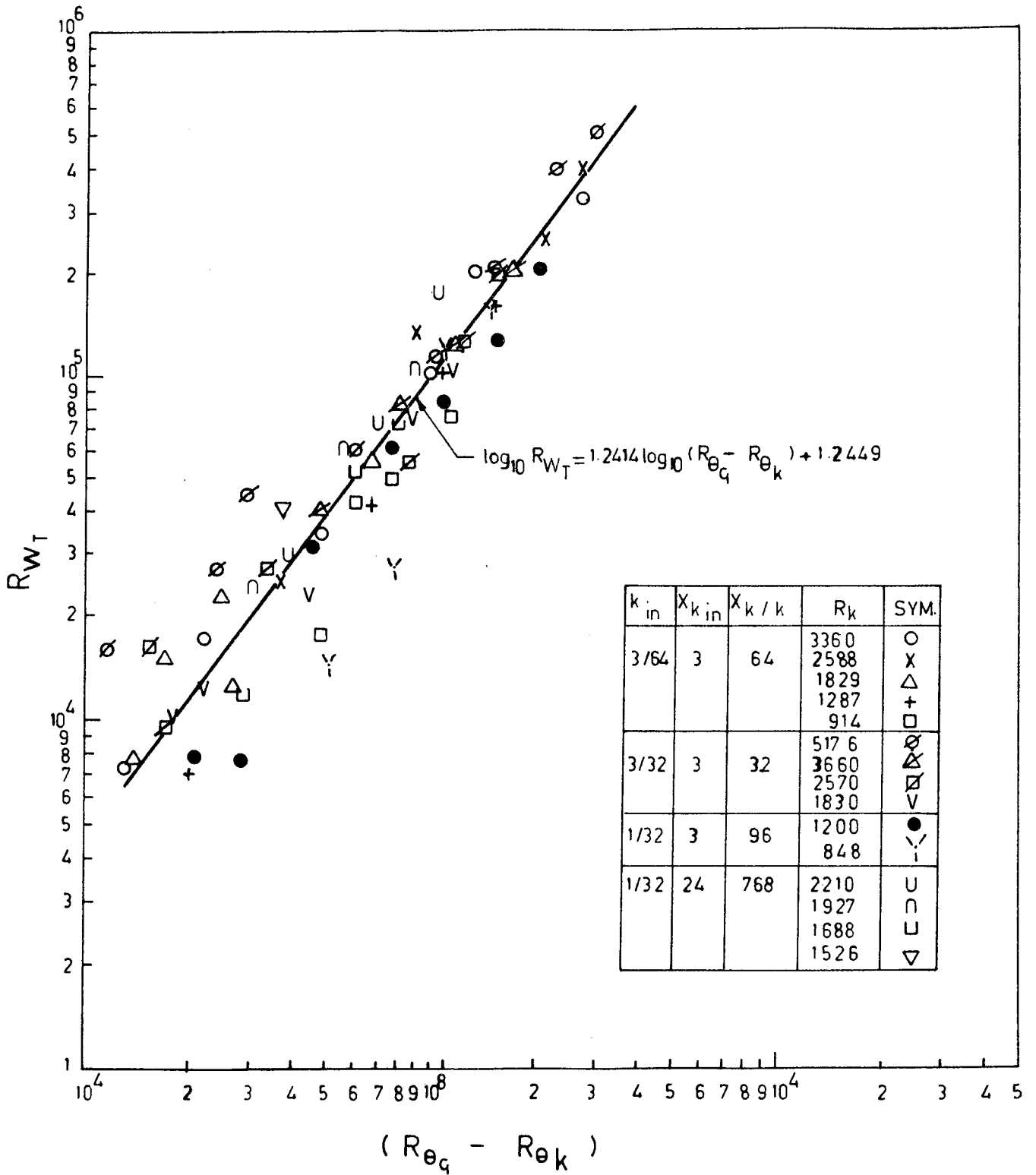
Fig.4.11 Correlation Between R_{W_T} and $R_{\theta_q} - R_{\theta_k}$.
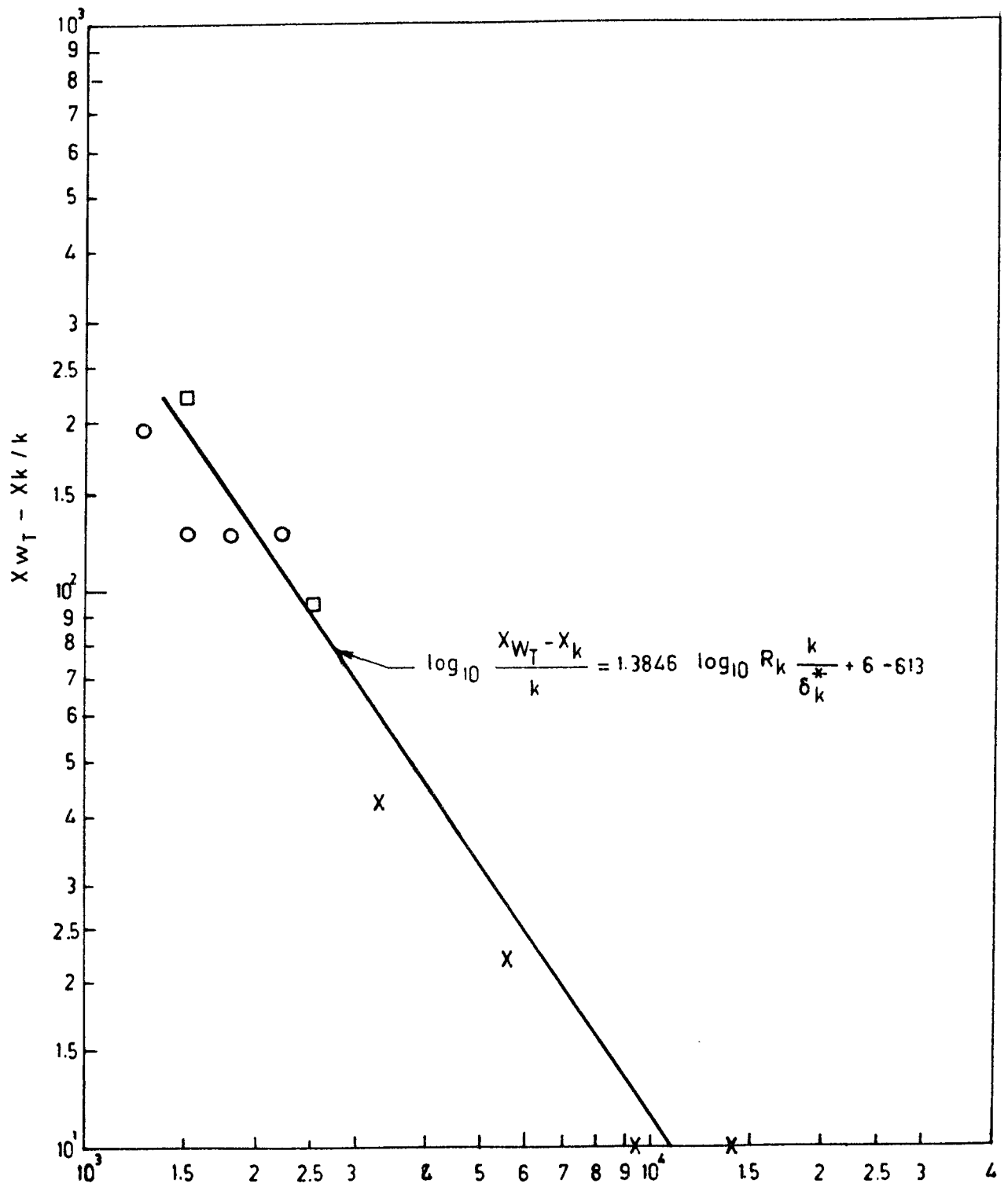
Fig. 4.14 Correlation Between $\dfrac{X_{W_T} - X_k}{k}$ and $R_k \dfrac{k}{\delta_k^*}$.

The figure shows a log-log plot with the vertical axis labeled $X_{W_T} - X_k / k$ and the horizontal axis labeled $R_k \dfrac{k}{\delta_k^*}$, with the fitted line:

$$\log_{10} \frac{X_{W_T} - X_k}{k} = 1.3846 \ \log_{10} R_k \frac{k}{\delta_k^*} + 6 - 613$$

111
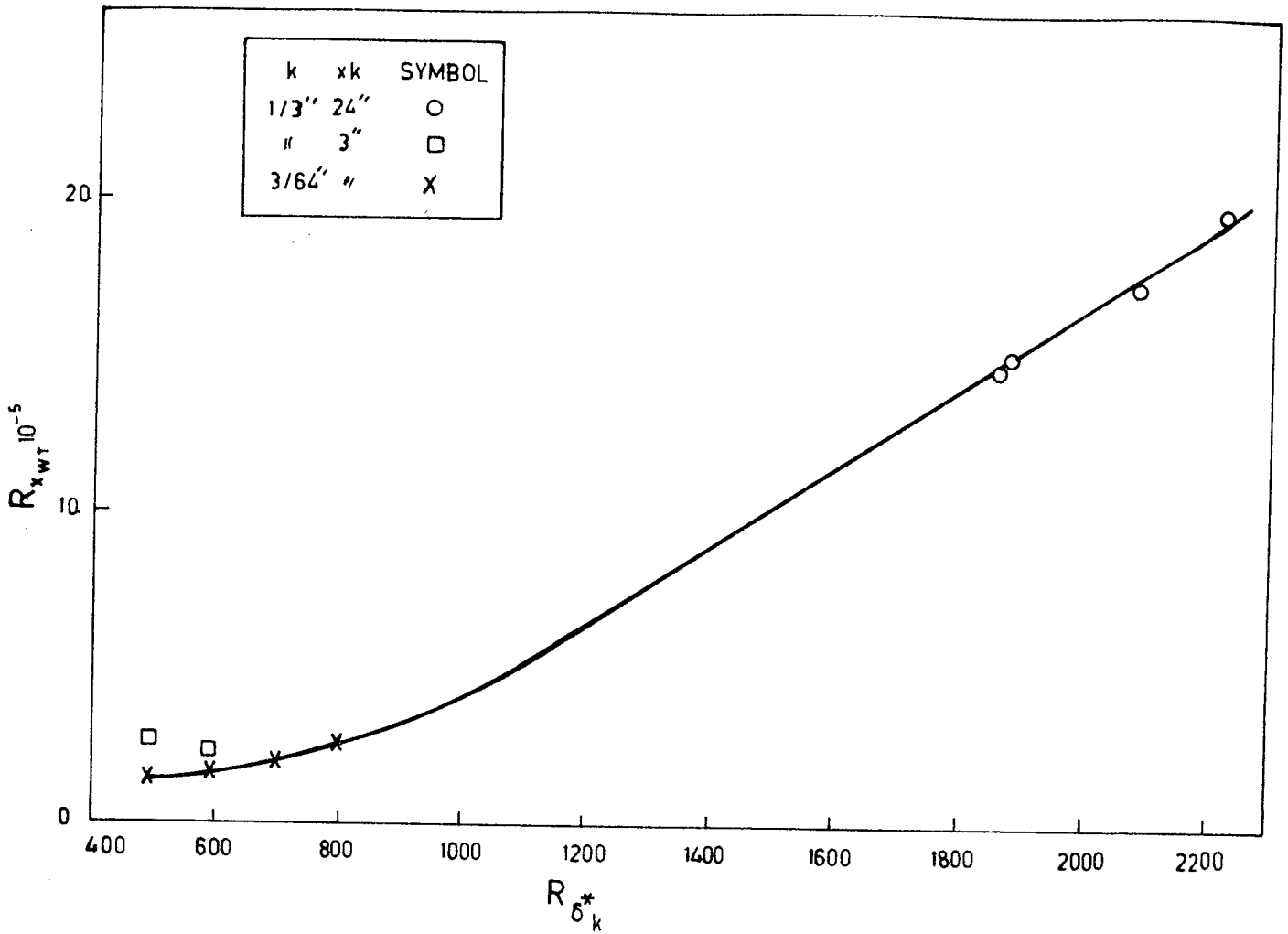
Fig.4.15 Variation of $R_{X_{W_T}}$ With $R_{\delta^*_k}$ Behind a Spherical Roughness Element Based on Göksel's Results (32).

112
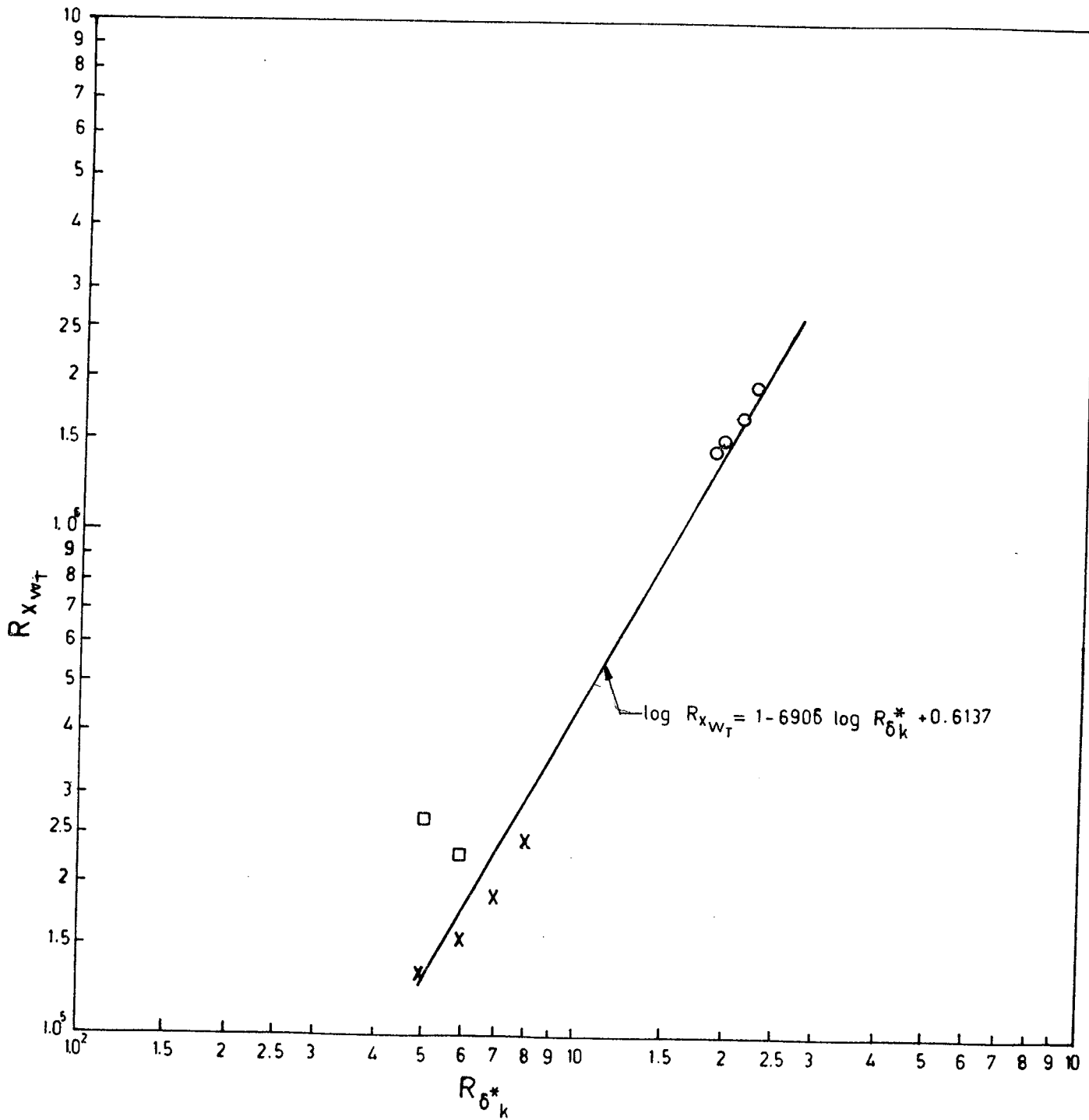
Fig.4.16 Correlation Between $R_{X_{W_T}}$ and $R_{\delta^*_k}$.
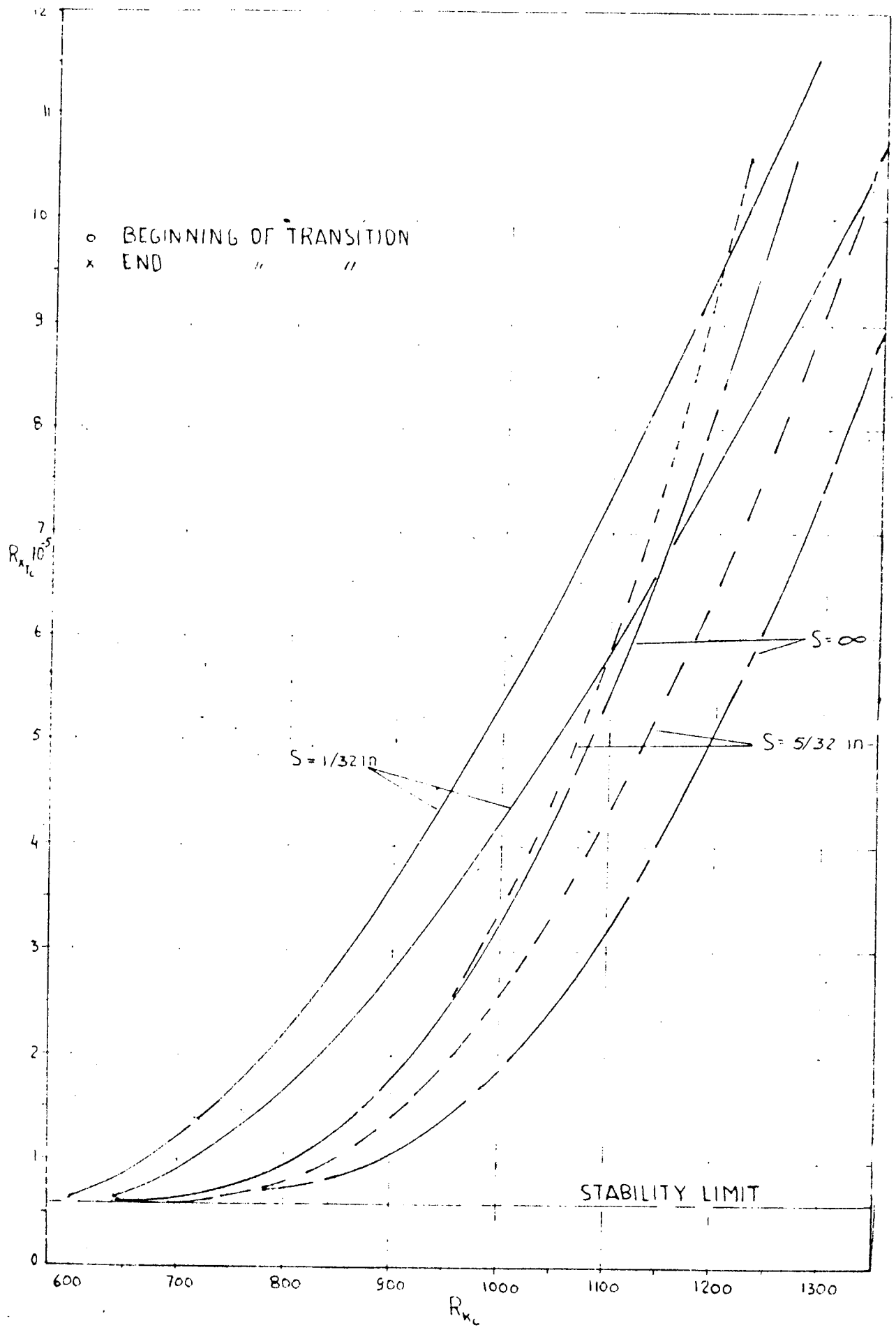
Fig.5.1   Variation of $R_{x_{Tc}}$ With R_{nkc} for a Row of Spherical

Roughness Elements $k = \dfrac{1}{32}$, $s = \dfrac{1}{32}''$, $n = 11$, $= 0$

From Reference 32.

114
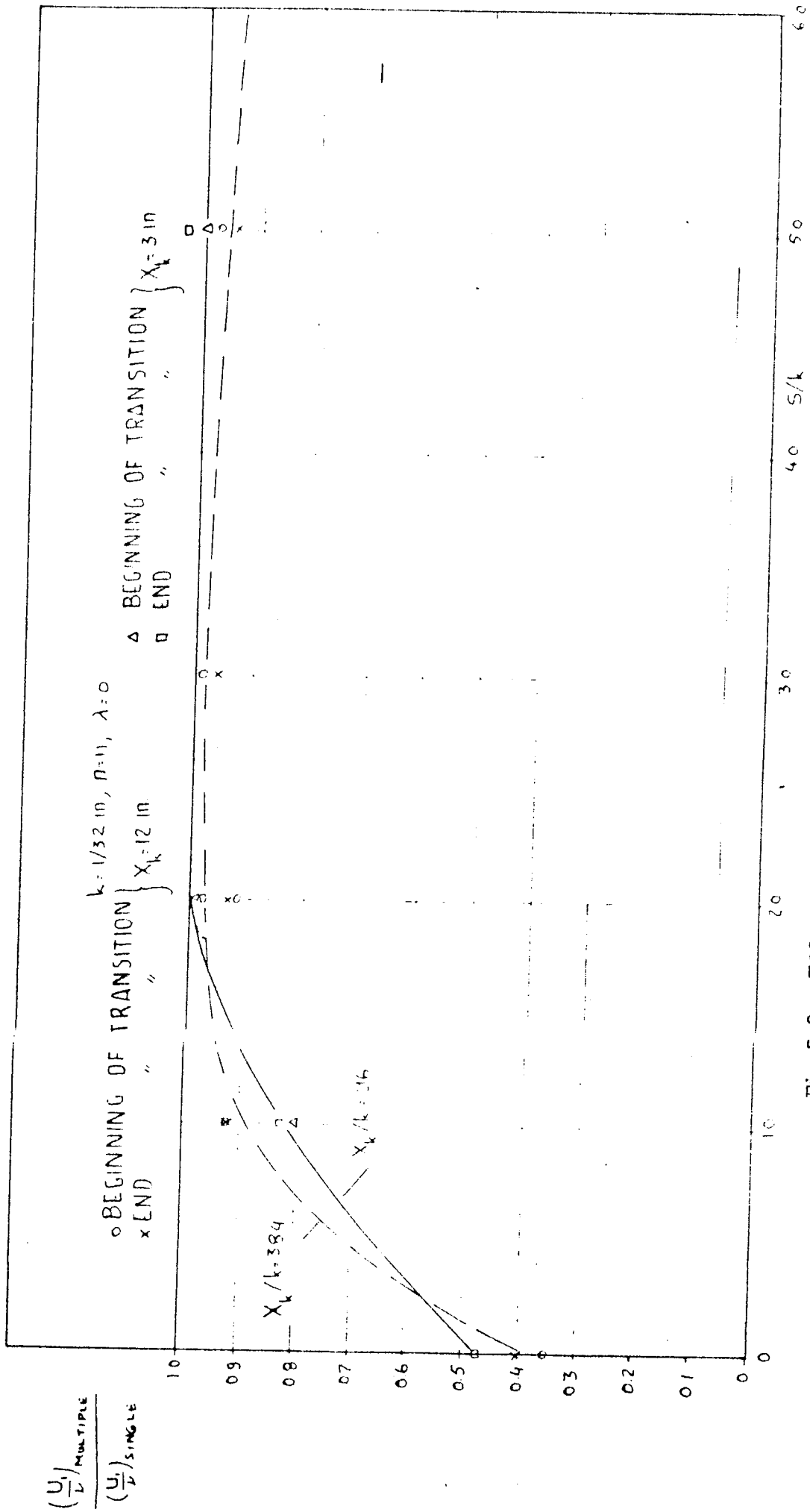
Fig.5.2 Effect of Spacing of the Elements on the Critical Roughness
Reynolds Numbers. From Reference 32.

115
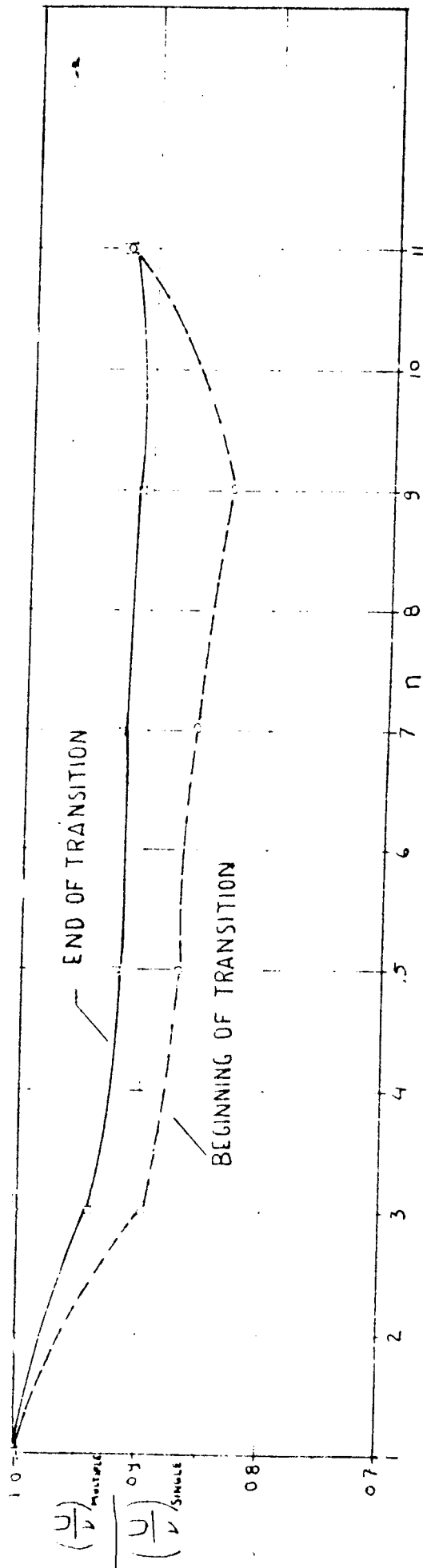
Fig.5.3   Effect of   Number of   Spheres   in one Row on R_{kc}.   From Reference 32.
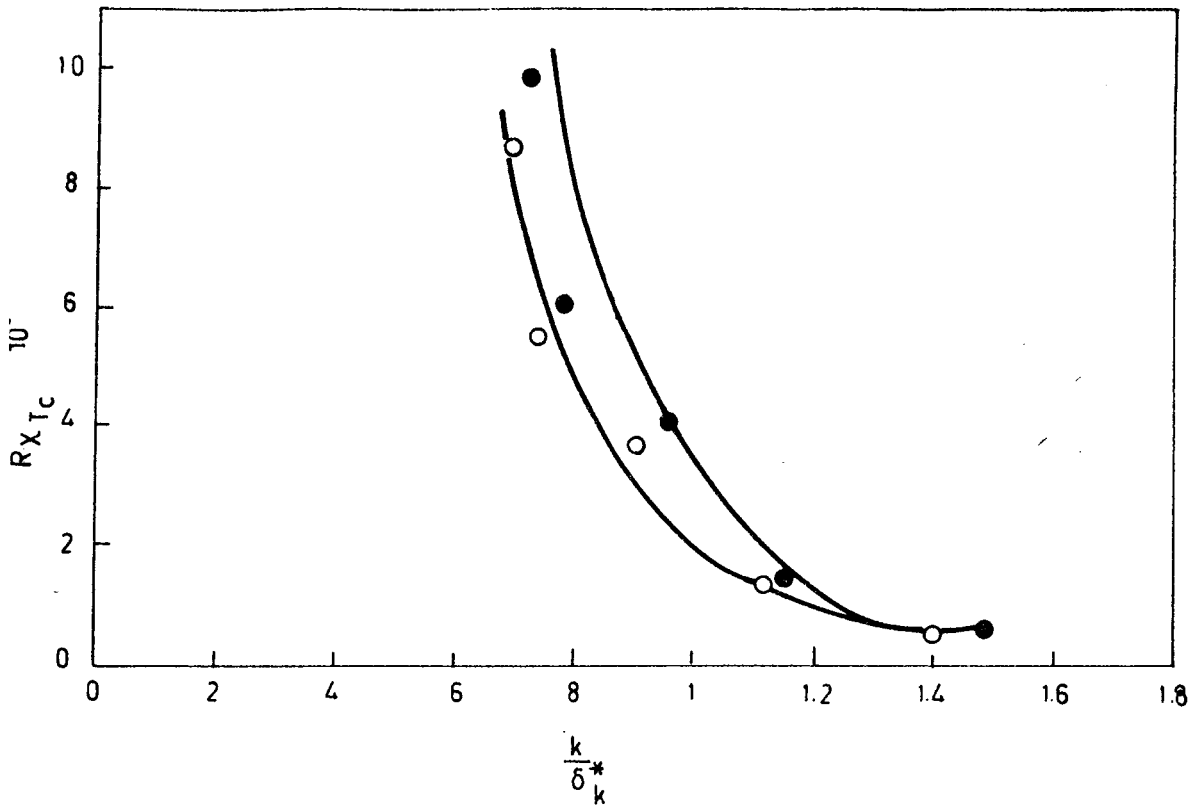
Fig.5.4.a Variation of $R_{X_{T_c}}$ With $\dfrac{k}{\delta^*_k}$ for a Row of Spheres , n = 11,

$s = \dfrac{1}{32}''$, $k = \dfrac{1}{32}''$, $X_k = 12''$. Based on the Experimental
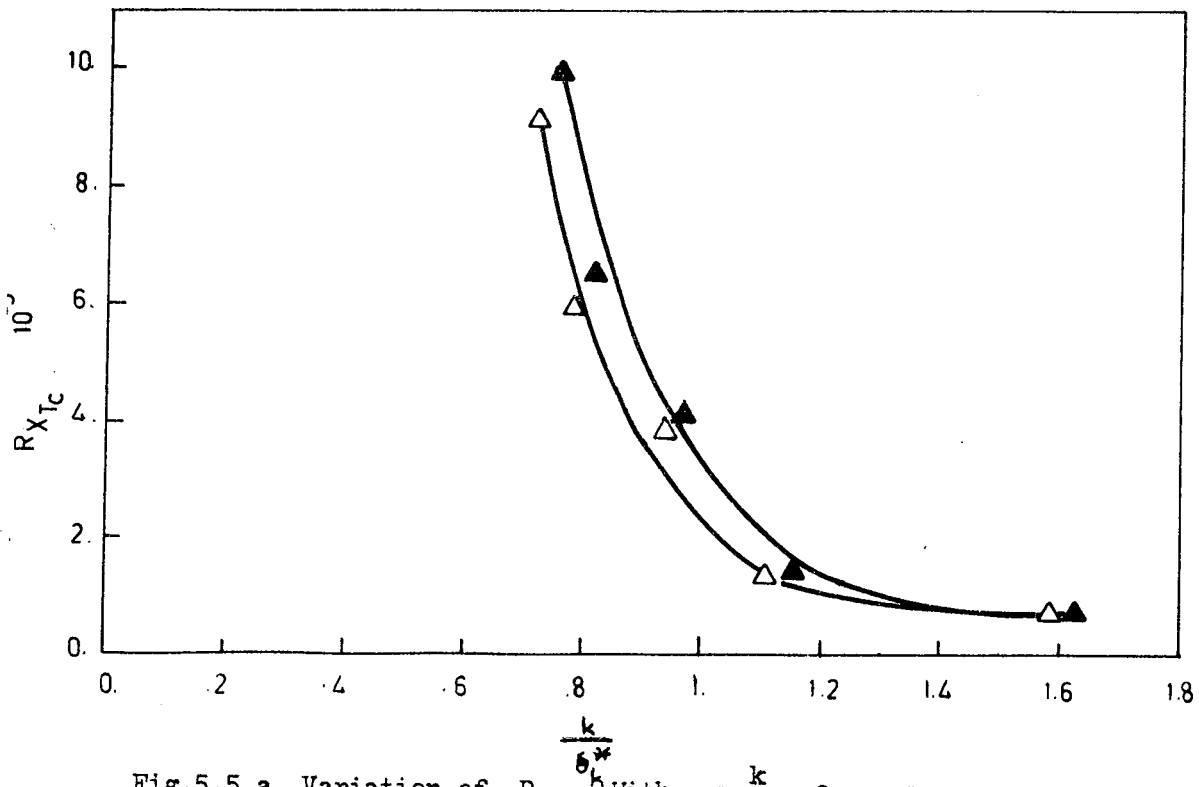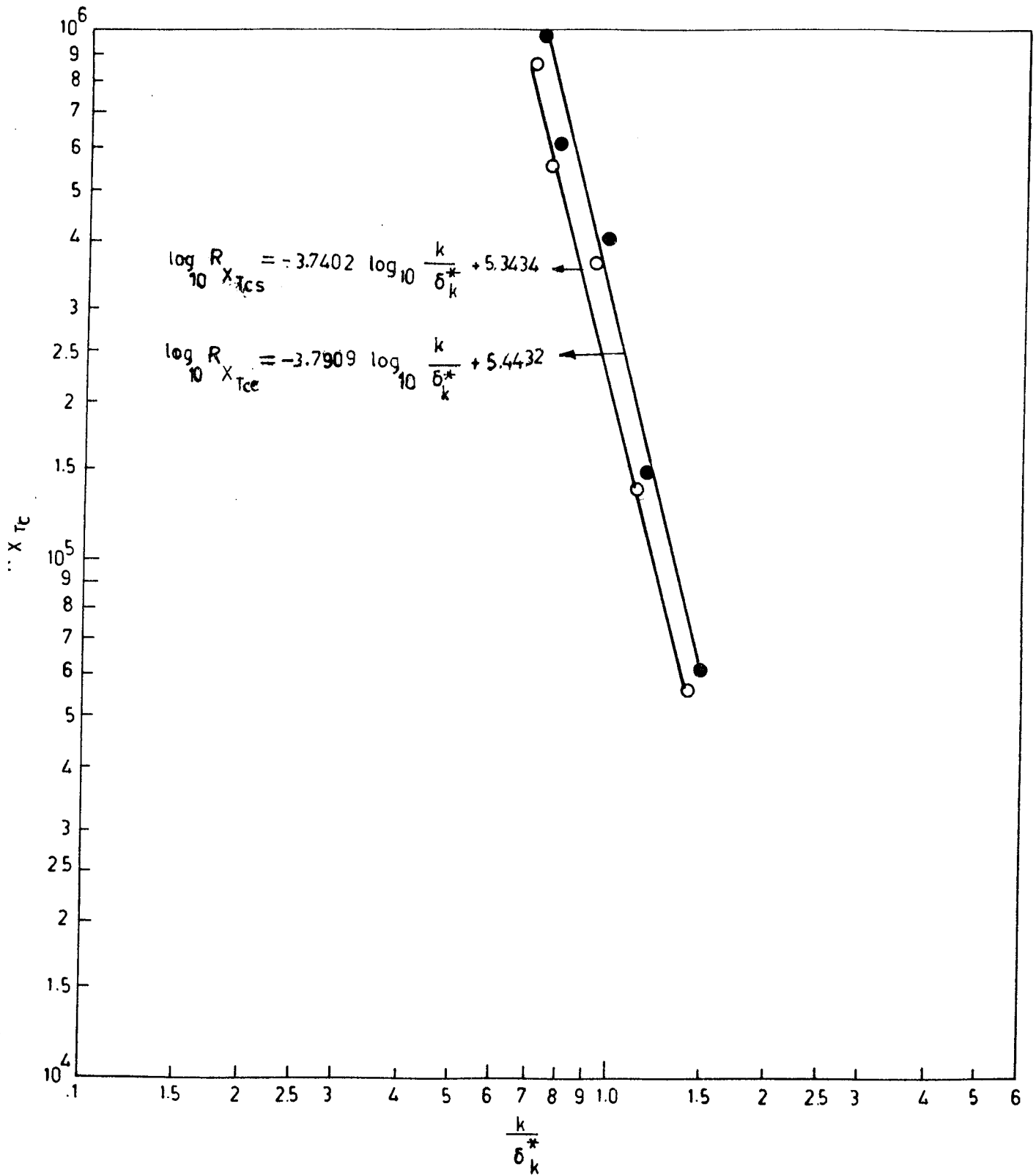
Results of Göksel.

Fig.5.5.a Variation of $R_{X_{T_c}}$ With $\dfrac{k}{\delta^*_k}$ for a Row of Spheres, n = 11,

$s = \dfrac{5}{32}''$, $k = \dfrac{1}{32}''$, $X_k = 12''$. Based on Experimental Results of

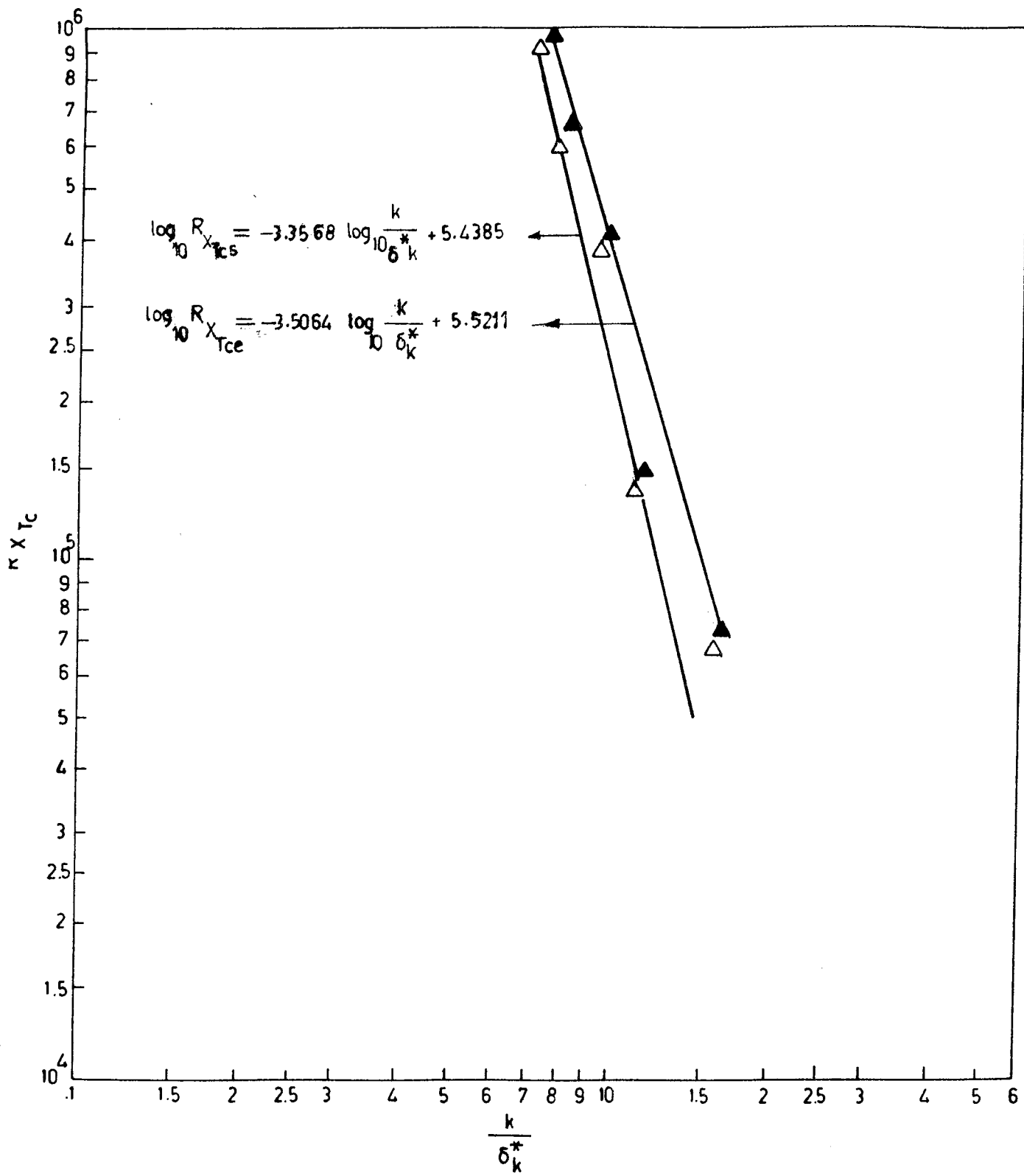Göksel.   117

Fig.5.4.b Correlations Between $R_{X_{Tc}}$ and $\dfrac{k}{\delta_k^*}$ for a Row of Spheres,

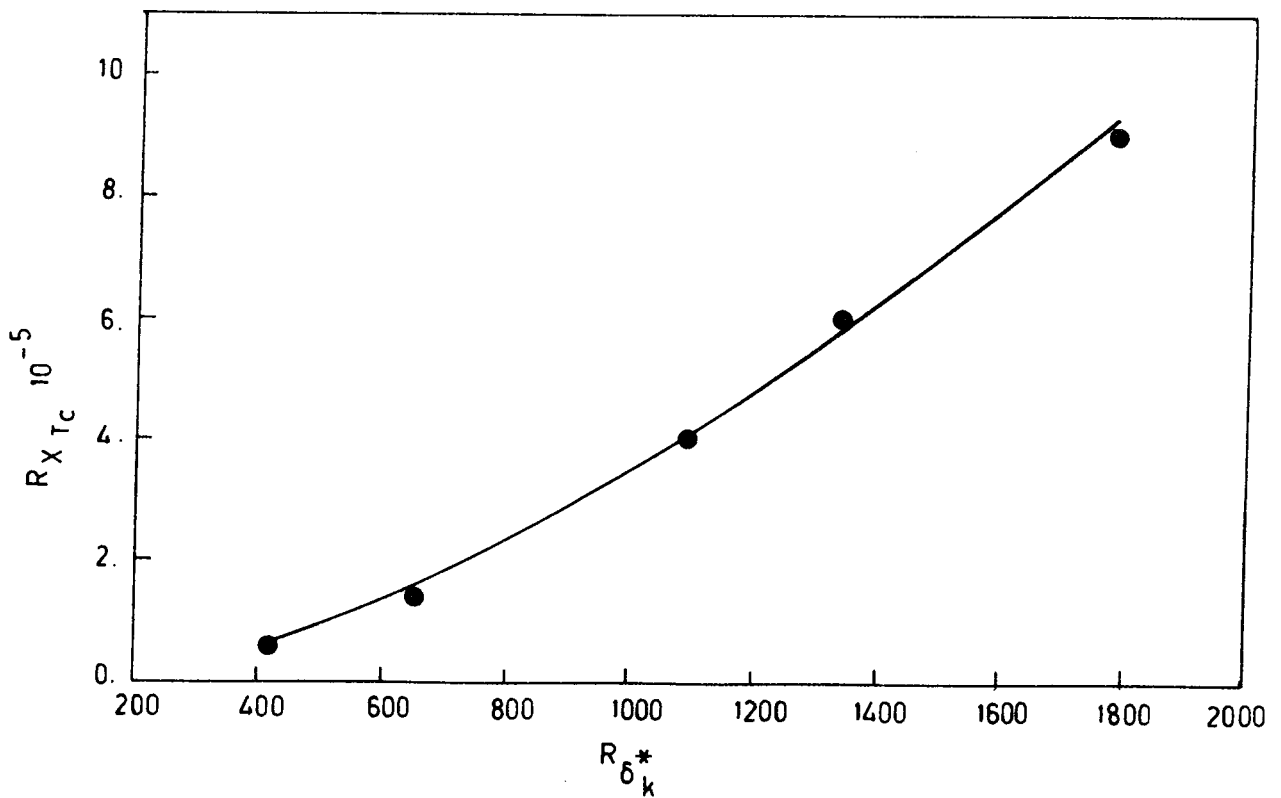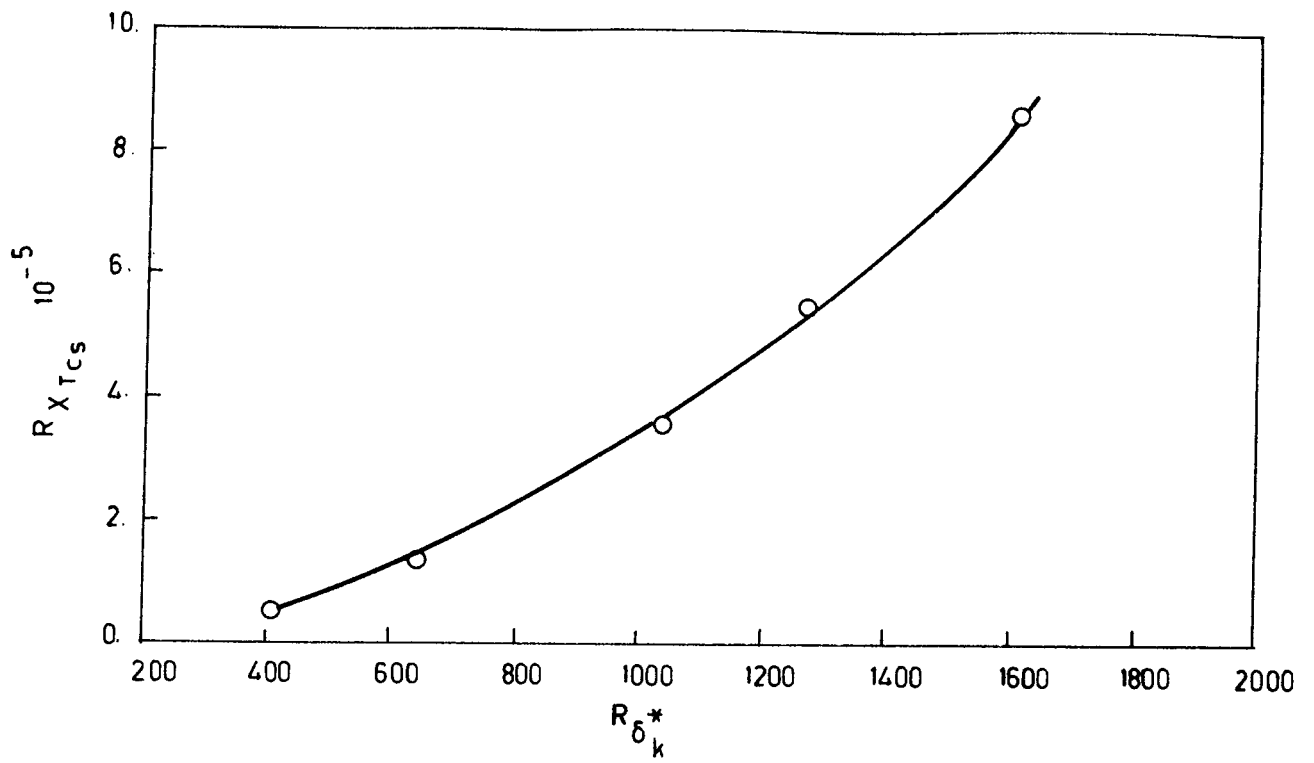$n = 11$, $s = \dfrac{1}{32}^{m}$, $k = \dfrac{1}{32}$, $X_k = 12^{k}$.

The equations shown on the figure:

$$\log_{10} X_{Tcs} = -3.7402 \ \log_{10} \frac{k}{\delta_k^*} + 5.3434$$

$$\log_{10} X_{Tce} = -3.7909 \ \log_{10} \frac{k}{\delta_k^*} + 5.4432$$

$$\log_{10} R_{X_{Tcs}} = -3.3568 \, \log_{10}\frac{k}{\delta^*_k} + 5.4385$$

$$\log_{10} R_{X_{Tce}} = -3.5064 \, \log_{10}\frac{k}{\delta^*_k} + 5.5211$$

Fig.5.5.b Correlations Between $R_{X_{Tc}}$ and $\frac{k}{\delta^*_k}$ for a Row of Spheres,

$n = 11$, $s = \frac{5}{32}''$, $k = \frac{1}{32}''$, $X_k = 12''$.

119

Fig.5.6.a Variation of $R_{X_{Tc}}$ with $R_{\delta_k^*}$ for a Row of Spheres, n = 11,

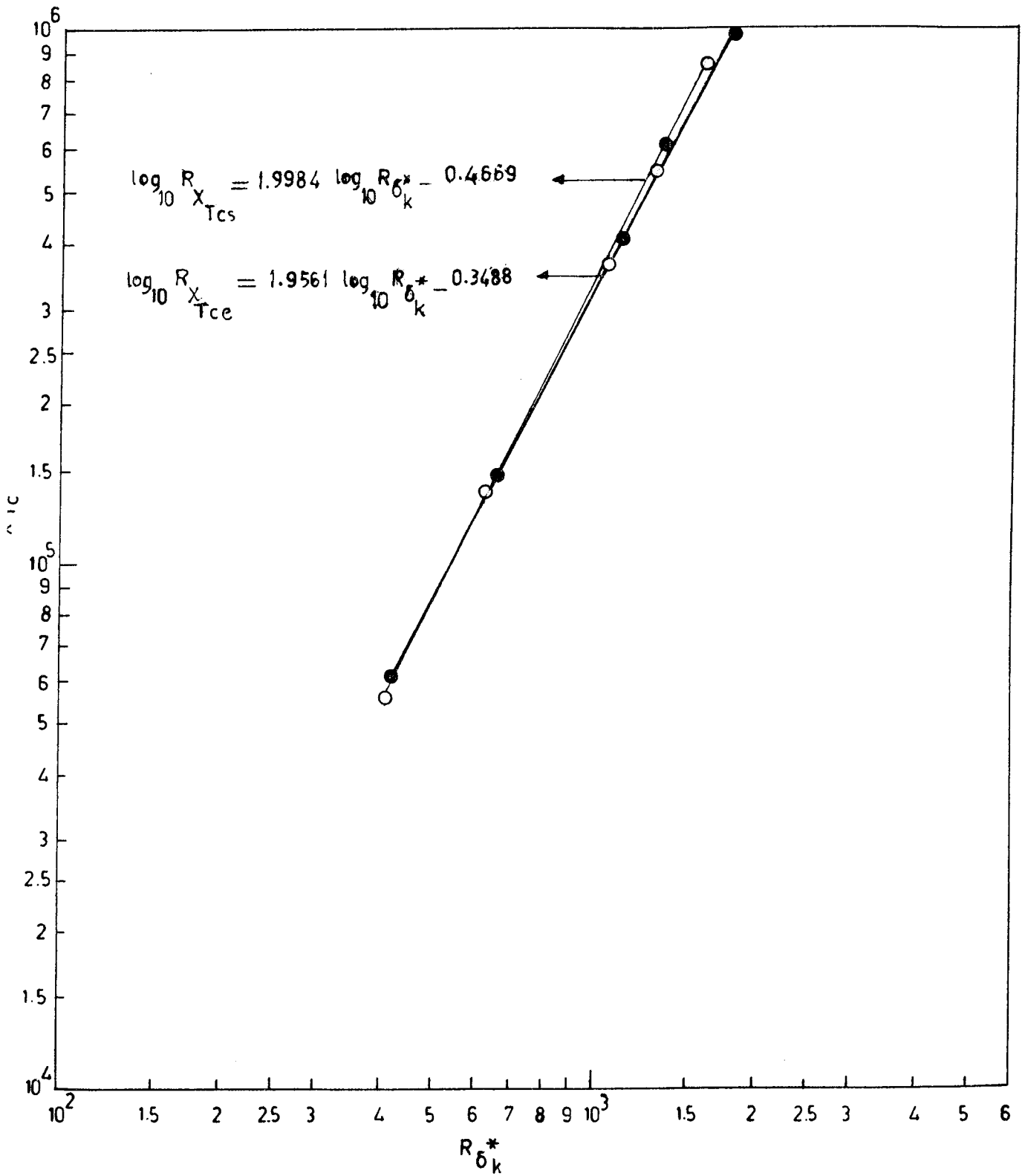$s = \dfrac{1}{32}$, k $= \dfrac{1}{32}$, $X_k = 12$.

Fig.5.6.b Correlation Between $R_{X_{Tc}}$ and $R_{\delta_k^*}$ for a Row of Spheres,

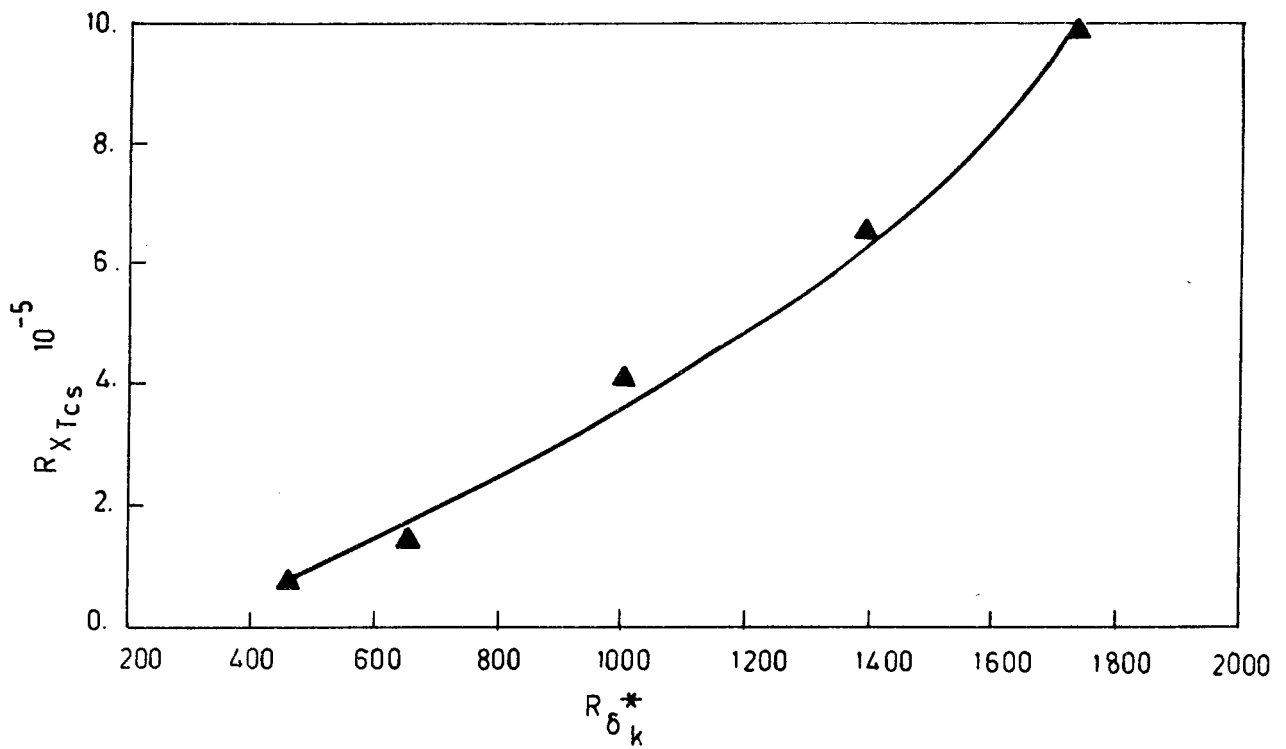$n = 11$, $s = \dfrac{1}{32}''$, $k = \dfrac{1}{32}''$, $X_k = 12''$.

121
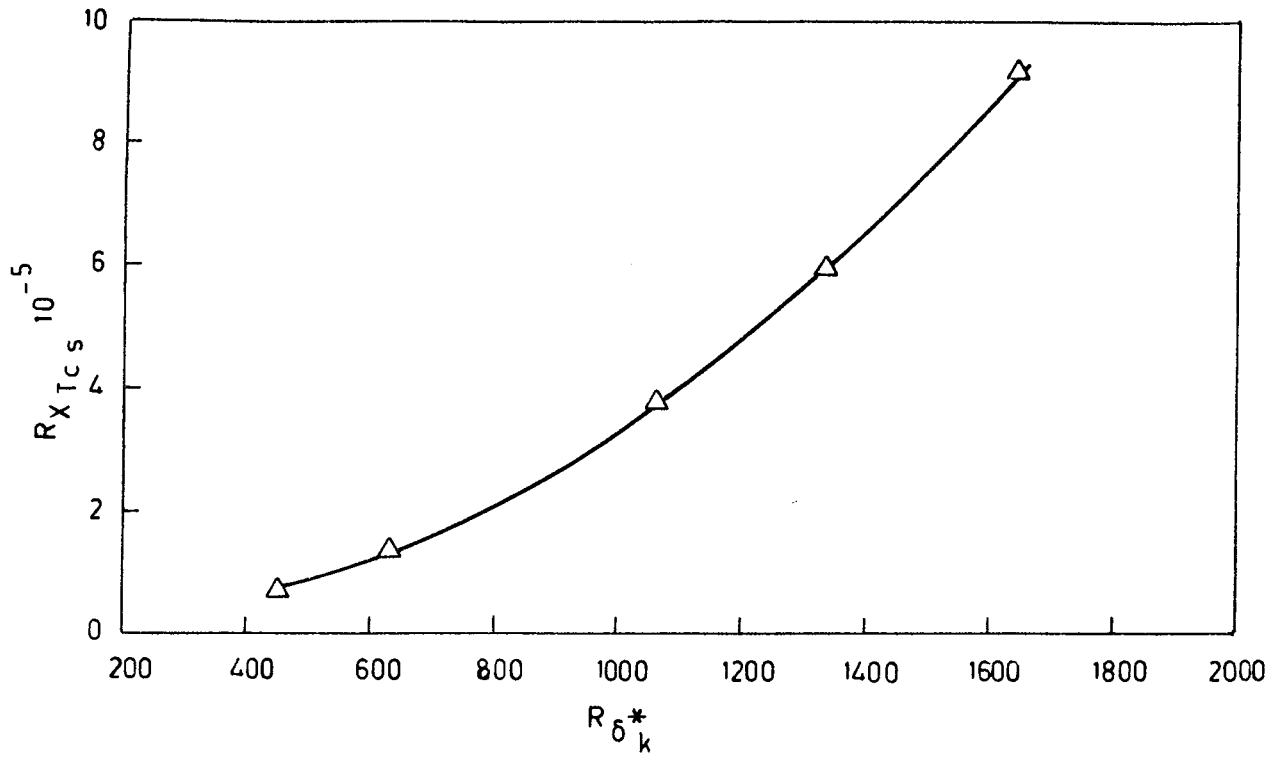
Fig.5.7.a Variation of $R_{X_{Tc}}$ With $R_{\delta^*_k}$ for a Row of Spheres $n = 11$, $s = \dfrac{5}{32}$ '', $k = \dfrac{1}{32}$ '', $X_k = 12$ ''.
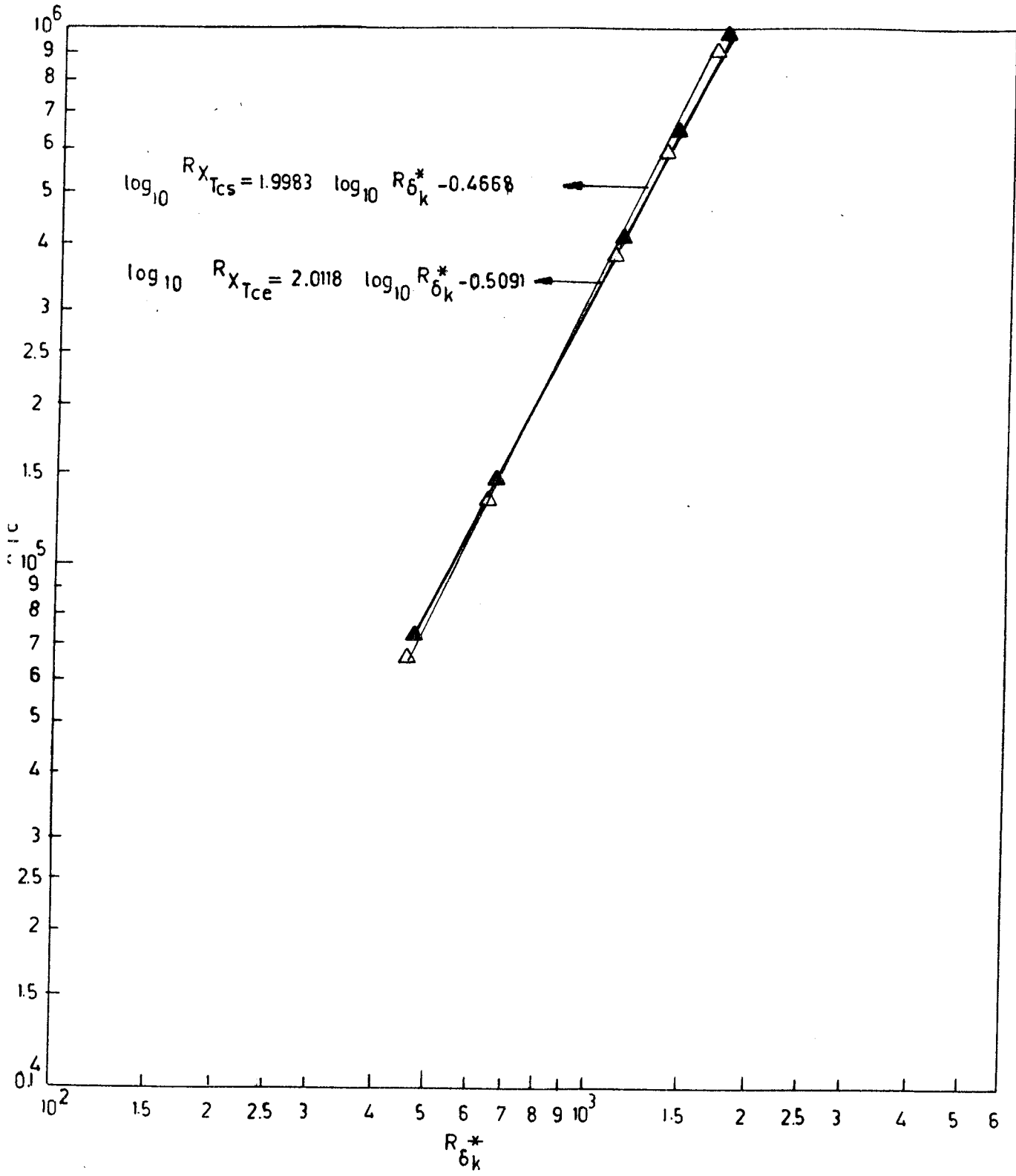
Fig.5.7.b   Correlation Between $R_{X_{Tc}}$ and $R_{\delta_k^*}$ for a Row of Spheres,

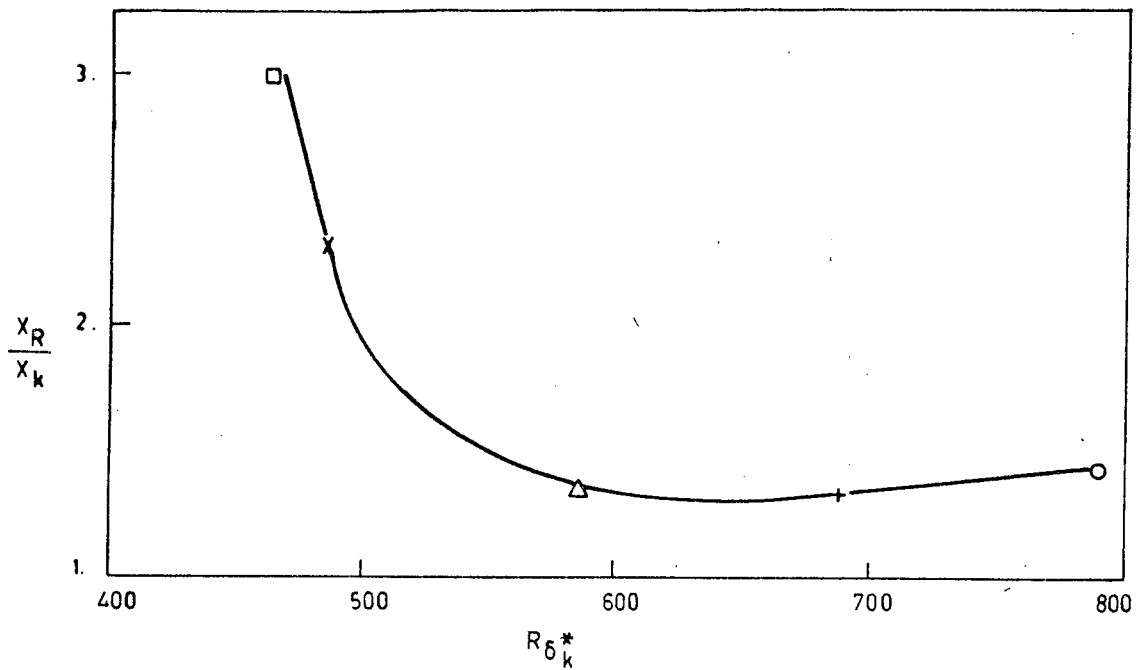$n = 11$, $s = \dfrac{5}{32}''$, $k = \dfrac{1}{32}''$, $X_k = 12''$.

The equations shown on the plot:

$$\log_{10} {}^R X_{Tcs} = 1.9983 \; \log_{10} R\delta_k^* - 0.4668$$

$$\log_{10} {}^R X_{Tce} = 2.0118 \; \log_{10} R\delta_k^* - 0.5091$$

123

Fig.5.8.a   Variation   of $\dfrac{X_R}{X_{k}}$ With $R_{\delta^{*}_{k}}$ Behind a Rof Spheres, n = 11,

$s = \dfrac{5}{32}^{"}$, $k = \dfrac{1}{32}$, $X_k = 3^{"}$,   Measured at $z = 0^{"}$.

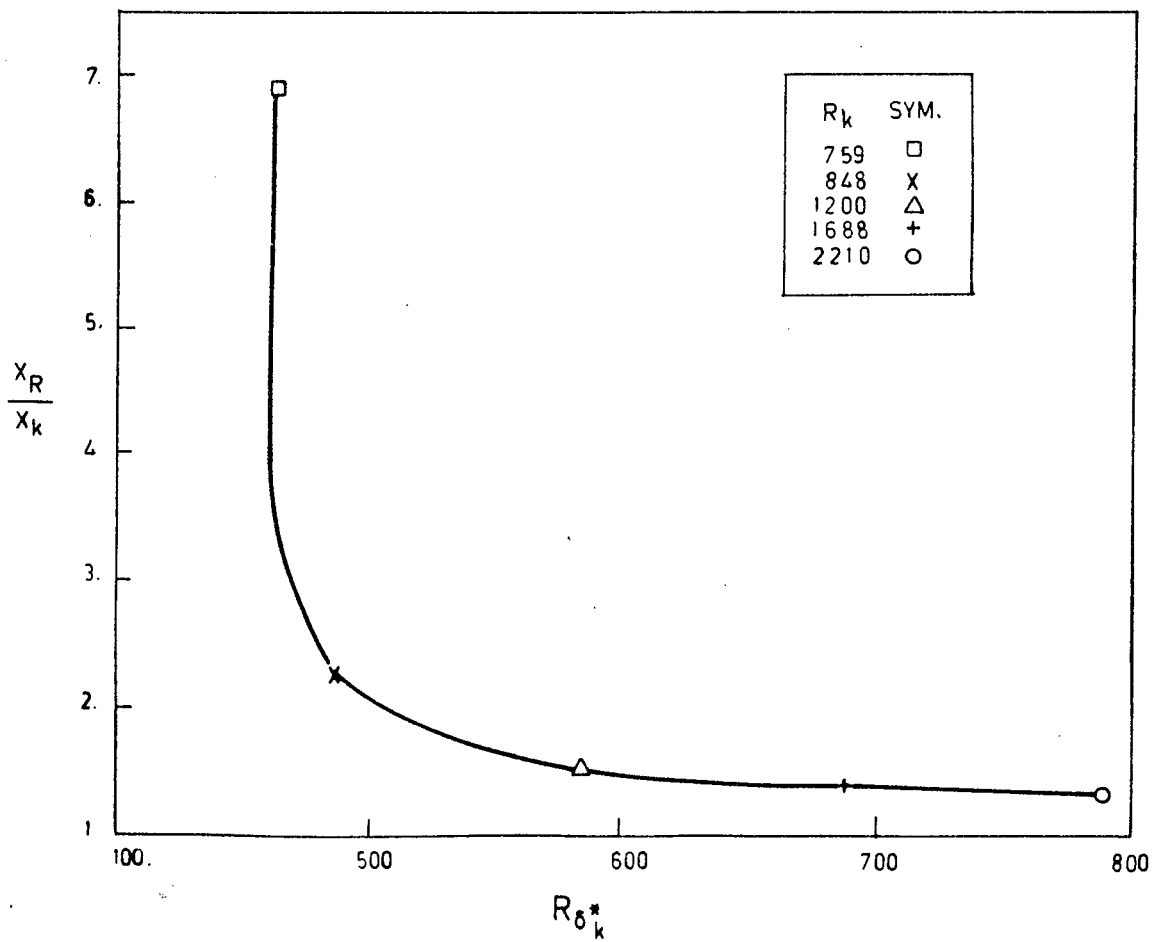| R_k	SYM.
759	□
848	X
1200	△
1688	+
2210	O

Fig.5.8.b   Variation of $\dfrac{X_R}{X_k}$ With $R_{\delta^{*}_{k}}$ Behind a Row of Spheres, n = 11,

$s = \dfrac{5}{32}^{"}$, $k = \dfrac{1}{32}^{"}$, $X_k = 3^{"}$,   Measured at $z = -\dfrac{15}{32}^{"}$.

124

Fig.5.9.a Variation of R_{X_L} With $R_k \dfrac{k}{\delta^*_k}$ Behind a Row of Spheres, n = 11, s = $\dfrac{5}{32}''$, k = $\dfrac{1}{32}''$, X_k = 3'' , Measured at z = 0'' .
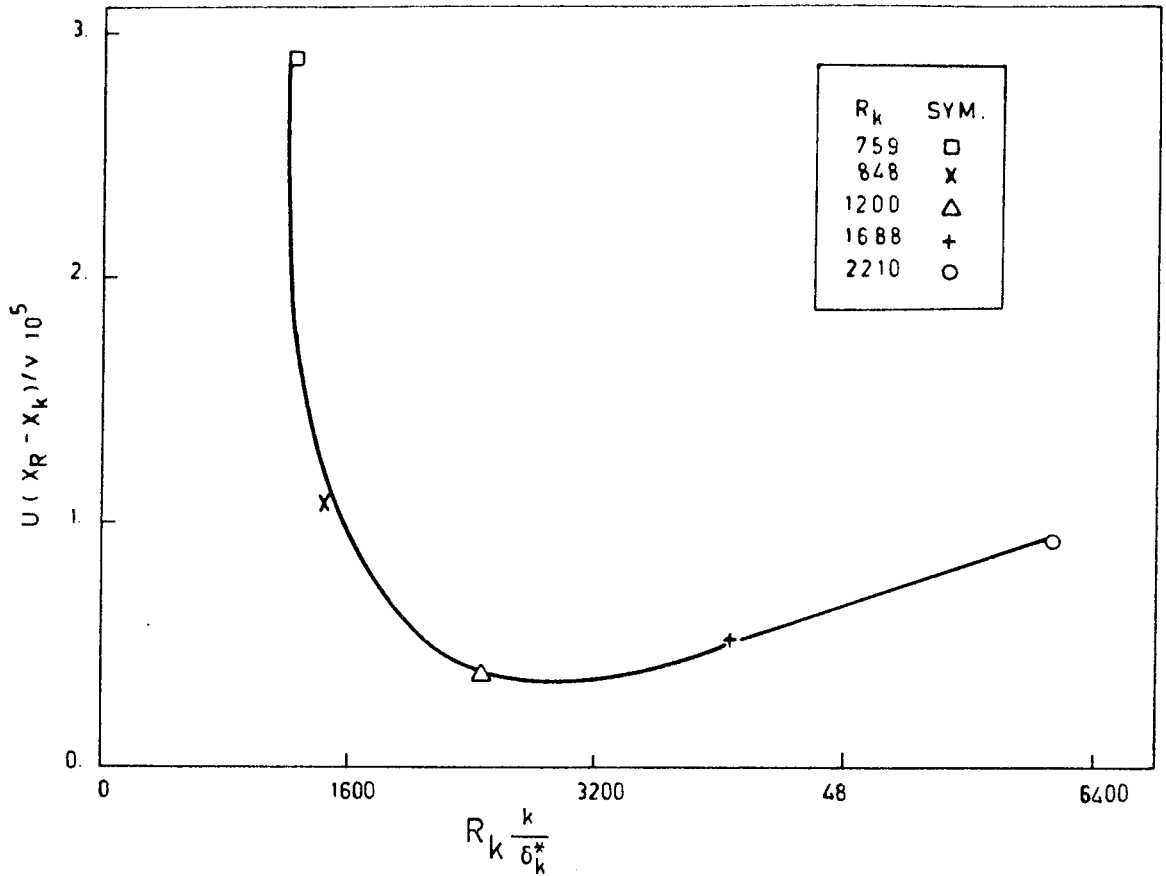

Fig.5.9.b Variation of R_{X_L} With $R_k \dfrac{k}{\delta^*_k}$ Behind a Row of Spheres, n = 11, s = $\dfrac{5}{32}''$, k = $\dfrac{1}{32}''$, X_k = 3'' , Measured at z = $-\dfrac{15}{32}''$.
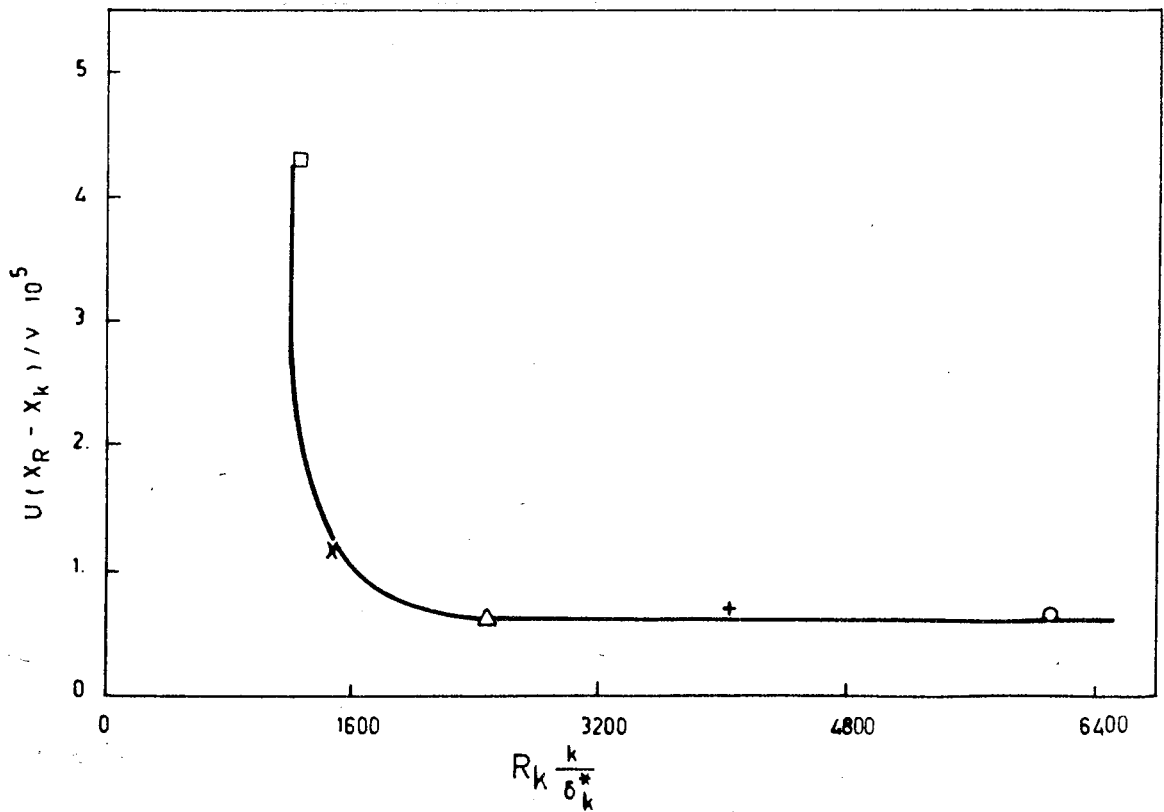
125

Fig.5.10.a Variation of R_{X_L} With $\dfrac{k}{\delta_k^*}$ Behind a Row of Spheres,

n = 11, s = $\dfrac{5}{32}''$, k = $\dfrac{1}{32}''$, X_k = 3$''$, Measured at z= 0$''$.

Fig.5.10.b Variation of R_{X_L} With $\dfrac{k}{\delta_k^*}$ Behind a Rof of Spheres,

n = 11, s = $\dfrac{5}{32}''$, k = $\dfrac{1}{32}''$, X_k = 3$''$, Measured at
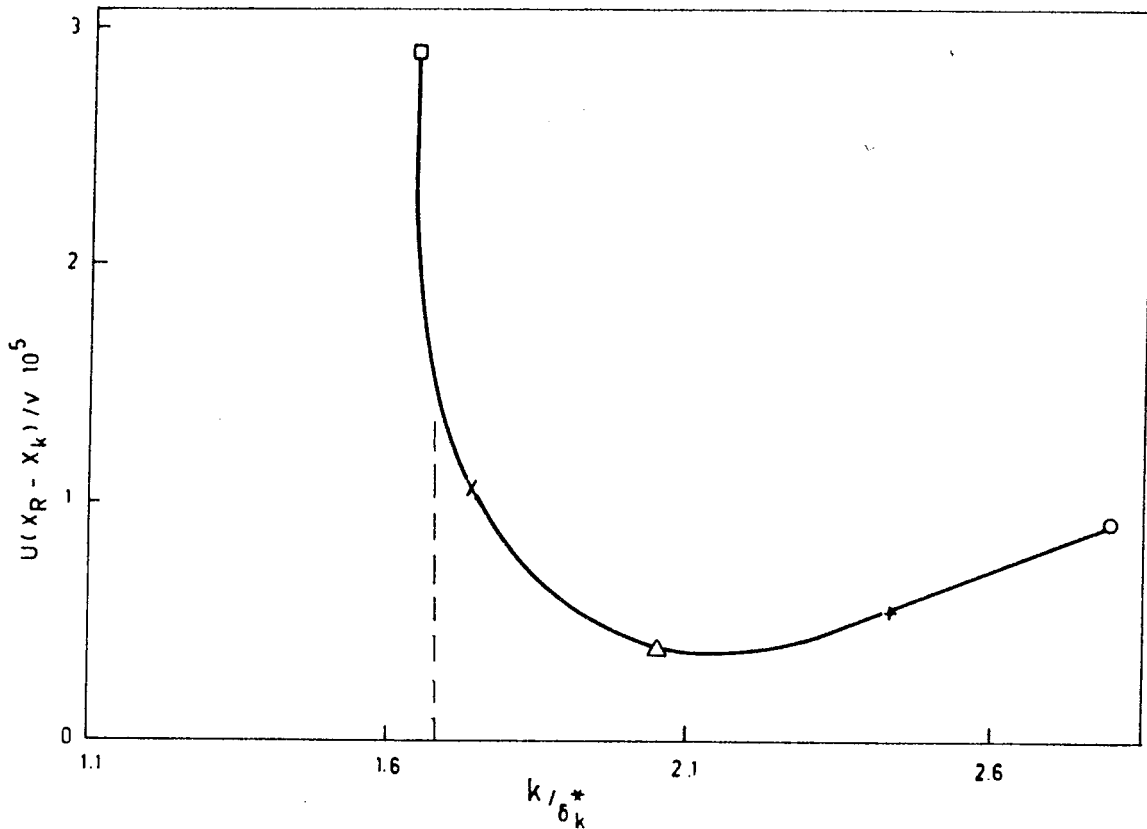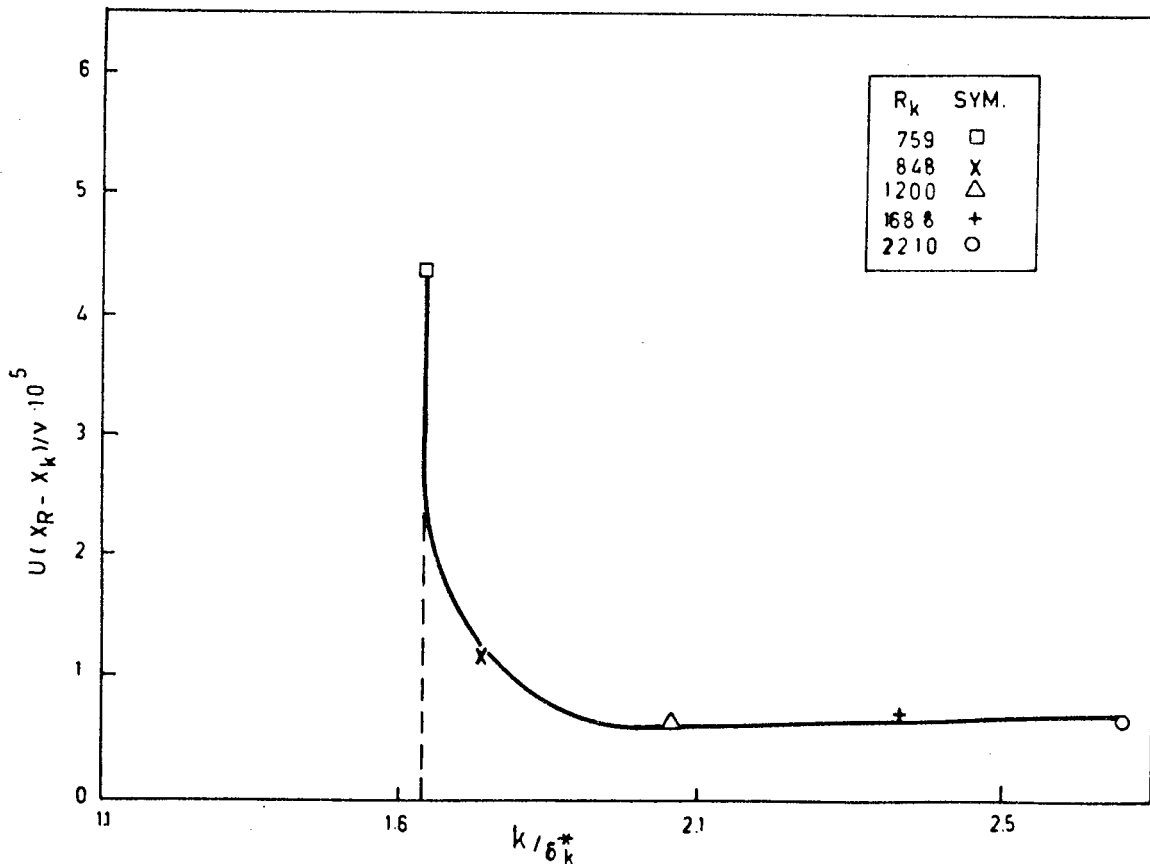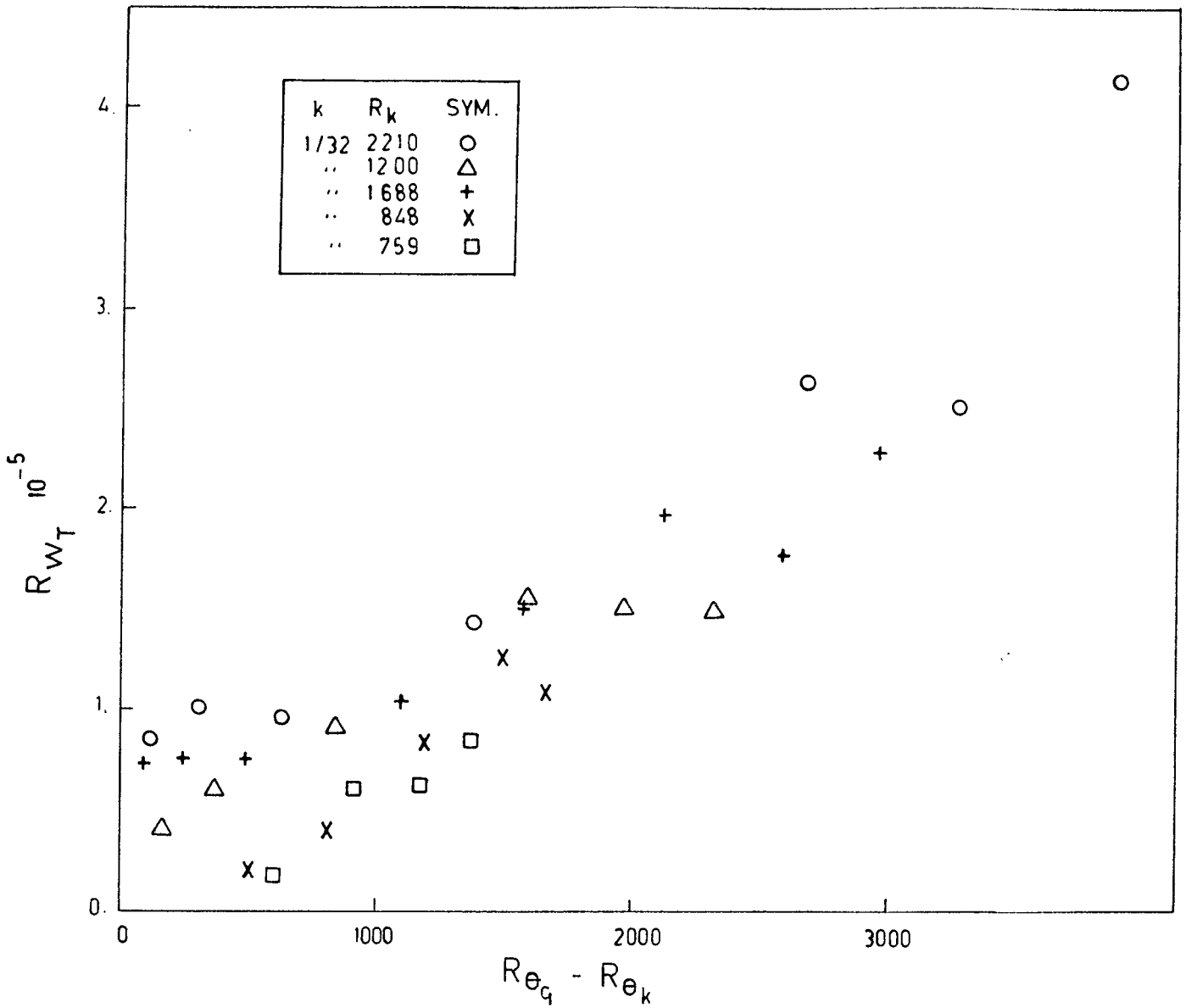
z = $-\dfrac{15}{32}''$.

126

Fig.5.11   Variation of R_{W_T} With $R_{\theta_q} - R_{\theta_k}$ for a Row of Spheres,

$n = 11$, $s = \dfrac{5}{32}"$, $k = \dfrac{1}{32}"$, $X_k = 3"$.

LIST OF REFERENCES

1. SCHLICHTING H. " Boundary Layer Theory " 6th Edition Mc - Graw - Hill Series in Mechanical Engineering Mc - Graw - Hill Book Company, New York, U.S.A., 1968

2. SCHUBAUER, G.B. - SCRAMSTAD, H.K. " Laminar Boundary Layer Oscillations and Stability of Laminar Flow " National Bureau of Standards Research Paper 1772. Reprint of Confidential NACA Rep. Dated April 1943.

3. KLEBANOFF, P.S., TIDSTROM, K.D. " Evalution of Amplified Waves Leading to Transition in a Boundary Layer With Zero Pressure Gradient " N.A.S.A. Techn.Note No : D - 195 Sept. 1959.

4. KLEBANOFF, P.S., TIDSTROM, K.D., SARGENT, L.M. " The Three - Dimensional Nature of the Boundary Layer Instability " Journal of Fluid Mechanics Vol : 12 Part, 1, 1962 pp. 1 - 34

5. TANI, I. " Some Aspects of Boundary Layer Transition at Subsonic Speeds " Advances in Aeronautical Sciences Vol:3, pp.143, 1962.

6. TANI, I., KOMODA, H. " Boundary Layer Transition in the Presence of Streamwise Vortices " Journal of Aerospace Sciences Vol :29, pp.440, April 1946.

7. SQUIRE, H.B. Proc, Roy. Soc. A.142, 621, 1933

8. DRYDEN, H.L. N.A.C.A. Rept 392, 1931.

9. TAYLOR, G.I. " Statistical Theory of Turbulence v. Effects of Turbulence on Boundary Layers " Proc.Roy. Soc. (London) Ser.A; Vol.156 No : 888, pp.307, 1936.

10. LIEPMANN, H.W.- FILA, G.H. " Investigations of Effects of Surface Temperature and Single Roughness Elements on Boundary Layer Transition " N.A.C.A. Rept. No : 890, 1947.

11. TANI, I., SATO, H. " Boundary Layer Transition by Roughness Element " Journal of the Physical Society of Japan Vol : 11, No : 12, December 1956 pp.1284

128

12. HAMA, F.R., LONG, J.D., HEGARTY, J.C. " On Transition from Laminar to Turbulent Flow ".

13. HAMA, F.R., NUTANT, J. " Detailed Flow Field Observations in the Transition Process in a Thick Boundary Layer " Proc.Heat Transfer and Fluid Mechanics Inst. pp.77 1963.

14. EMMONS. H.W " The Laminar Turbulent Transition in a Boundary Layer " Journ. Aero. Scie. Vol:18, pp.490, 1951.

15. SCHUBAUER, G.B., KLEBANOFF, P.S. " Contributions on the Mechanics of Boundary Layer Transition " N.A.C.A. Techn. Note 3489.

16. DHAWAN, S., NARASHIMA, R. " Some Properties of Boundary Layer Flow During the Transition from Laminar to Turbulent Motion " Journal of Fluid Mech. Vol.3, No : 1953 pp.418 - 436.

17. NAGEL, L.A., " Compressible Boundary Layer Stability by Time Integration of the Navier - Stokes Equations and an Extension of Emmons " Transition Theory to Hypersonic Flow " Flight Sci.Lab. Rept.119, September 1967.

18. CHEN, K.K., THYSON, A.N. " Extension of Emmons'spot Theory to Flows on Blunt Bodies " July 1970.

19. MORKOVIN, M.V., " Instability, Transition to Turbulence, and Predictability " AGARDOGRAPH No : 236, 1978.

20. GRANVILLE, P.S. " The Calculations of Viscous Drag of Bodies of Revolution " Rept.849, 1953.

21. HALL, A.A., HISLOP, G.S. " Experiments on the Transition of the Laminar Boundary Layer on a Flat Plate " A.R.C. R.M. 1843, 1938.

22. DRYDEN, H.L. " Turbulence and the Boundary Layer " J.A.S.6, 85 - 100 and 101 - 105 1939.

23. MICHEL, R. " Etude de la Transition Sur les Profiles d'aile; e tablissement d'un Crite're de Determination du Point de Transition et calcul de la trainee de Profilen Incompressible " ONERA Rapport 1/1578 A, 1951.

24. SMITH, A.M.O. " Transition, Pressure Gradient and Stability
    Theory " Paper presented at the IX. Intern Congress of Appl.
    Mech. 4.234 - 244 Brussels 1957.

25. KLEBANOFF, P.S., SCHUBAUER, G.B., TIDSTROM, K.D. " Measurements
    of the Effect of Two - Dimensional and Three - Dimensional
    Roughness Elements on Boundary Layer Transition " Journal Aero.
    Sci. Vol.22 pp.803 - 804 1955.

26. GREGORY, N., WALKER, S. " The Effect on Transition of Isolated
    Surface Excrescences in the Boundary Layer " British A .R.C.
    13436 October 1950.

27. WESKE, J.R. Techn. Note BN - 91, Inst. Fluid Dynamics and .
    Applied Mathematics University Maryland, 1957.

28. PETERSON, J.B., HORTON, E.A. " An Investigation of the Effect of
    a Highly Favourable Pressure Gradient on Boundary Layer Transi-
    tion as Caused by Various Types of Roughness in a 10 Foot
    Diameter Hemi - Sphere " N.A.S.A. Memo. No : 2 - 8 - 59L, 1959.

29. TANI, I. " Einige Bemerkungen Über den Laminar - Turbulenten
    Umschlag in Grenzschichtstromungen " Zeitschrift für Angewandte
    Mathematik und Mechanic, Vol.53, pp.T25 - T32, 1973.

30. MOCHIZUKI, M. " Smoke Observation on Boundary Layer Transition
    Caused by a Spherical Roughness Element " J.Phys. Soci. Japan Vol.16
    pp.905 - 1008 1961.

31. HALL D.J. " Boundary Layer Transition " Ph.D Thessis 1968
    Liverpool University U.K.

32. GÖKSEL, Ö.T., " Some Effects of Spherical Roughness Upon the
    Incompressible Flow of a Boundary Layer With a Zero Pressure
    Gradient ". Ph.D. Thessis Liverpool University UK 1968.

33. FRASER, C.J., MILNE, J.S. " Boundary Layer Development from
    Transition Provoking Devices " International Journal of Heat and
    Fluid Flow, Vol.2, No:4, 1980 pp.165 - 173.

34. YEĞEN, İ. " The Effect of Spherical Roughness Elements on Transi-
    tion and Boundary Layer Development " Ph.D. Thessis METU 1982.

35. ALBAYRAK, K. " Investigation of the Boundary Layer Transition the Turbulent B.L Development and the Recovery Length of the Turbulent Boundary Layer Behind 3-D Roughness Elements " Ph.D Thessis METU May 1984.

36. VON DOENHOFF, A.E., HORTON, E.A. " A Low Speed Experimental Investigation of the Effect of a Sand Paper Type of Roughness on Boundary Layer Transition N.A.C.A. Rept. No : 1349, 1958.

37. HOLSTEIN, H. " Versuche an einer parallel angeströmten ebenen Platte über den Rauhigkitsein-fluss auf den Umschlag laminar / turbulent ZWB, UM 3110.

38. BRASLOW, A.L. " Review of the Effect of Distributed Surface Roughness on Boundary Layer Transition " A.E.A.R.D.Rept. No:254, 1960.

39. CARMICHAEL, B.H. " Critical Reynolds Number, for Multiple Three - Dimensional Roughness Elements " Northrop Air - Craft Rept. No:NAI 58 - 589 (BLC - 112) 1958.

40. CARMICHAEL, B.H. " Prediction of Critical Reynolds Number for Single Three - Dimensional Roughness Elements " Northrop Air-Craft Rept. No:NAI - 58- 412 (B.L.C - 109), 1958.

41. TANI, I., KOMODA, H., KOMATSU, Y., 1UCHI, M. " Boundary Layer Transition by Isolated Roughness " Aeronautical Research Inst.Univ. Tokyo Rept.No : 375 November 1962.

42. FAGE, A. " The Smallest size of a Spanwise Surface Corregation which Affects Boundary Layer Transition on an Aerofoil " A.R.C. Rept. and Memo. No : 2210, 1943.

43. STÜPER, J. " The Influence of Surface Irregularities on Transition With Various Pressure Gradients Division of Aeronautics, Australia Rep, A 59 Melborne, 1949.

44. HALL, D.J., GIBBINGS, J.C. " The Criterion for Tolerable Roughness in a Laminar Boundary Layer ". Fluid Mechanies Division Univ. of Liverpool.

45. TANI. I., HAMA, F.R., MITUISI, S. " On the Permissible Roughness in the Laminar Boundary Layer " Rep. Aero. Res.Inst.Tokyo Imp. Univ. No : 199, 1940.

46. LOFTIN, L.K, Jr " Effects of Specific Types of Surface Roughness on Boundary Layer Transition " N.A.C.A. War time Rept L - 48

47. COWLED, " The Effects of Surface Irregularities on Transition in the Laminar Boundary Layer ".

48. SCHILLER, L. Handbuch der Experimentalphysik, 4. Part. 4. pp.189 - 192 Leipzig, 1932.

49. GOLDSTEIN, S. " A Note on Roughness " ARC RM 1763, 1936.

50. GÖKSEL, Ö.T., " The Recovery Length of a Turbulent Boundary Layer Upon a Flat Plate Behind Two and Three - Dimensional Roughness Elements " METU Ankara February 1973.

51. TANI - HAMA - MITUISI On the Effect of a Single Roughness Element on Boundary Layer Transition Rep. Aero.Res.Inst.May 1984

52. FAGE, A., PRESTON, J.H. " On Transition From Laminar to Turbulent Flow in the Boundary Layer " Proc.Ray. Soc. A178 201 - 225 1941.

53. DRYDEN,H.L. " Review of Published Data on the Effect of Roughness on Transition From Laminar to Turbulent Flow." Presented at the Aerodynamics Session, 21th Annual Meeting IAS New York January 26 - 29, 1953.

54. WHITE F.M. " Viscous Fluid Flow " Mc.Graw - Hill, Inc. 1974.